ANALYSIS AND OPTIMIZATION OF THE SCHEFFLER SOLAR CONCENTRATOR

A Thesis

presented to

the Faculty of California Polytechnic State University,

San Luis Obispo

In Partial Fulfillment

of the Requirements for the Degree

Masters of Science in Mechanical Engineering

by

Simone Alberti

December 2014

COMMITTEE MEMBERSHIP

TITLE:	Analysis and Optimization of the Scheffler Solar Concentrator
AUTHOR:	Simone Alberti
DATE SUBMITTED:	December 2014
COMMITTEE CHAIR:	Andrew Davol, PhD Professor of Mechanical Engineering Department Chair of Mechanical Engineering
COMMITTEE MEMBER:	Peter Schwartz, PhD Associate Professor of Physics
COMMITTEE MEMBER:	Glen Thorncroft, PhD Professor of Mechanical Engineering

ABSTRACT

Analysis and Optimization of the Scheffler Solar Concentrator

Simone Alberti

The Scheffler reflector is a new solar concentrator design which maintains a fixed focus while only having a single axis tracking mechanism. This design makes the construction and operation of high temperature solar concentrators accessible to developing nations. In this project, I wrote computer simulation codes to better understand the dynamics and the effect of deformation or deviations from ideal conditions in order to define necessary manufacturing and operational tolerances. These tools and knowledge drove the prototyping of new reflector concepts by myself and other students on my team. A fiberglass prototype was able to drive the cost of a reflector to sub-$50 and a wood reflector was manufactured with accessible materials and techniques used in boat building.

ACKNOWLEDGMENTS

I would like to acknowledge and thank the great research and effort made by all the students involved in Dr. Schwartz Solar Concentrator group throughout the years of my involvement and the work done by the senior project team that I advised in 2013. A great portion of the work was performed by these bright undergraduate students. I would finally like to thank Dr. Schwartz and Dr. Davol for the continuous support and passion on this project and the great relationship the three of us built between the Mechanical Engineering and Physics Departments. Thank you all.

TABLE OF CONTENTS

LIST OF TABLES

LIST OF FIGURES

NOMENCLATURE

β	-	Angle of paraboloid cutting plane wrt (+) x-axis
ϕ	-	Angle of crossbar cutting plane wrt (-) x-axis
$\delta_{\odot}$	-	Solar Declination
Θ (ΔΘ)	-	Horizontal angle (deformation) on reflector
Φ (ΔΦ)	-	Vertical angle (deformation) on reflector
Δ_{hrz}	-	Horizontal displacement of the light at the focus
Δ_{vrt}	-	Vertical displacement of the light at the focus
A	-	Lowermost point of reflector, intersection between parabola and cutting plane line
B	-	Uppermost point of reflector, intersection between parabola and cutting plane line
C	-	Point on parabola with 45 degree slope, close to midpoint between A and B
F	-	Focus of the parabola and reflector
a	-	Semi-minor axis of elliptical dish
b	-	Semi-major axis of elliptical dish
$R(\theta)$	-	Rotation Matrix
N	-	Day of the year
n	-	Number of horizontal cross sections, total number of points $\sim\frac{n^2}{2}$
$_p$	-	Parabola subscript
$_l$	-	Reflector cutting plane line subscript
$_Q$	-	Crossbar cutting plane line subscript
$_n$	-	n^{th} crossbar or cross section
$_N$	-	Nth day of the year
$_e$	-	Ellipse coordinate system subscript

CHAPTER 1: INTRODUCTION

The energy of the sun accounts for nearly all sources of energy used by nature and mankind. The sun drives all that is alive, but only few sources of energy rely directly from the energy from sunlight. Even though the sun provide about 1 kW of thermal power per meter square on the surface, resulting in enough energy to power the winds, maintain temperate climates and grow all photosynthetic life over the surface of the earth, mankind has not been able to harness it because of the relatively low energy density.

To generate the type of energy the humans need, from cooking to electricity, we usually need elevated temperatures. Biomass and fossil fuels have been a great source of high temperature energy for centuries but have always produced smoke and other undesirable byproducts. In many developing nations fire is used to cook indoors, trapping smoke in living areas. Studies show that indoor air pollution due to combustion of biomass results in more children's deaths than malaria in developing nations (Ezzati and Kammen). Furthermore, the need to find wood or other fuels can bring dangers such as long trips and exposure to violence, but also environmental impacts such as deforestation or pollution from drilling and mining.

In order to harness the power of the sun for practical human applications it is necessary to focus its energy to an area of concentrated heat. Though this seems like an easy task to achieve since we've all played with magnifying glasses or bent mirrors, in the long run it becomes a challenge because the sun is not stationary. Maintaining a high quality focus through the sun's apparent rotation around the earth requires a significant engineering effort. Often, the simplest methods to track the sun yield a concentrator with a moving focus, which poses a number of inconveniences. The solution to this problem are fix focus concentrators, of which many pedigrees exist requiring sophisticated mechanisms.

The Scheffler solar concentrator was introduced by namesake engineer Wolfgang Scheffler as a unique fixed focus solar concentration device with the intent to empower developing nations. The core of the idea behind the Scheffler is to create a high quality focus which requires reduced tracking mechanisms and structure so that it could be easily built, maintained, and operated in all parts of the world. The Scheffler concentrator achieves this goal because it can maintain a fixed focus while only having single daily axis tracking. Figure 1.1 shows a graphics representation of a Scheffler Concentrator in a solar cooking application. The shape of the reflector is defined by the parabola, show in red, and its focus, shown in yellow. As the day progresses, the reflector is rotated about the rotation axis to track the sun while maintaining a fixed focus.

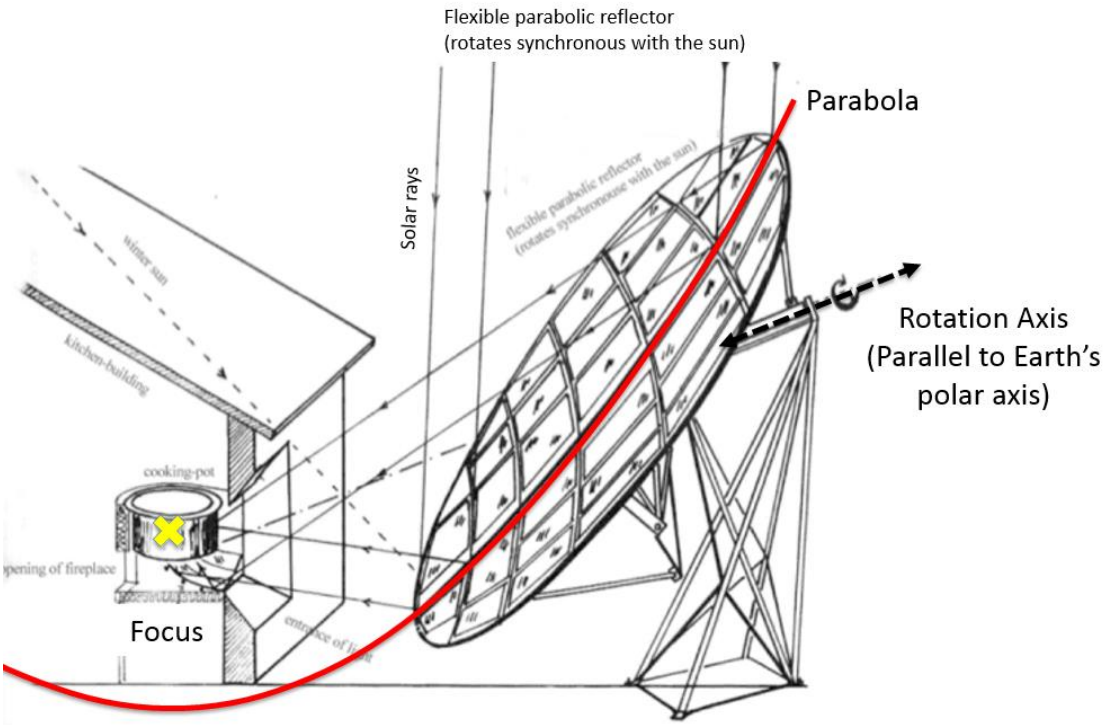

Figure 1.1: A simple representation of the Scheffler Concentrator in a solar cooking application. The solar rays are focused inside a building to a cooking surface. As the reflector rotates about its axis to track the sun daily, the focus remains fixed.

Like for Scheffler, our goal is to give access to solar concentration technology to developing nations rather than driving down the cost of production for sale. The strongest quality of the Scheffler reflector is that it reduces complexity of the technology, allowing nations with abundance of human labor to access its technology. The mission of Cal Poly's Scheffler Reflector research group, led by Pete Schwartz, is to improve on Scheffler's design to allow for construction with more sustainable and appropriate materials which are in abundance in rural areas of developing nations. Due to the very unique nature of the Scheffler design and its recent introduction, very few research and development has been done outside of Scheffler's Solar Brucke foundation.

The scope of my research and role in Cal Poly's Scheffler Reflector group can be broken into four categories.

1. To develop an in-depth understanding of very complex dynamics of the Scheffler reflector.
2. To analyze the sensitivity of the focus of a Scheffler reflector to define manufacturing tolerances required to create an effective concentrator.
3. To design a reflector constructed from accessible materials for developing nations.
4. To drive cost of raw material and manufacturing down while maintaining a high quality concentrator.

To achieve these goals I developed a computer simulation and analysis tool for the Scheffler reflector. I assisted my advisor, Pete Schwartz, in managing a group of 4-6 undergraduate research students working on the Scheffler reflector. I sponsored and advised a Mechanical Engineering senior project with 3 Cal Poly seniors though three quarters investigating alternative

construction methods for the parabolic reflector. Finally, in collaboration with Pete Schwartz and Tyler Murphey, developed a dual mirror polar tracking reflector derived from the Scheffler design.

CHAPTER 2: CURRENT SCHEFFLER CONCENTRATOR

Cal Poly built the first Scheffler reflector in North America in 2010 based on the instructions provided by Scheffler for a 2 square meter reflector. The building process took 4 students a total of 1000 man-hours over the course of a summer with a budget of approximately $2,000. The instructions were not always very clear and were provided in German resulting in a working reflector with a few errors or missing components.

Figure 2.1: Scheffler reflector built at Cal Poly in 2010, first in North America

Scheffler provides building instructions for a 2 square meter horizontal reflector (also known as “laying down” reflector, see Section 3.5), the one Cal Poly built, and a larger 2.7 square meter vertical reflector. The instructions are for a reflector mostly built out of aluminum square stock, nuts, and bolts, all rather accessible components. Though it was not easy building the first prototype with the instruction because everything was unfamiliar, the process would be easier and results would be better after building several reflectors. Scheffler’s plan to spread the use of his reflectors is not to expect people to build them just from the instructions, like the Cal Poly students did. Instead they run workshops teaching people in developing nations how to manufacture the reflectors (like Barefoot College in India, www.barefootcollege.org), making it

much easier to produce a high quality product. The reflector still remains rather expensive, though much more affordable and accessible that other solar concentrator technologies.

In addition to the Scheffler reflector built in house at Cal Poly, we have recently purchased a similar reflector built in Germany by the Scheffler team which required only minor assembly on our part. This reflector was expensive, costing us about $4700, and the delivery was not easy but its build quality was considerably better than the first prototype built here. Most importantly it allowed us to notice a few design aspects and features that were not included in our reflector build. The new reflector focused the light better and overall was easier to use, but that can mostly be attributed to the experience of the team who constructed it. One significant difference between the two is a clever pivot mechanisms design into the frame of the new reflector which aids the seasonal adjustment by automatically deforming the reflector surface as its angle is adjusted for seasonal changes. This mechanism makes adjusting the reflector throughout the seasons very easy and straightforward (Scheffler, Hensel and Munir). Yet, the designs were near identical and the cost was still high.

The Scheffler that was built here at Cal Poly has been used on a daily or weekly bases for the past 4 years and been through various tests. It currently focuses most the light to a 15 by 15 centimeter target, though a majority of the light is focused in a much smaller area as small as 5 by 5 centimeters depending on how well it is adjusted and the time of the year. Figure 2.2 shows the light distribution at the focus during a test with moonlight, allowing us to better visualize the focus without igniting anything or blinding ourselves. Each small square is 1/5 of an inch, the outline drawn on the paper represents where almost all of the light was focused and it measures 10 by 15 centimeters, while the really bright spot at the center measures less than 5 by 5 centimeters.

In additional tests we found that it could boil one liter of water in approximately 10 minutes, delivering as much as 900 Watts of thermal power during a test in July.

Figure 2.2: Light distribution at the focus of the Cal Poly built Scheffler concentrator during a test with moonlight

The goal of the research team that has been working on the Scheffler reflector since 2010 is to engineer a simpler Scheffler reflector that can be built in less time and with less resources. Prototypes for a simpler frame have been designed and built costing less than $20, a simple tracking circuit was engineered to cost about $5, and other various components were improved and added, such as a thermal storage unit for cooking after sunset. The greatest challenge has been to engineer and manufacture the reflective dish less expensively yet maintain loose enough tolerances to achieve a small focus throughout the year. This required us to better understand the dynamics and optics of this rotating and deforming reflector as well as exploring interesting new

manufacturing ideas with an interdisciplinary team of both physics and mechanical engineering students.

CHAPTER 3: SCHEFFLER CONCENTRATOR DESIGN

3.1 Selecting a Parabola

The first step in constructing a Scheffler concentrator is to decide the equation of the parabola and the start and end points of our dish section for equinox (Scheffler, Hensel and Munir). These parameters are defined by the ratio between the area of the dish and the position of the focus with respect to the dish. Once this ratio is defined, the dimension of the parabola can be adjusted for smaller or bigger dish areas by simply scaling everything up or down.

To simplify calculations the parabola is set to have the vertex at the origin, taking the form,

$$y_p = m_p x^2 \tag{3.1}$$

which will then be revolved around the y-axis to form the three dimensional paraboloid. The paraboloid must then be sliced by a plane to define the dish section. The slice will create the dish with an elliptical rim, see Figure 3.1. The following calculation will be made on the 2-D x/y-plane, illustrated in Figure 3.2, using Equation 3.1 to define the parabola and the equation of a line to represent the intersecting plane. The intersection points between the parabola and the line, *A* and *B*, represent the lowermost and uppermost ends of the dish section and the slope of the line is represented by the angle β with respect to the x-axis. In this representation, the sun rays are incoming parallel to the y-axis and reflect off the paraboloid toward the focus on the y-axis, see Figure 3.1.

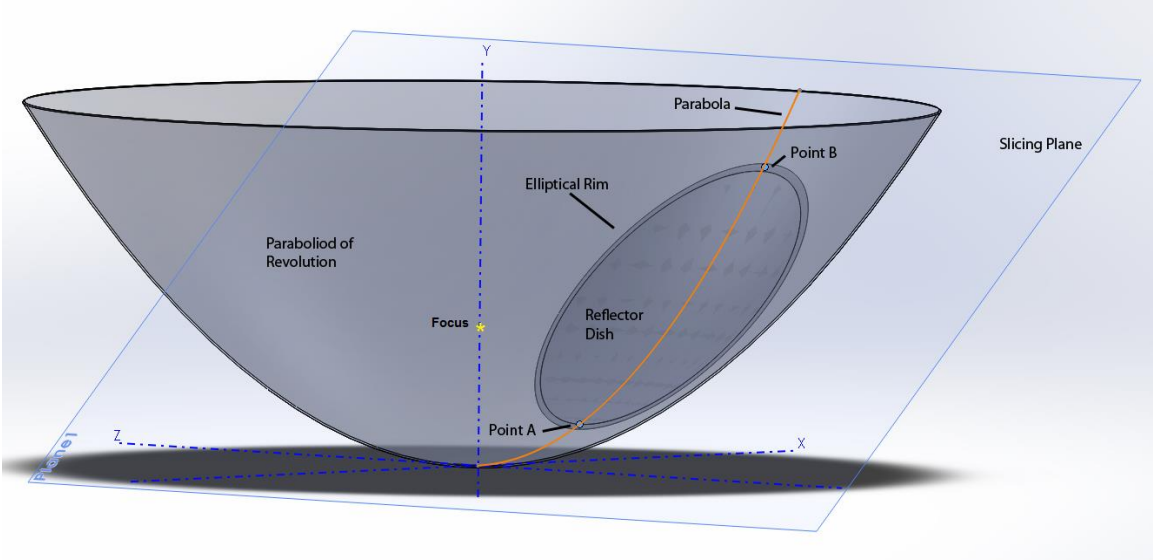

Figure 3.1: The parabola is revolved around the y-axis to form a paraboloid of revolution, which is the slices by the plane connecting points A and B to form the reflector dish.

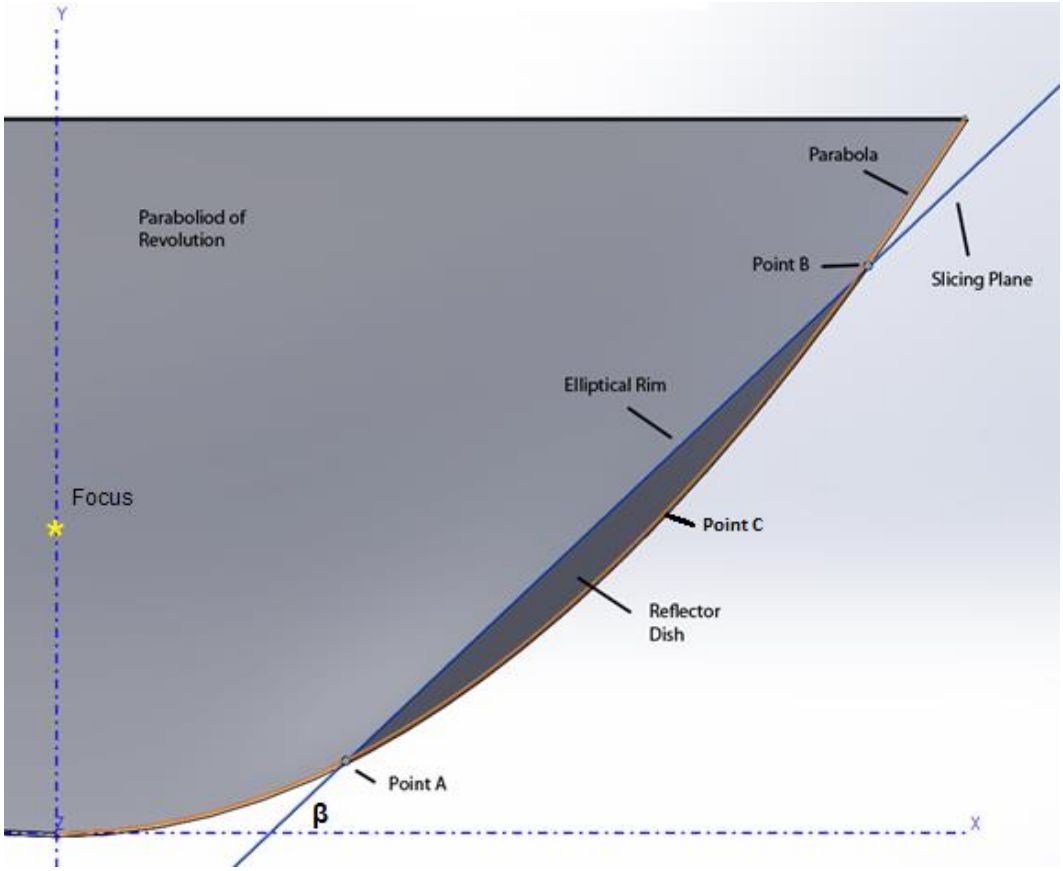

Figure 3.2: 2D view of Figure 3.1 on X-Y plane used to define the function of the parabola, points A and B, and the slicing plane.

Taking the derivative of Equation 3.1 yields the equation for the slope,β

$$\frac{dy_p}{dx} = 2m_p x$$

3.2

Point *C* is defined on the parabola as the point with slope of 45 degrees. This point is of interest because it represents the point where the incoming vertical light rays will reflect by 90 degrees and proceed horizontally to the focus. The horizontal light ray from point C to the focus defines the axis of rotation of the physical reflector for the daily tracking of the sun. This characteristic point should be placed very close to the center of the dish to create a balanced frame with respect to the daily rotation axis. If *C* is located near the center of gravity of the reflector then it will be very easy to rotate the reflector, minimizing the need to counter balance.

The most important point in the analysis is the focus of the parabola, *F*, is located on the y-axis at a height

$$y_F = \frac{1}{4m_p}$$

3.3

Since the vertex was positioned at the origin Equation 3.3 also represents the focal length of the parabola which is defined as the distance between the vertex and focal point along the axis of symmetry.

Since we reserve the ability to scale the reflector at a later point, at this stage we will choose parameters that simplify the design of the reflector. For mathematical simplicity, m_p was then chosen to be 0.25, which positions the focus at $= (0,1)$,

$$y_F = \frac{1}{4 \cdot 0.250} = 1$$

and the 45° point at $C = (2,1)$ from Equation 3.1. Yielding a very elegant equation for the parabola to be used in the rest of the project,

$$y_p = 0.25x^2$$

3.4

The start and end point of the dish section, point A and B respectively, are then chosen to be equidistant from C, their distance from each other determines the ratio between the size of the reflector and the distance to the focus. If A and B are placed farther apart, the ratio between the distance CF to the area of the dish will decrease. This increases the curvature of the dish and makes it easier to focus the light at the focus. This is desirable because it will allow for looser tolerances in the manufacturing of the dish making it easier and less expensive to make. If points A and B are chosen to be closer, the focus will be effectively farther away and the dish less curved. This will require tighter tolerances in the production of the dish but will give various advantages such as the ability to focus the sunlight a greater distance away, such as inside a house.

The x-coordinate of A and B were then chosen to be $x_A = 1$ and $x_B = 2.8$ so that the arclength between them was about 25% more than the distance from C to the focus. Since the biggest challenge in reducing the cost of the Scheffler design is producing a good reflective dish, we chose to keep the focus closer to the dish. The y-coordinates of A and B can be calculated using the parabola equation, 3.4. The equation for the arclength on an upright parabola is,

$$h = \frac{x}{2}$$

$$q = \sqrt{f^2 + h^2}$$

where h and q are parameters for describing the two points confining the arc on the parabola, defined by x_1 and x_2. The length of the arc between points 1 and 2 is defined as,

$$\Delta s_{1,2} = \frac{h_1 q_1 - h_2 q_2}{f} + f \ln\left(\frac{h_1 + q_1}{h_2 + q_2}\right)$$

3.5

where $\Delta s_{1,2}$ is the arclength between point 1 and 2 and f is the focal length of the parabola.

The line that connects points A and B is defined as

$$y_l = m_l x + b_l$$

3.6

with a slope angle of

$$\beta = \tan^{-1}(m_l)$$

3.7

With the known coordinates of A and B, the slope and y-intercept are calculated with,

$$m_l = \frac{y_B - y_A}{x_B - x_A}$$

$$b_l = y_A - m_l x_A$$

Yielding the following function,

$$y_l = 0.95 x_l - 0.7$$

3.8

Table 3.1: Key points on parabola with $m_p = 0.250$

	x	y
F - focus	0	1.00
C - mid point	2.00	1.00
A - bottom point	1.00	0.250
B - top point	2.80	1.96

The reflector dish is now fully defined by Equations 3.4, and 3.8, representing the parabolic line to be revolved about the y-axis and the cutting plane, respectively, shown in Figure 3.3. The significant points and their coordinates are shown in

Table 3.1. It is important to remember that the dish was designed considering ratios instead of dimensions, allowing this design to be scaled depending on the application.

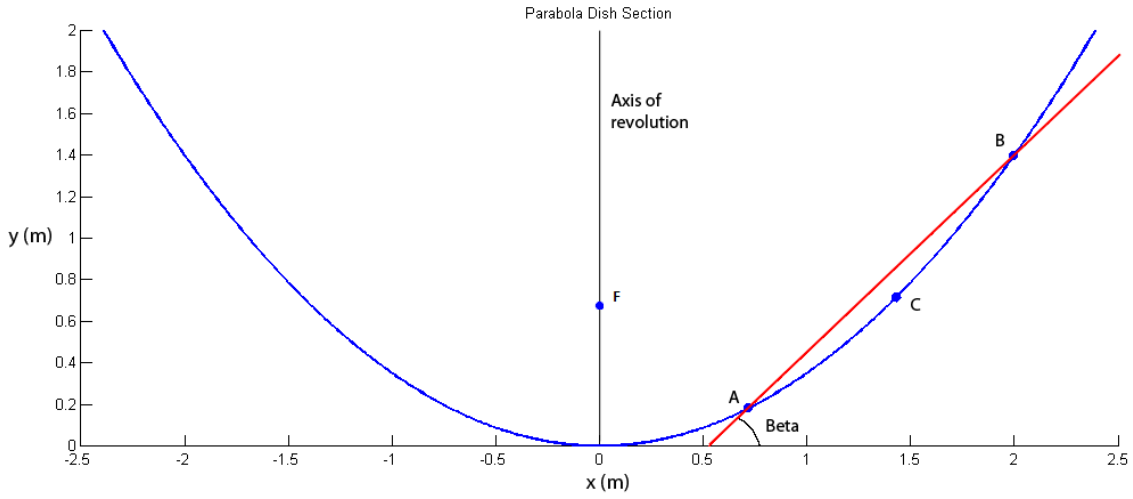

Figure 3.3: Graph of the parabolic curve of our dish. Red line delimits the section used as the dish, between points A and B, while point C shows its midpoint and 45 degree slope point

The MATLAB code ParabolaSec.m calculates all the properties of the dish given the parabolic equation and points A and B .

3.2 Resizing the Dish

Since parabolas are geometrically similar, it is possible to scale Equation 3.4, while maintaining the ratios that define points A, B, and C, to obtain any desired dish area. By geometrical properties, the intersection of a paraboloid of revolution and an inclined plane will create an ellipse, defined by semi-minor axis, a, normal to both the x and y-axis and semi-major axes, b, connecting points A and B. The vertical projection of the ellipse tilted at angle β onto the horizontal plane (x-z) is a circle of radius $a = \frac{x_B - x_A}{2}$, which represents the effective area seen by the sun. The x value of A and B can be found by setting Equation 3.1 and 3.6 equal to each other and solving using the quadratic formula,

$$x_{A,B} = \frac{m_l}{2m_p} \pm \sqrt{\left(\frac{m_l}{2m_p}\right)^2 + \frac{b}{m_p}}$$

3.9

Then finding the difference to calculate the semi-minor axis,

$$a = \frac{x_B - x_A}{2} = \sqrt{\left(\frac{m_l}{2m_p}\right)^2 + \frac{b}{m_p}}$$

3.10

Using Pythagorean's theorem it is possible to relate *a* and *b* to the angle β, Figure 3.4,

$$\frac{a}{b} = cos(\beta)$$

3.11

Then the elliptical area of the dish can be rewritten using Equations 3.11 as,

$$Area = \pi \cdot a \cdot b = \frac{\pi a^2}{cos(\beta)}$$

3.12

The *Area* as defined in Equation 3.12, will be the parameter by which we resize the dish.

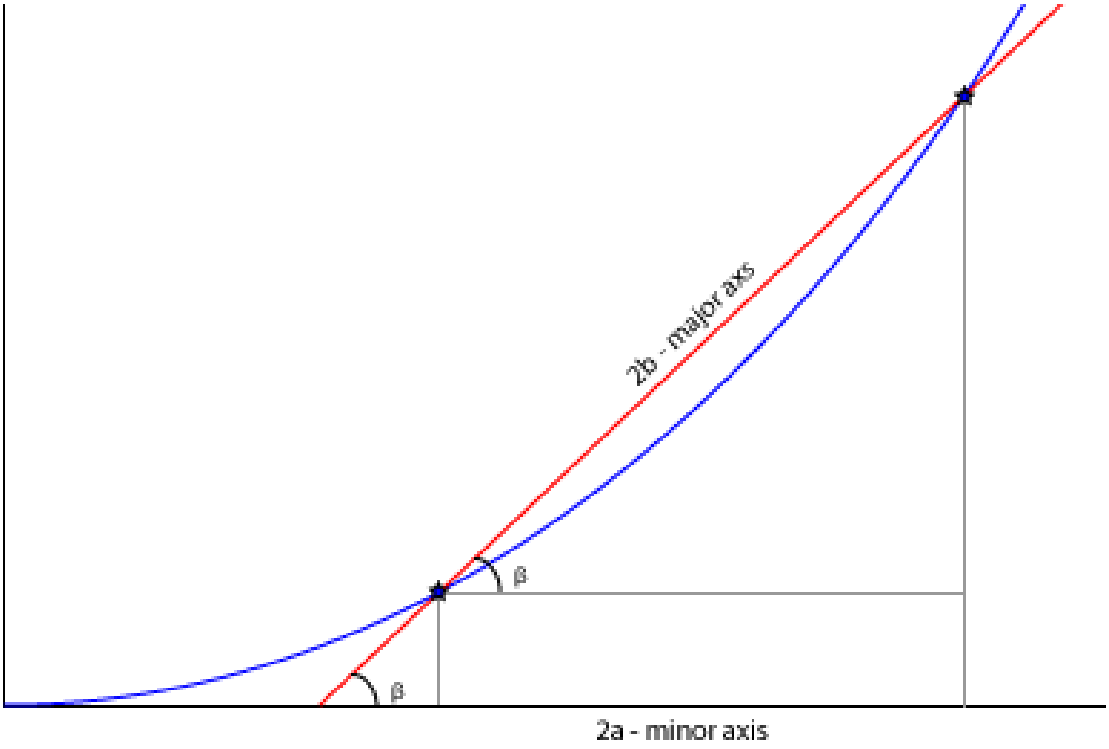

Figure 3.4: Pythagorean relation between angle of slicing plane, β, and the major and minor axes of the resulting ellipse

To derive a resizing equation it is first necessary to formulate a relation between the original parabola, $y_1 = m_1 x_1^2$, and the resized parabola, $y_2 = m_2 x_2^2$, and the x and y coordinates of points A and B. The original parabola, now being denoted by subscript 1, is the same defined in Section 3.1 , therefore $m_p = m_1$. Using Equations 3.1 and 3.3 we can define the x-coordinate of points C,

$$x_{C_1} = \frac{1}{2m_1}$$

$$x_{C2} = \frac{1}{2m_2}$$

Using the geometric similarity of parabolas we can require that the ratios between the x-coordinates of A to C and of B to C to remain constant after the resize,

$$\frac{x_{A1}}{x_{C1}} = \frac{x_{A2}}{x_{C2}}$$

$$\frac{x_{B1}}{x_{C1}} = \frac{x_{B2}}{x_{C2}}$$

which can be solved in terms of the x_2s and y_2s using Equation 3.1,

$$x_{A2} = x_{A1}\frac{m_1}{m_2}$$

$$x_{B2} = x_{B1}\frac{m_1}{m_2}$$

3.13

and

$$y_{A2} = \frac{{m_1}^2}{m_2}{x_{A1}}^2$$

$$y_{B2} = \frac{{m_1}^2}{m_2}{x_{B1}}^2$$

3.14

To use Equation 3.12 we must find an expression for a_2 in terms of m_1, m_2, and x_1s. We must rewrite Equation 3.10 in the following form,

$$a_2 = \sqrt{\left(\frac{m_l}{2m_2}\right)^2 + \frac{b}{m_2}}$$

3.15

and find expressions for m_l and b.

Knowing that the slope of a line is equal to rise over run and substituting Equations 3.13 and *3.14* we can define,

$$m_l = \frac{y_{B2} - y_{A2}}{x_{B2} - x_{A2}} = \frac{\frac{{m_1}^2}{m_2}({x_{B1}}^2 - {x_{A1}}^2)}{\frac{m_1}{m_2}(x_{B1} - x_{A1)})} = m_1 \frac{({x_{B1}}^2 - {x_{A1}}^2)}{(x_{B1} - x_{A1)})} = m_1(x_{B1} + x_{A1})$$

3.16

The value of *b* can then be found by substituting point (x_{A2}, y_{A2}) into Equation 3.6 then substituting in Equations 3.13, *3.14*, and 3.16.

$$b = y_{A2} - m_l x_{A2} = \frac{{m_1}^2}{m_2}{x_{A1}}^2 - m_1(x_{B1} + x_{A1}) \cdot x_{A1}\frac{{m_1}^2}{m_2} = -\frac{{m_1}^2}{m_2}x_{B1}x_{A1}$$

3.17

Equation 3.15 can now be rewritten as,

$$a = \sqrt{\frac{{m_1}^2(x_{B1} + x_{A1})^2}{4{m_2}^2} - \frac{{m_1}^2}{{m_2}^2}x_{B1}x_{A1}} = \frac{m_1}{m_2}\sqrt{\frac{1}{4}(x_{B1} + x_{A1})^2 - x_{B1}x_{A1}}$$

3.18

Which leaves β the only undefined variable in Equation 3.12. This angle is the arctangent of the slope of the line connecting points A and B and can thus be rewritten using Equation 3.16 as,

$$\beta = tan^{-1}(m_l) = tan^{-1}[m_1(x_{B1} + x_{A1})]$$

3.19

Substituting Equations 3.17 and 3.18 into 3.12 yields,

$$Area = \frac{\pi \frac{{m_1}^2}{{m_2}^2}\left[\frac{1}{4}(x_{B1} + x_{A1})^2 - x_{B1}x_{A1}\right]}{cos\{tan^{-1}[m_1(x_{B1} + x_{A1})]\}}$$

Solving for the only unknown, m_2,

$$m_2 = \sqrt{\frac{\pi m_1^2\left[\frac{1}{4}(x_{B1} + x_{A1})^2 - x_{B1}x_{A1}\right]}{Area \cdot cos\{tan^{-1}[m_1(x_{B1} + x_{A1})]\}}}$$

3.20

We now have an equation in terms of all the predefined properties and dimensions of the original dish defined in Section 3.1 and the desired reflector area. For the parabolic dish used in the project a surface area of 1.8 m^2 was chosen yielding the parabolic equation below and the key points A, B, C, and F show in in Table 3.2 in meters,

$$y_p = 0.349{x_p}^2$$

3.21

$$y_l = 0.95x - 0.501$$

3.22

Table 3.2: Key points on parabola with $m_p = 0.349$

	x (m)	y (m)
C - mid point	1.43	0.716
A - left point	0.716	0.179
B - right point	2.01	1.40
F - focus	1.43	0
β	43.5°	
Geometrical Mid-Point	1.36	0.791

The area we have been discussing in Section 3.2 is referring to the elliptical area that is the physical dish that we build. This is a key parameter used in describing how large the dish is for practical and construction purposes but may be misleading during the analysis. It is easy to think that the elliptical area represents the area of sunlight captured, in reality it is not because the dish is tilted at approximately 45° from the incoming sun rays. The important area to consider is the projected area on the plane perpendicular to the incoming light rays, which corresponds to the earth surface during the equinoxes. This projection, as mentioned previously, is a circle of radius a. By comparing the two area equations we find the following relation,

$$\frac{A_{projected}}{A_{dish}} = \frac{\pi a^2}{\pi ab} = \frac{a}{b} = cos(\beta) \approx \cos\left(\frac{\pi}{4}\right) = 0.707$$

Due to the design parameters described previously, a Scheffler concentrator will have a β angle very close to 45° at equinox. We then know that the area of sunlight captured by the reflector is about 70% of the elliptical area of the reflector at equinox.

The MATLAB code Resize.m executes the resizing of the dish.

3.3 DISH SECTION AND CROSSBARS

As explained in detail in the previous sections, when a paraboloid of revolution is intercepted by an inclined plane it forms an ellipse. The ellipse created by intersecting the paraboloid of revolution from Equation 3.20 and the plane from Equation 3.22 is the rim of the parabolic dish to be used in our Scheffler concentrator. The solid part outside this intersection is the dish which has a parabolic profile on its vertical axis and an elliptical profile on its horizontal axis.

The equation for an ellipse can be written in standard from as

$$1 = \left(\frac{x}{a}\right)^2 + \left(\frac{y}{b}\right)^2$$

3.23

Using Equation 3.11 we can simplify the formula in terms of the angle β and the semi-minor axis *a* defined by Equation 3.10,

$$y_e = \frac{1}{\beta}\sqrt{a^2 + x_e^2}$$

3.24

Equation 3.24 is not to be represented on the original x-y plane used by the parabola and all the analysis in Section 3.1 . We have now shifted to a new coordinate system on the intersecting plane (formed by Equation 3.22) since this is the plane on which the elliptical rim of the dish is located. In this new ellipse coordinate system the y_e-axis is coincident with the major axis of the ellipse and the x_e-axis is coincident with the minor axis, the z_e-axis is normal to this plane, pointing

toward the inside of the paraboloid of revolution, Figure 3.5 illustrates the coordinate system visually.

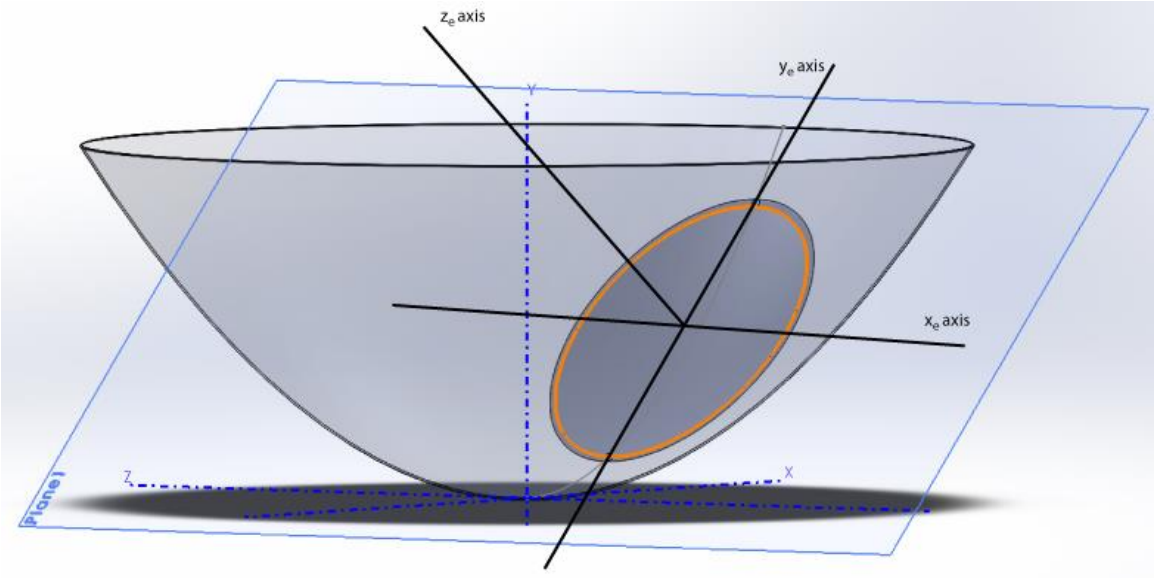

Figure 3.5: Ellipse plane coordinate system denoted by subscript 'e'

For the analysis and the construction of the reflector, it is necessary to analyze various cross-sections of the reflector, which can then be also used to construct crossbars. The first crossbar needs to be located at the center of the ellipse and coincident with the x_e-axis, while the other crossbars should be equally spaced to both ends of the ellipse and parallel to each other. The number of cross-sections are chose to be a large number for analysis purposes to increase the resolution but for construction purposes numbers can be low, Scheffler states that seven crossbars can be sufficient for a reflector of up to 8 m^2 (Munir, Hensel and Scheffler). We will continue this section considering 11 crossbars, but the analysis can be easily generalized for any larger number.

11 crossbars are equally spaced at $\Delta y = 0.148$ meters and the crossbar count must be odd so that the middle crossbar can be placed at the center of the ellipse. Figure 3.6 shows the location of the crossbars on the ellipse plane as lines.

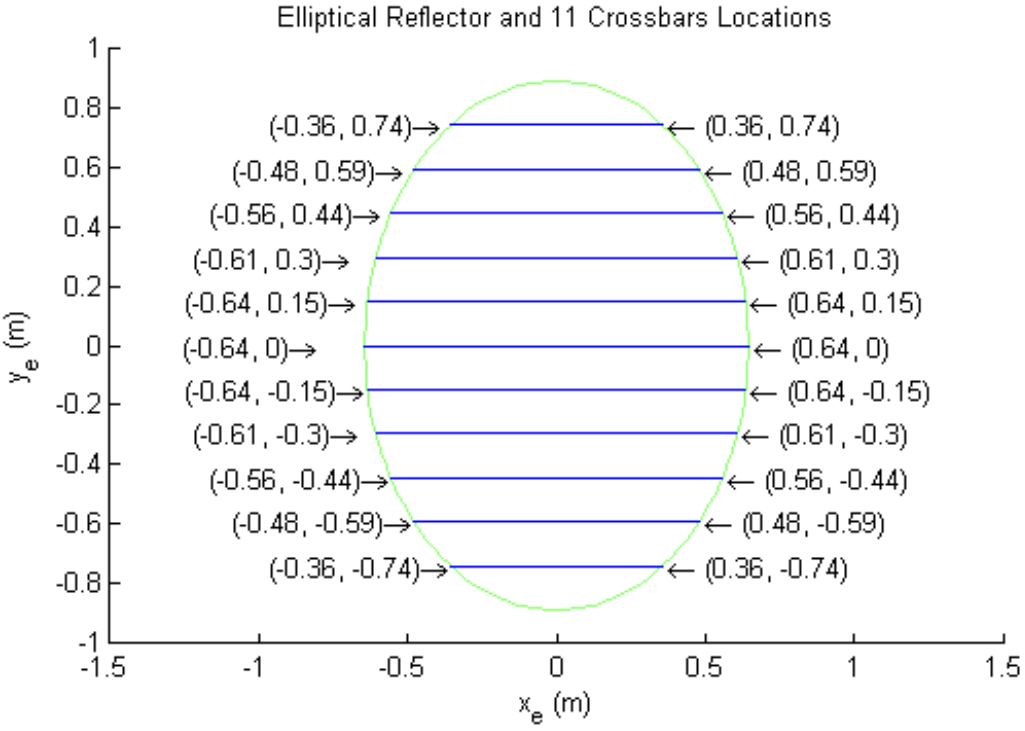

Figure 3.6: Elliptical reflector shape and the location and intersection points of the 11 crossbars, represented on the ellipse coordinate system

The cutting planes of each crossbar are normal to the ellipse plane and can be represented on the parabola coordinate system as lines perpendicular to the cutting plane on the x-y plane, Figure 3.7.

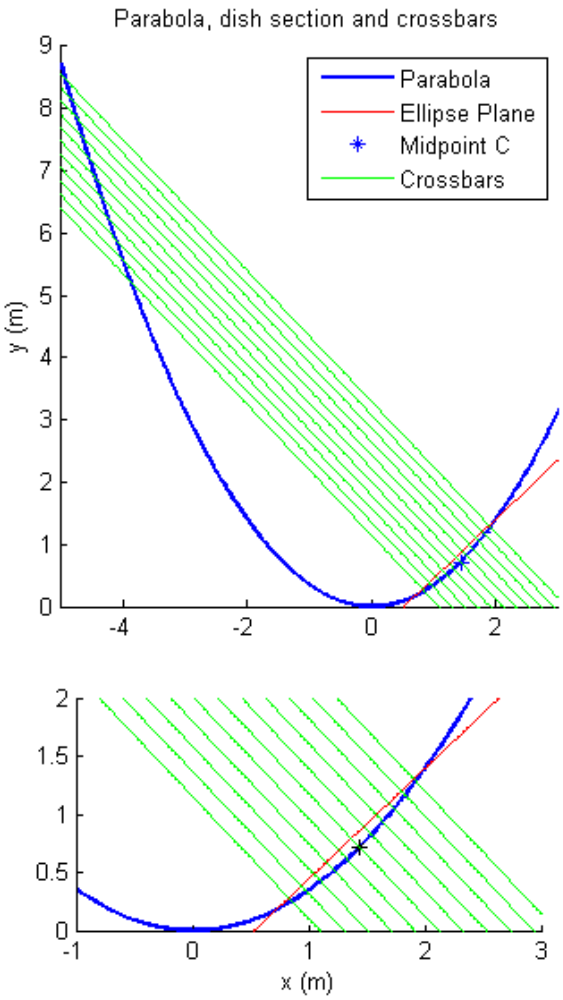

Figure 3.7: Parabola (blue), elliptical cutting plane (red), and crossbar cutting planes (green)

The equation for these lines can be found by knowing the angle with the negative x-axis, ϕ, which is equal for all cross section planes and at 90° with the reflector cutting plane angle, β. The angle of the cross section cut planes and the resulting line slope is calculated with

$$\phi = \frac{\pi}{2} - \beta \tag{3.25}$$

$$m_Q = \tan(-\phi) \tag{3.26}$$

The y-intercepts are equally spaced proportional to the spacing on the ellipse plane. The middle crossbar line can be calculated by using the result from Equation 3.26 and the geometric mid-point of the parabola from Table 3.2. The y-intercepts for all other lines can be found by adding and subtracting the crossbar spacing projected on the y-axis, where Δb is the change is y-intercept,

$$\Delta b_Q = \frac{\Delta y}{\cos(\phi)}$$

3.27

The resultant equations for the 11 crossbar cutting sections are shown in Table 3.3 and Figure 3.7. It is easy to notice that the crossbar cutting planes (green in Figure 3.7) intersect the paraboloid in the same way the reflector cutting plane (red) does and thus will result in similar elliptical profiles. The semi-major and semi-minor axes of each elliptical crossbar profile can be calculated using Equation 3.11 and is shown in Table 3.3. With the properties of the elliptical crossbars it is possible to reconstruct the shape of the reflector.

The profile of the reflector along the y_e-axis at x_e=0 is that of the parabola we defined in Section 3.1 and 3.2 , we can say that the profile along the vertical axis of the reflector is parabolic. On the other hand, the profile along the x_e-axis is that of an ellipse defined by each of the crossbars, we can say that the profile along the horizontal axis of the reflector is elliptical.

Table 3.3: Properties of the 11 crossbars

Crossbar #	Equation of cutting section on parabola plane	Semi-minor axis a_n (m)	Semi-major axis b_n (m)	± x-coordinate on ellipse plane x_n	y-coordinate on ellipse plane y_n
1	$y_1 = -1.05x + 1.15$	2.36	3.42	0.356	-0.741
2	$y_2 = -1.05x + 1.36$	2.49	3.61	0.480	-0.593
3	$y_3 = -1.05x + 1.58$	2.61	3.78	0.558	-0.444
4	$y_4 = -1.05x + 1.79$	2.72	3.95	0.608	-0.296
5	$y_5 = -1.05x + 2.01$	2.83	4.11	0.636	-0.148
6	$\boldsymbol{y_6 = -1.05x + 2.22}$	**2.94**	**4.27**	**0.644**	**0**
7	$y_7 = -1.05x + 2.44$	3.04	4.42	0.636	0.148
8	$y_8 = -1.05x + 2.65$	3.14	4.56	0.608	0.296
9	$y_9 = -1.05x + 2.87$	3.24	4.70	0.558	0.444
10	$y_{10} = -1.05x + 3.08$	3.33	4.84	0.480	0.593
11	$y_{11} = -1.05x + 3.30$	3.42	4.97	0.356	0.741

3.4 APPROXIMATING ELLIPTICAL CROSSBARS WITH CIRCULAR PROFILES

To simplify the construction of the crossbar, Scheffler suggests approximating the elliptical horizontal profile with a circular profile. He argues that the approximation helps produce the crossbars cheaply without significantly harming the focus of the reflector. Since the segment of the ellipse used in the crossbar is very small, they can be taken as circular segments. Our analysis, see Section 4.2 , supports Scheffler conclusion, finding that 99.7% of light is concentrated in a small 5x5 cm focus.

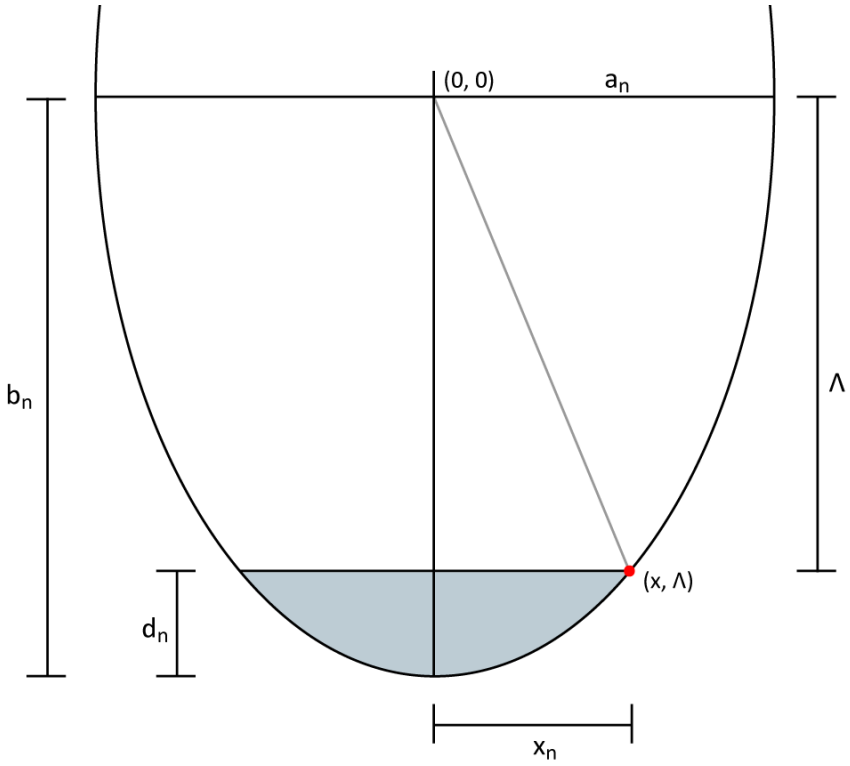

Figure 3.8: Ellipse of a crossbar, shaded area the section of the reflector with depth d_n

While the width of each crossbar is known, double the x_e-coordinate show in Table 3.4, the depth must be calculated with some geometry. Using Figure 3.8 for reference we can see that the depth of each crossbar is,

$$d_n = b_n - \Lambda$$

where Λ is defined by the general ellipsoidal equation to be

$$\Lambda = \frac{\sqrt{a_n^2 - x_n^2}}{\cos(\phi)}$$

With the depth of the crossbar calculated we have three points from which a circle can be approximated, the center bottom and the two edges. The radius and the angle made with the half arc length of the circles are,

$$R_n = \frac{d_n^2 + x_n^2}{2d_n}$$

$$\omega_n = \sin^{-1}\left(\frac{x_n}{R_n}\right)$$

The resultant values for our reflector design are shown in Table 3.4. All the calculations for the crossbars, including those of Chapter 3.3 , are performed by the crossbar.m Matlab function. The Matlab function works for any parabola and any cutting plane

Table 3.4: Crossbar depths and circular approximations

Crossbar #	Depth d_n (m)	Circular Approximation Radius R_n (m)	Half arc angle ω_n (deg)
1	0.0393	1.635	12.59
2	0.0680	1.730	16.12
3	0.0878	1.818	17.88
4	0.0997	1.901	18.64
5	0.1048	1.979	18.73
6	**0.1038**	**2.052**	**18.31**
7	0.0974	2.121	17.43
8	0.0861	2.187	16.13
9	0.0704	2.249	14.37
10	0.0505	2.309	12.01
11	0.0270	2.365	8.66

3.5 SEASONAL CHANGES

One of the greatest advantages of the Scheffler design is that is allows for simple adjustments to maintain the same focus as the seasons change. The Scheffler is built and optimized for the equinox, when the sun is positioned half way between summer and winter

solstices. While the adjustments are simple and are well approximated by simply flexing the reflector inward or outward, the engineering analysis of the new reflector shapes can be instrumental to optimizing the concentrator.

The solar declination, $\delta_{\odot}$, is the angle of the sun at noon with respect to the aforementioned y-axis, or the plane of the equator, where north is positive (Duffie and Beckman). The declination is 0° at the equinoxes, it reaches a maximum angle equal to the Earth's axial tilt of 23.44 degrees during the summer solstice after moving north, then decreases to a minimum of -23.44 degrees during the winter solstice after moving south. The plot of the solar declination resembles a sine curve but is actually much more complex. For instance, the curves at the maximum and minima are more acute and the Earth moves slower about the sun on July 4th, close to the northern hemisphere summer solstice, because it's at the aphelion (point farthest to the sun in the elliptical orbit) making the declination change slower during the summer. Two equations for the solar declination are to be considered. The first has a lower accuracy, with an error of about +1.5^{o} at the autumn equinox, but is simpler to use and can be instrumental when adjusting the reflector in developing nations. The low fidelity equation uses a parameter N which represents the day of the year at GMT,

$$\delta_{\odot} = -23.44° \cdot \cos\left[\frac{360°}{365} \cdot (N + 10)\right]$$

3.28

where the number 10 represents the number of days from the winter solstice to the first day of the year (Sproul) (Szokolay). The second equation is more accurate, with a maximum error of 0.035^{o}, but considerably more complicated (Duffie and Beckman).

$$\delta_{\odot} = \frac{180^{\circ}}{\pi}\left[0.006918 - 0.399912\cos\left(B_{day}\right) + 0.070257\sin\left(B_{day}\right) - 0.006758\cos\left(2B_{day}\right)\right.$$
$$\left. = 0.000907\sin\left(2B_{day}\right) - 0.002697\cos\left(3B_{day}\right) - 0.00148\sin\left(3B_{day}\right)\right]$$

3.29

Where B_{day} is defined by the day of the year as,

$$B_{day} = \frac{2\pi}{365}(N - 1)$$

3.30

The Scheffler concentrator is positioned with the axis of rotation (which passes through the middle of the reflector and the focus) pointing north/south and parallel to the axis of rotation of the Earth. This is easily achieved by tilting the axis of rotation by the current latitude angle with respect to the ground. This insures that during the equinox, when the solar declination is zero, the sun's rays are coming in perpendicular to the rotation axis regardless of where the Scheffler concentrator is positioned in the world. It is also necessary so that the reflector rotates about the same axis as the Earth as it tracks the sun throughout the day. With these constraints, the Scheffler can be positioned standing up or laying down. This geometry is reversed when moving between the northern and southern hemisphere. We arbitrarily define our direction as follows: a concentrator which "points north" has the focus on the north side and the reflector on the south side. A "vertical" Scheffler concentrator points towards the equator (pointing south in the northern hemisphere and pointing north in the southern hemisphere) and a "horizontal" points towards the closest pole (pointing north in the northern hemisphere and pointing south in the southern hemisphere), Figure 3.9: Visual representation of a horizontal north facing reflector and a vertical south facing reflector in the northern hemisphere. While a physical concentrator can be relatively easily rotated or flipped to match any configuration, mathematically the sign of the solar

declination changes between configurations as shown in Table 3.5. For this project, we choose to consider the horizontal configuration in the northern hemisphere as it matches the configuration of the reflector built in 2010 at Cal Poly. Moving forward, all references to summer and winter configurations refer to a horizontal configuration in the northern hemisphere.

Table 3.5: Concentrator configuration and sign of declination angle

	Northern Hemisphere	Southern Hemisphere
Vertical	1	-1
Horizontal	-1	1

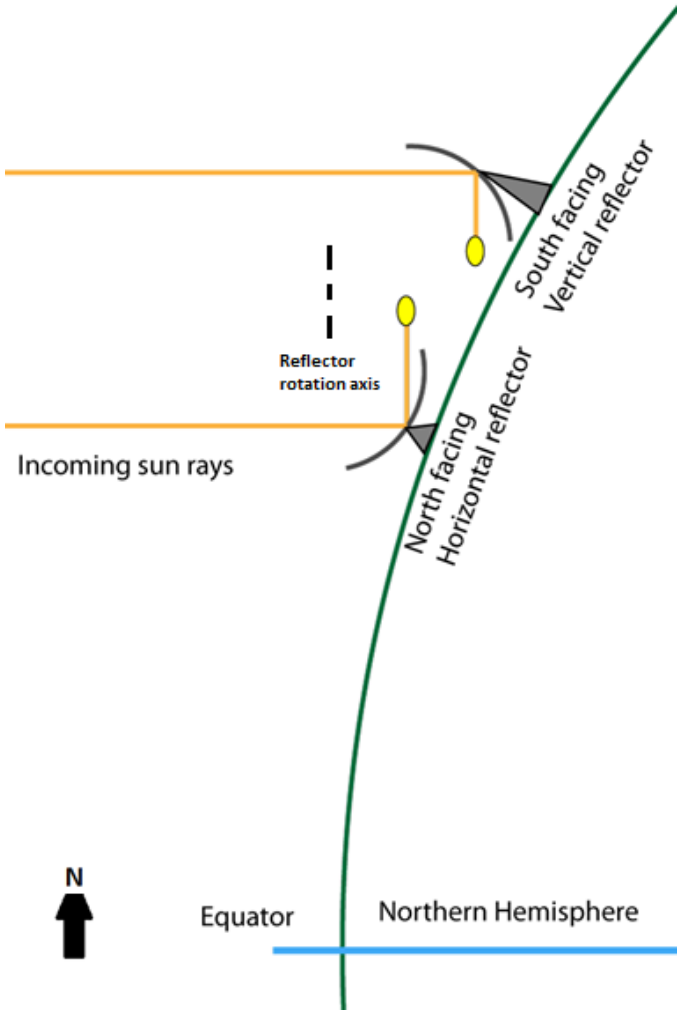

Figure 3.9: Visual representation of a horizontal north facing reflector and a vertical south facing reflector in the northern hemisphere.

As the solar declination changes throughout the year, the reflector must be adjusted to account for light rays coming in at angles not perpendicular to the axis of rotation. The best way to visualize the adjustments is that the axis of symmetry of the parabola needs to rotate by the solar declination, $\delta_{\odot}$, about the focus so that its axis of symmetry remains parallel to the incoming light rays, see Figure 3.10. Furthermore, the slope of the shared point of the parabolic section used for the reflector, which was previously at 45^{o}, must rotate by $\delta_{\odot}/2$ (a rotation of a reflective surface by $\theta/2$ causes the reflected light to rotate by θ) and hence the section of the parabola used shifts up or down the y-axis. Say the parabolic section used as the reflector lies in quadrant

1 and we want to adjust it for summer, so we need to rotate the parabola about the focus clockwise to follow the sun, which has moved right. After the rotation, the section used as the reflector is moved higher up on the parabola and has a reduced curvature, making the rays reflect at larger angles to reach the same focus. Similarly, if the sun moves left, the parabola must rotate counterclockwise, the reflector section will move lower in the parabola and increasing the curvature, making the rays reflect at more acute angles to reach the focus. Figure 3.10 shows a graphical representations of this phenomenon for the cases of the two solstices.

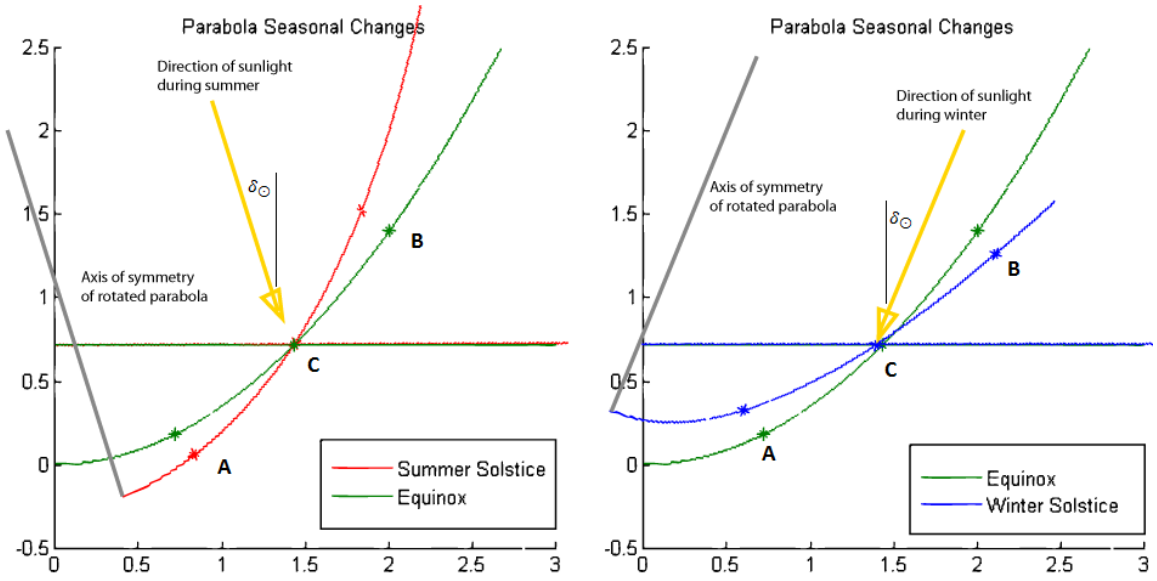

Figure 3.10: The parabola rotates about the midpoint, C, to follow the sun as it moves throughout the year, the section of the parabola also shifts up and down the curve in order to increase and decrease its curvature.

In addition to having to either open up or close the parabolic profile of the reflector, there must also be a change in the horizontal profile. The change in the horizontal profile is opposite of the vertical one: when the parabolic profile is opened to a smaller curvature, the horizontal profile is closed to a larger curvature and vice versa. This is very fortunate, because as a concave circular structure is stretched in one direction it curves in in the other making it very simple to physically adjust the reflector.

Mathematically, it is more convenient to represent all the parabolas on the same axis. So even though we rotate the axis to follow the sun and adjust the parabola, we rotate the coordinate system back so that the light rays are always coming down vertically. The best way to visualize the following analysis (see Figure 3.11) is that instead of imagining the Scheffler being fixed on Earth with the sun drifting North and South through the year, we visualize the sun as fixed and the earth as rotating on its axis.

The shared point between all parabolas of the year is chosen to be the point C because it is the point at the end of the rotation axis, the point with a slope of 45° in the equinox configuration. This point must be rotated about the focus (which we are to keep fixed in space) by $\delta_{\odot}$ using the rotation matrix,

$$R(\theta) = \begin{bmatrix} \cos(\theta) & -\sin(\theta) \\ \sin(\theta) & \cos(\theta) \end{bmatrix}$$

3.31

Since we are rotating about the focus and not the origin the x and y coordinates of the new point C_N can be found by,

$$[x_{C,N}, y_{C,N}] = R(\delta_{\odot}) \cdot [x_C, 0] + [0, y_C]$$

3.32

where $\delta_{\odot}$ is a function of the day of the year, N. Figure 3.11 shows the rotation of point C, represented by the star, for the extreme conditions of summer and winter solstice. This point is shown to move in the mathematical model because we are working in a reference frame where the sun is fixed and the Scheffler is rotating. In practice, the sun rotates and point C remains fixed in space, though the slope at C does change.

The slope of the parabola at the new point C_N must be adjusted by $\delta_\odot/2$ so that vertical light rays still reflect to the original focus. With this second constraint, the equations of the parabola can be easily found for any day of the year, N. The general parabolic equation is,

$$y_N = m_N x^2 + b_N$$

Calculating m_N

$$\frac{dy_n}{dx} = 2m_N x_{C,N} = \tan\left(\frac{\pi}{4} + \frac{\delta_\odot}{2}\right)$$

3.33

$$m_N = \frac{\tan\left(\frac{\pi}{4} + \frac{\delta_\odot}{2}\right)}{2x_{C,N}}$$

3.34

and b_N

$$c_N = y_{C,N} - m_N x_{C,N}^2$$

3.35

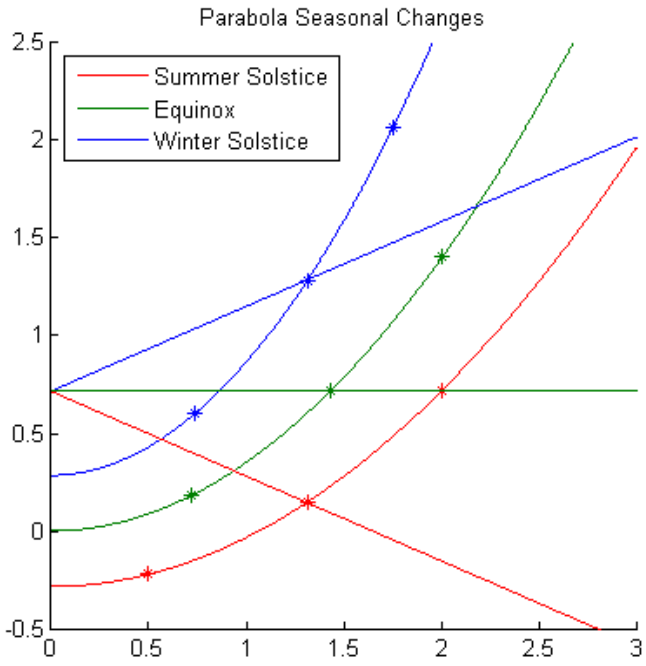

Figure 3.11: Equinox and solstice parabolic shapes with sun rays incoming parallel to axis of symmetry of the parabolas, the star point represents the shared point between the three parabolas.

The angle between the elliptical cutting plane and the x-axis can be also found by adding $\delta_{\odot}/2$ to its original value, from which points A_N and B_N can be found using the assumption that the area of the parabolic section of reflector remains constant during this transformation.

Table 3.6: Properties of the parabola at summer and winter solstice compared with equinox

	Parabola Eq^n	C (x,y)	Vertical Curvature at C (m^{-1})	Horizontal Curvature at C (m^{-1})	β (°)
Summer Solstice	$y_p = 0.250x^2 - 0.2850$	(1.314, 0.146)	0.292	0.421	32.0
Equinox	$y_p = 0.349$	(1.432, 0.716)	0.247	0.487	43.5
Winter Solstice	$y_p = 0.570x^2 + 0.2850$	(1.331, 1.312)	0.192	0.608	55.3

Calculated values for summer and winter solstice compared with equinox are show in Table 3.6 and Figure 3.11. We notice that the winter parabola, at $\delta_{\odot} = +23.44$ (positive because of horizontal configuration, see Table 3.5, is smaller but point C is further up yielding a smaller vertical curvature and hence a larger reflection angle. The horizontal curvature changes in the opposite direction, yielding a larger horizontal curvature in order to focus. Conversely, the summer parabola, at $\delta_{\odot} = -23.44$, is bigger but point C is closer to the origin yielding a larger vertical curvature and a smaller horizontal curvature. The fact that the horizontal and vertical curvatures trend in inverse directions is very convenient mechanically. If you imagine stretching a bowl shaped object in one axis, the other axis will deform in an opposite manner. This facilitates the seasonal adjustments because one axis will automatically adjust the other in a favorable direction. To help visualize these adjustments, Figure 3.10, shows the three parabolas with their axes tilted as following the declination of the sun as described earlier in this section.

Another important factor to consider is that the angle β changes as the parabola changes through the seasons. As was described in Section 3.2 , the angle β is directly related to the projected area of the reflector which defines how much area of sunlight is captured. We previously defined that at Equinox, when β≈45°, the ratio between the physical area of the reflector and the effective area is approximately 70%. For the reflector designed in this paper, the ratio becomes 57% at winter solstice and 85% at summer solstice, therefore a larger area of sunlight is captured during the summer for this particular configuration of reflector.

3.6 Reflector 3D Model

The previous sections outlined the procedure and equations to calculate the reflective surface of a Scheffler concentrator for any day of the year. The method is based on slicing the

reflective surface and creating a finite number of crossbars, which can either be exact elliptical sections or circular approximations. Calculating the shapes of a small number of crossbars is useful for manufacturing. All these calculations are coded in Matlab with a considerable number of adjustable variables.

In this section we show sample values for a reflector built using 11 crossbars, while the original Scheffler design calls for 7. Running the Matlab code with 11 crossbars will output the parameters and values shown in the tables in Section 3.3 but can also be used to construct a model of the cross bars as shown in Figure 3.12.

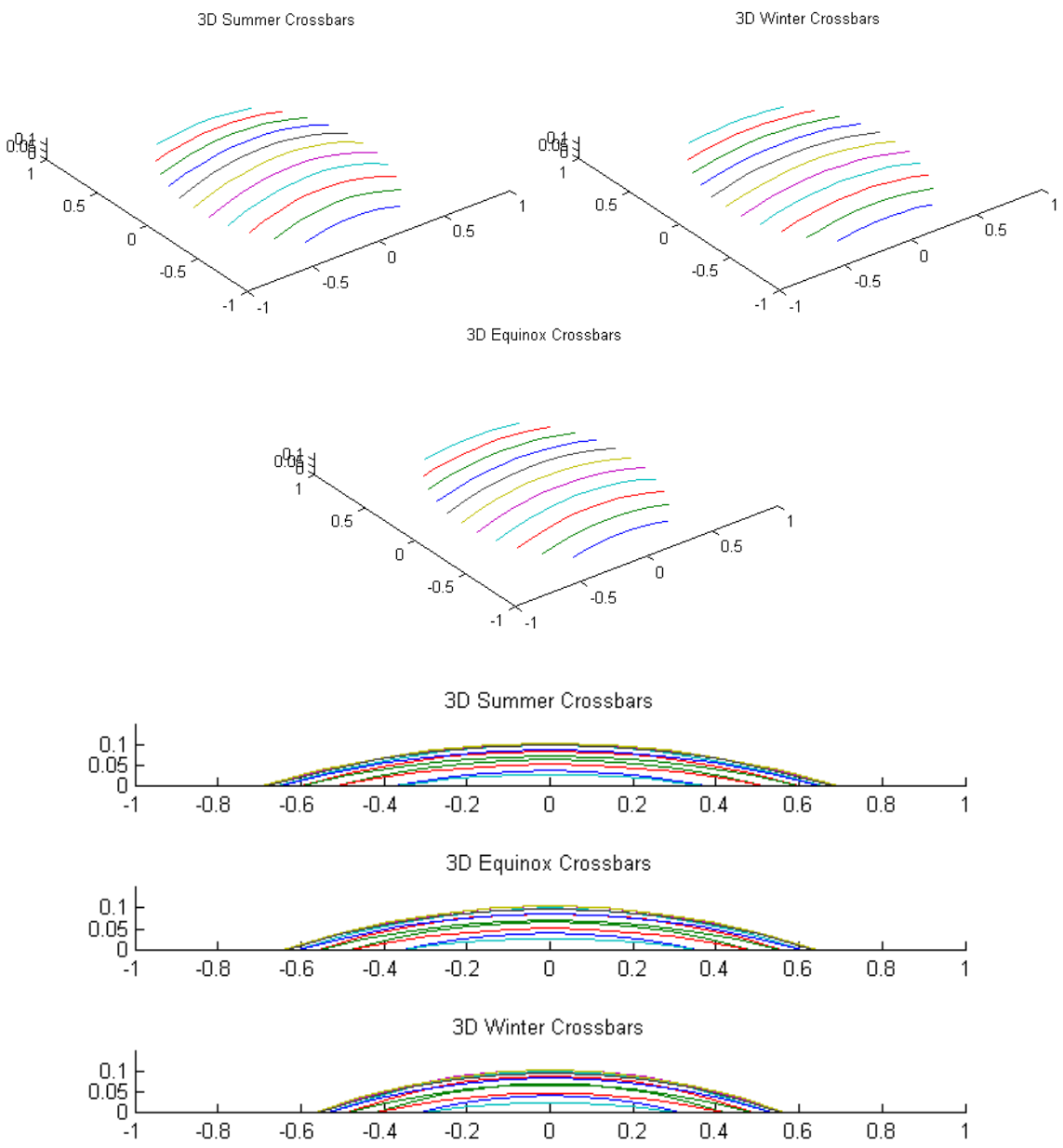

Figure 3.12: The 11 elliptical crossbars of the reflector for equinox and solstices

Increasing the number of crossbars will increase the resolution of the reflector surface. With a crossbar count of 1001, over 1 million points are calculated on the surface with a resolution of about 1 millimeter. This level of detail is useful to create a 3D model of the reflector surface that can then be imported into 3D modeling software and to perform in depth ray tracing analysis in Matlab. Figure 3.13, shows the *.dxf part.

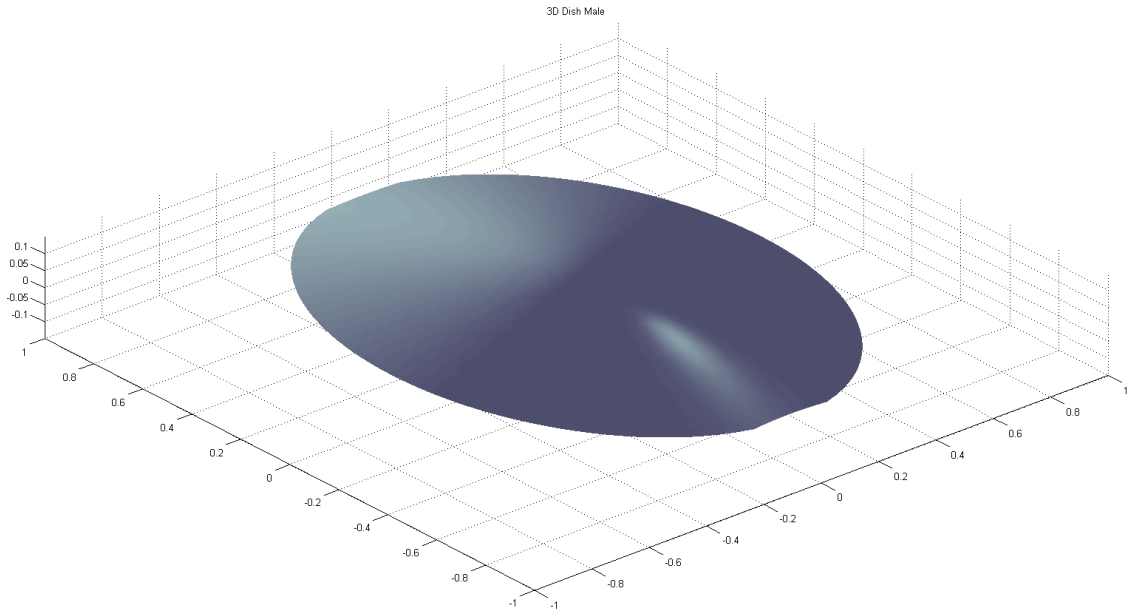

*Figure 3.13: Matlab generated *.dxf 3D model of reflector with 1001 crossbars*

In the method above, the number of crossbars is set by the user with the variable *n*, and each crossbar is then defined by *n* equally spaced points between the two ends of the crossbar. This method is very effective in creating an accurate surface model because there is always a point on the elliptical edge of the reflector. This causes the horizontal spacing between points to not be the same for all crossbars and is thus not optimal for mathematical calculations.

A second surface model is created with the points being equally spaced apart in a quadrilateral structured mesh with an aspect ratio of 1 and a skewness of 0 (a square mesh) throughout the surface. With this method the point density is uniform and all the points are aligned with the axes allowing for calculations of derivatives in the two directions. The surface was also rotated and moved to match the location in Figure 3.3 on the global coordinate system. Figure 3.14 shows a 3D rendering of this point surface in the golobal coordinate system.

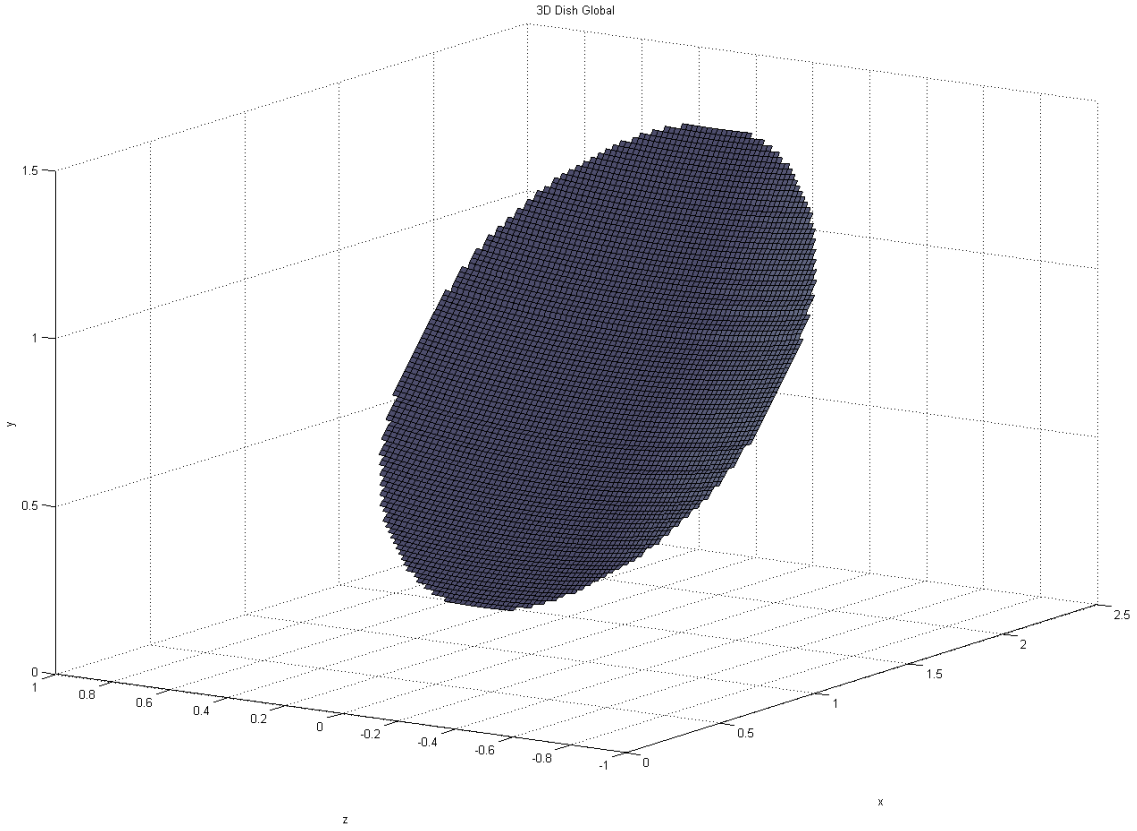

Figure 3.14: Reflector dish with grid mesh points in global coordinate system

CHAPTER 4: THEORETICAL RAY TRACING ANALYSIS

The ability to compute a high-resolution 3D model of the reflector surface at any time of the year allows for detailed ray tracing analyses of the sunlight converging at the focus. By applying various types of deviation to the surface to simulate manufacturing inaccuracies or imperfections it is possible to calculate the size of the focus and the power delivered to a certain area. For the purposes of a Scheffler concentrator with cooking applications a focus area of about 15 cm by 15 cm is considered to be a reasonable target.

Two Matlab functions were created for ray tracing analysis. The first compares the difference in angle and position between the theoretical shape and a slightly deformed shape. The second is a global ray tracing code that traces rays from any direction though a reflection from an arbitrarily shaped surface with a square mesh.

4.1 Ray Tracing from Crossbar Equations

The first function is to be used for theoretical calculations of the light deviation at the focus using user-defined fictitious deviation from the perfectly shaped reflector. It starts by knowing the exact shape of the reflector and calculating the difference in angle to the deformed reflector surface in order to determine the displacement from the theoretical focus. The analysis is done at equally spaced points on the surface as determined in Section 3.6 .

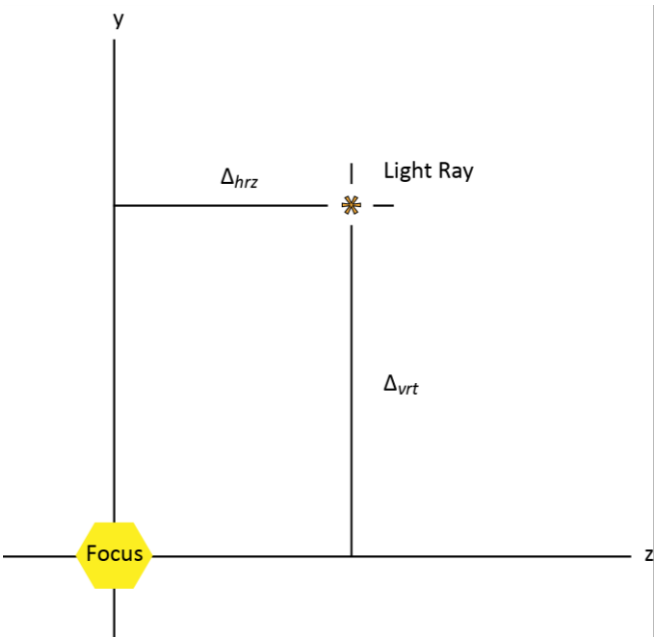

Figure 4.1: Visual representation of vertical and horizontal components of the ray displacement at the focus

The vertical, y-direction, and horizontal, z-direction, components of the ray displacement at the focus are separated and calculated independently, Figure 4.1. The length of the ray, *r*, from the point on the reflector from which it emanates to the focus is calculated, as well as r_{xz}, the length of the ray's projection onto the xz-plane,

$$r = \sqrt{x^2 + z^2 + \left(y - F_y\right)\text{^}2}$$

$$r_{xz} = \sqrt{x^2 + z^2}$$

4.1

For the horizontal displacement, the horizontal angle of the crossbar is calculated by taking the derivative of the elliptical function of the crossbar as described in Section 3.3 and as shown in

Table 3.3. This slope is now assumed to have the angle that will focus the light directly at the focus, any deviation, $\Delta\Theta$, from this angle will cause a horizontal deviation, Δ_{hrz}. The slope and angle are calculated with respect to the slope of the reference point C to be,

$$s_{hrz} = \frac{b}{a^2}\frac{x}{\sqrt{1-\left(\frac{x}{a}\right)^2}}$$

$$\Theta = \tan^{-1}(s_{hrz})$$

For the vertical displacement, the slope of the parabola is calculated. Since the reflector is formed by revolving the parabola about the vertical axis, y-axis, if the reflector is sliced by any plane containing the axis the parabola is rotated around, the intersection would be that same parabola, see Figure 4.2. Therefore the vertical slope of any point on the reflector facing the focus is equal to the slope of the parabola given the xz-plane distance from the origin. This slope is the angle that will focus the light vertically directly at the focus, any deviation, $\Delta\Phi$, from this angle will cause a vertical deviation, Δ_{vrt}. The vertical slope and angle are calculated to be,

$$s_{vrt} = 2mr_{xz}$$

$$\Phi = \tan^{-1}\left(s_{vrt} - \frac{\pi}{4}\right)$$

The 45° offset is to adjust the angle to be with respect to the slope of the idealized reflector surface at the center point, C, of the dish, which has a slope of 45° with respect to the y-axis.

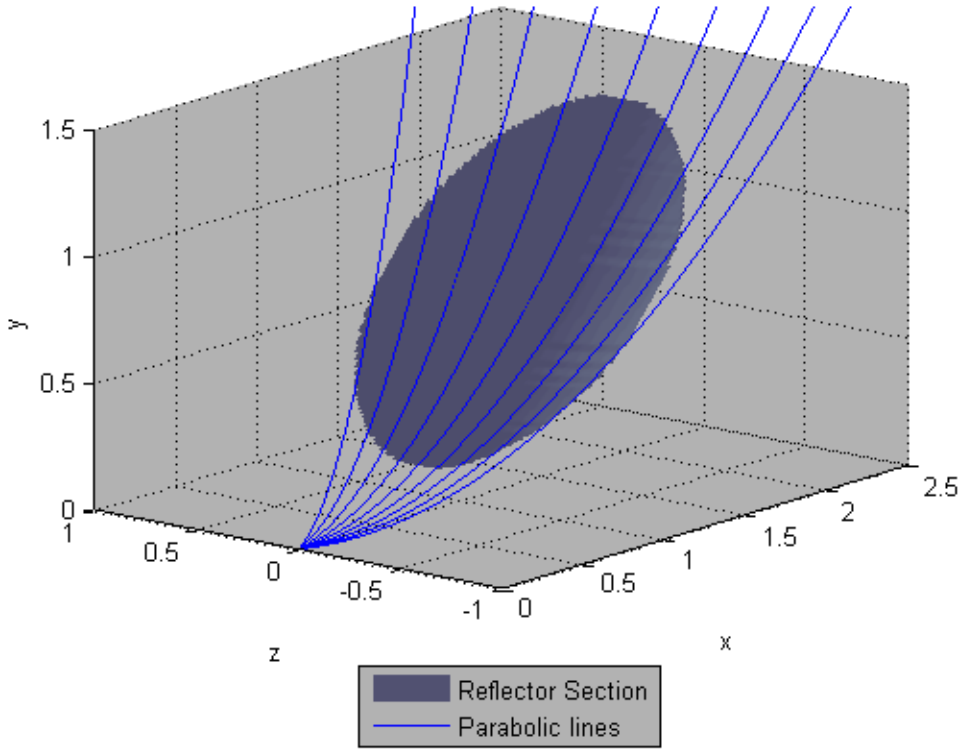

Figure 4.2: 3D model of reflector with superimposed identical parabolic lines defined in Equation 3.21

With the two slope angles calculated at each point on the parabola, a fictitious error in these angles is introduced, either by offsetting the angle by a certain percentage or by an absolute angle. For instance, we can define the angle at all points is off by 5%, making the center point of the reflector exact while the edges are most deflected, or we can define an absolute error of +1 degree throughout the surface.

Using the error deviation angle, $\Delta\Theta$ and $\Delta\Phi$, of the surface it is possible to calculate how far from the focus a reflected light ray will hit. Simple geometry and trigonometry a required to derive Equations 4.2 and 4.3 for the horizontal and vertical displacement of the reflected light ray at the focus, Figure 4.3 shows the geometrical setup for 4.3.

$$\Delta_{hrz} = \frac{r\sin(2\Delta\Theta)}{\sin\left(\frac{\pi}{2} - 2\Delta\Theta + 2\Theta\right)}$$

4.2

$$\Delta_{vrt} = \frac{r\sin(2\Delta\Phi)}{\sin\left(\frac{\pi}{2} - 2\Delta\Phi + \beta\right)}$$

4.3

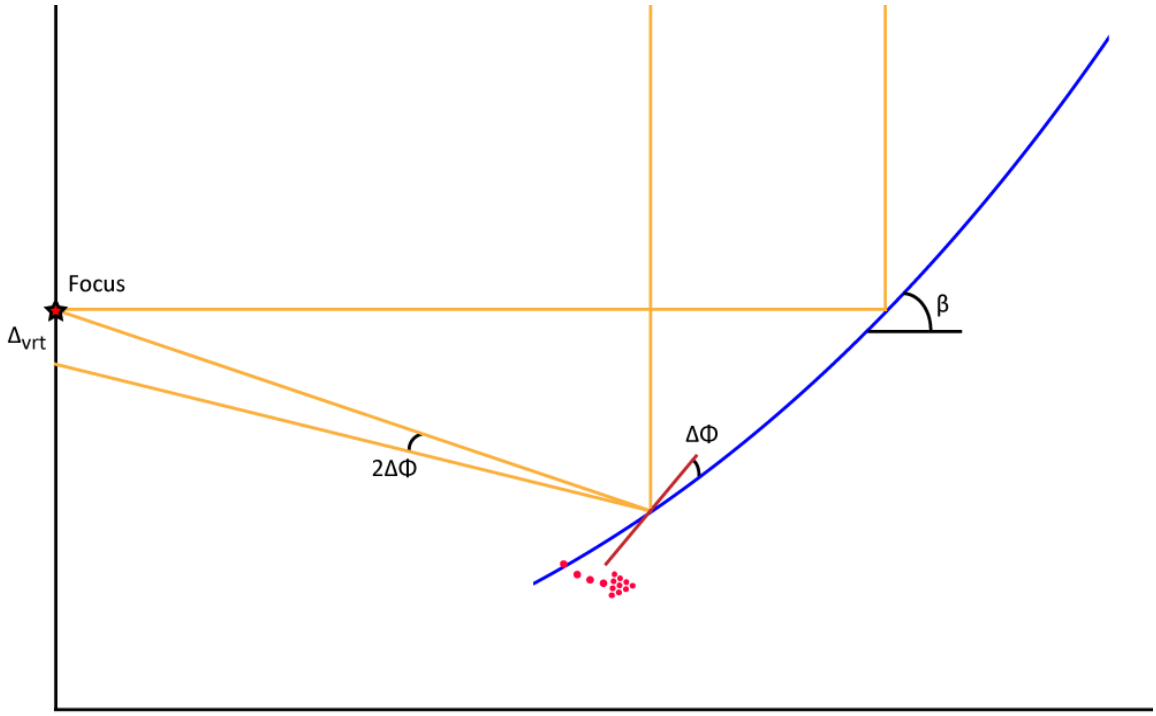

Figure 4.3: Optical geometry of ray tracing for simple vertical angle deflections on the reflector and resulting effect on focus.

The vertical and horizontal displacement can then be combined to determine the overall displacement of the light rays originating from every point on the reflector. The Matlab code keeps track of all these displacements and also computes a vector that represents the light ray originating from the reflector and ending on the focus plane so it can be easily plotted and visualized.

This method for calculating focus deviations is very simple and accurate but only works for theoretical calculations where the slopes are calculated from the known equations of the reflector surface. For experimental calculations or more complex conditions a new method needs to be used where the slope is calculated empirically from surrounding points. This is the second ray tracing function, which will be discussed in later sections of this chapter.

4.2 Theoretical Deviation Analysis from Surface Deviations

With the focus deviation code outlined above, FocusDeviation.m, a series of surface deviations and irregularities were tested to determine the susceptibility of the solar concentration to these deviations and to determine reasonable targets for manufacturing.

All simulations were run with n=1001 equidistant cross-sections distributed along the vertical axis of the reflector, each cross-section was then subdivided with equidistant points. For the particular reflector being analyzed in this paper, this configuration resulted in a resolution of 1.8 mm in both directions and approximately 500,000 points throughout the surface. The resolution necessary for accurate results was determined by running a range of resolutions varying from n= 11 to n=10001 on a surface with Gaussian distribution type defects (described in following sections), some results are shown in Figure 4.4. The results converge within 4 decimal places at resolutions above n=1001[1].

[1] Increasing the resolution above this value for more accurate results quickly increases memory requirements, with n=10001 the code requires about 18GB of memory to run - easily crashing most

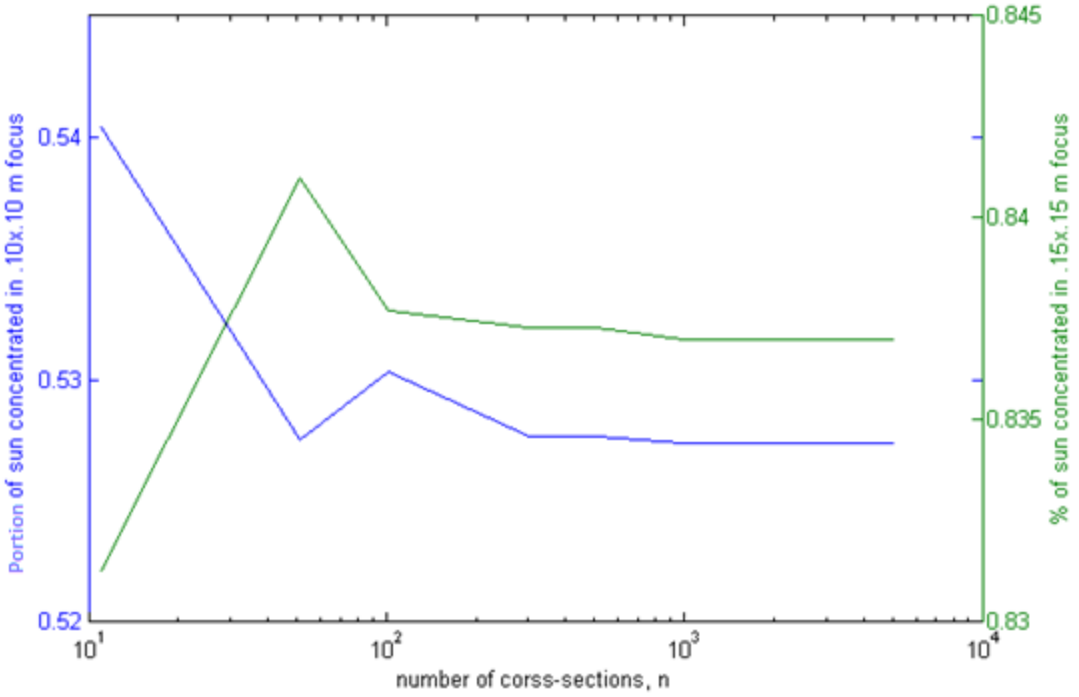

Figure 4.4: Simulation results for various point resolutions, converging within 4 decimal places at n=1001

We express the quality of the concentrator using three parameters: % of light collected (efficiency), power concentrated, and solar concentration ratio. The percent of collected light concentrated in a given area of the focus is the best indicator of the quality of the reflector surface. Ideally, 100% means that all sunlight incident on the reflector is concentrated in the defined focal region. In the attempt to minimize manufacturing costs, it is important to understand that 100% efficiency is impossible and achieving very high efficiency my not be necessary if the reflector is

machines without further optimization. Simple math reveals why, n^2 = 100 million points each with 64bit double precision which means 8 bytes per point and 800 Mb per each matrix and just to define their position in space we need 3 matrices for x, y and z coordinates (2.4Gb).

large enough. What is important to consider is the thermal power concentrated in the focus in Watts.

Considering the cooking application of this solar concentrator, 500 Watts will bring one liter of water to boil in 11 minutes while 1,000 Watts will bring it to boil in just over 5 minutes. Also, consider that most 6 inch electric stove-tops deliver 1,500 Watts of power in modern homes. Another important factor to consider is the radiative power dissipation of the focus as it heats up, the larger the area the more heat will be lost. Figure 4.5 shows a plot of the power focused by the concentrator compared to the radiative power dissipated at the focus given three common cooking temperatures, the difference between the two is the excess power which will be delivered to the cooking surface. As the cooking area increases, it captures more light from the reflector (which does not have a perfect focus) resulting in higher power focused, but it will also increase the power dissipated due to the larger radiating area. To put the cooking temperatures into prospective, meats require less than 100°C to cook, boiling water requires a temperature of 100°C, and oil can fry food between 160-190 °C. Figure 4.5 shows that the dissipated power due to the focus size is very small compared to the solar power that the Scheffler is delivering and that the focus area needs to be determined based on cooking conditions and pot sizes to maximize heat absorption instead of radiative cooling constraints.

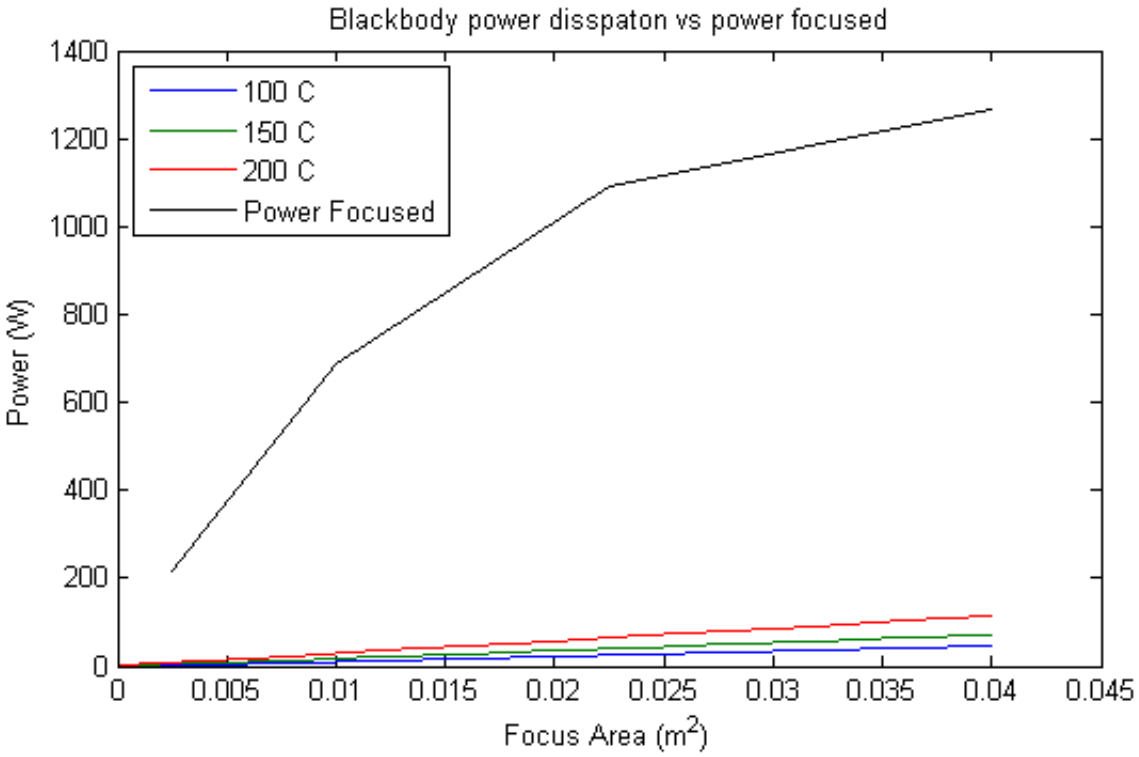

Figure 4.5: Power dissipated at focus at three common cooking temperatures compared to the power concentrated. A .15x.15 m focus has an area of 0.0225 m^2.

Finally the last parameter, solar concentration ratio, tells us how many suns are concentrated in that area. It describes the ratio between regular sunlight intensity and the concentrated sunlight intensity. For instance, 100 suns means that the light is 100 times more powerful, or concentrated, than the light coming from the sun, or about 100Kw/m^2.

A Perfect Reflector

The first simulation that we ran is that of a perfectly shaped Scheffler reflector. We must use this simulation to check that the shape that was created in the previous steps actually focuses the light to a point. The simulation was run with a very small but non-zero deviation of 0.01% in order to avoid dividing by 0 in the tracing code. Figure 4.6 and Figure 4.7 show how the light rays

focus nearly to a point. This exercise was trivial for this particular code since the rays are calculated from the difference between the theoretical shape and the deformed shape and not from the absolute global angles of the surface, as is done in the second ray tracing code. It was therefore expected that applying a very small deviation would result in a very small focus. This case is thus verifying the quality of the code and not the quality of the reflector (see Section 4.4).

In the following sections, various types of deviations will be simulated and figures will show a larger focus region.

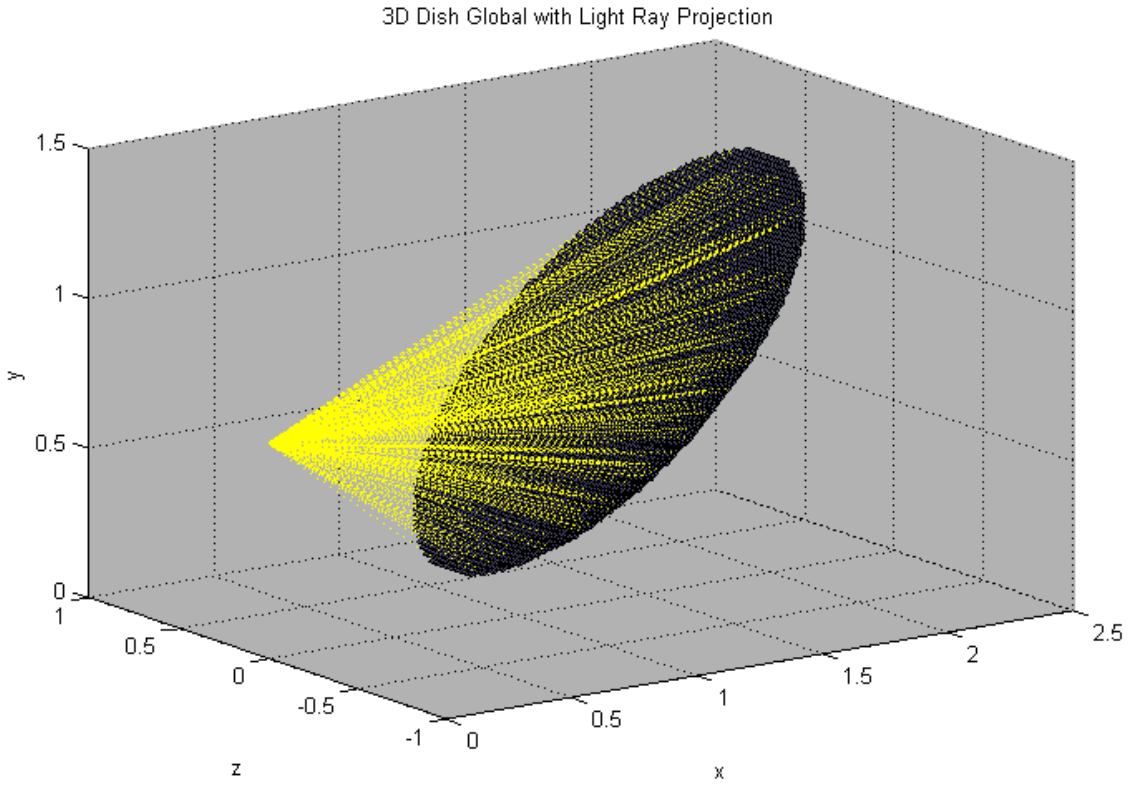

Figure 4.6: Light ray tracing to a perfect focus

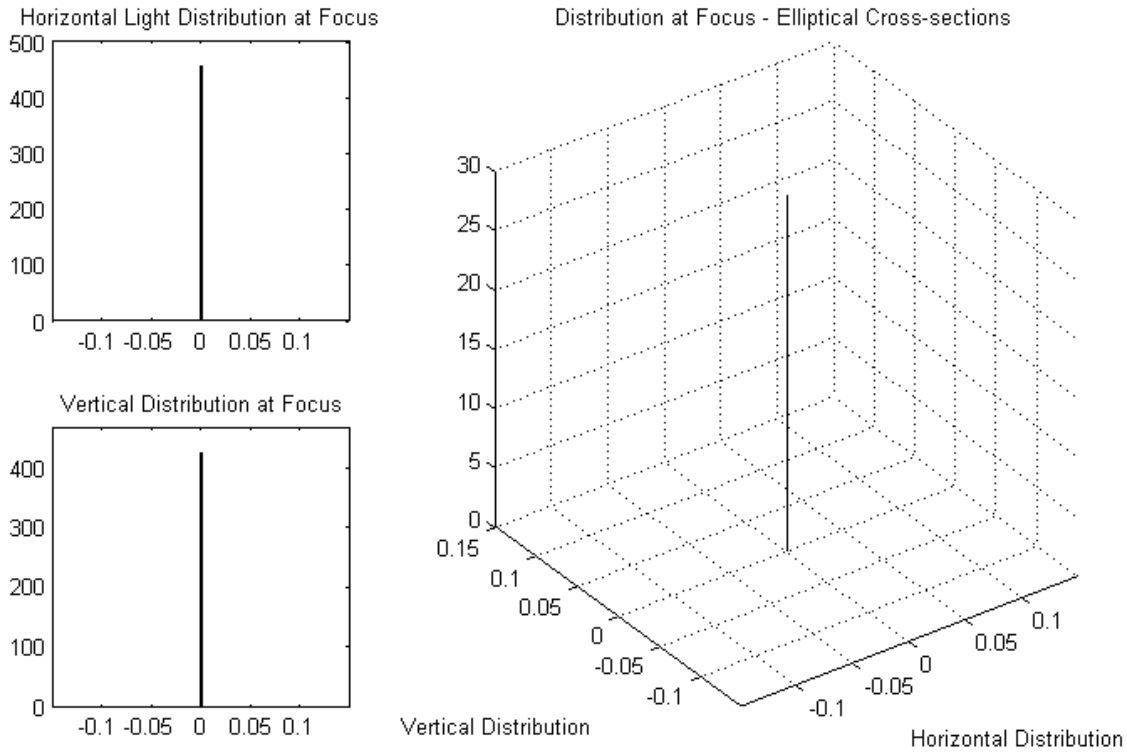

Figure 4.7: All light focused at one point at the focus

PERFECT REFLECTOR WITH A REAL SUN

The light rays coming from the sun are not all parallel, the sun acts as a circular light source in the sky with a subtending angle of 0.533°. The real sun is not a perfect source and it will not allow a perfect focus to occur, even with a perfect mirror. The simulation shown in Figure 4.8 explores the most tightly focused sunlight the concentrator can achieve on Earth. The light is still extremely focused within a very small area of a few centimeters, generating very high concentration on surface power density. It is important to keep these results in consideration when looking at other simulations because any deformation or imperfection of the reflector which defocuses the light less than the real sun will have a negligible effect on the performance in real world applications.

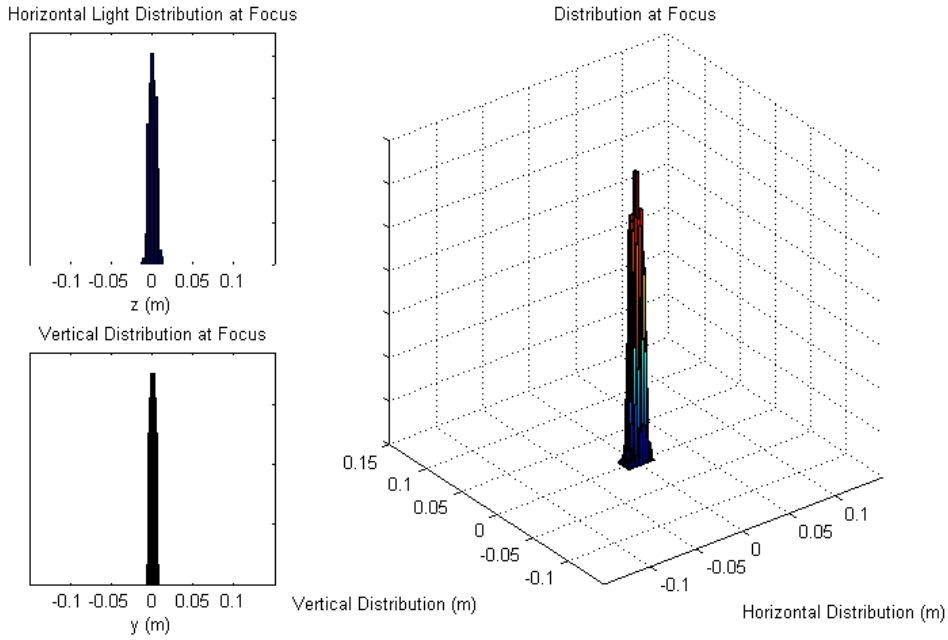

Figure 4.8: Light distribution at focus with a real sun with subtending angle of 0.533 degrees and a perfect reflector

CIRCULAR CROSSBAR PROFILE

A very important case to consider is that of a reflector constructed with circular crossbars profiles rather than elliptical. As mentioned in Section 3.4 Scheffler recommends constructing circular crossbars as they greatly simplify manufacturing while minimally affecting the focus. We see from the results of the simulation in Figure 4.9, the effects of the circular profile are minimal. The light spreads slightly in the horizontal direction and almost imperceptibly in the vertical direction, maintaining 99.6% of the sunlight within a 5 by 5 centimeter area. This level diffusion is comparable to the diffusion due to the subtending angle of a real sun and is thus not important. We can conclude that the circular crossbars have little to no effect on the quality of the focus but greatly increase the simplicity of manufacturing.

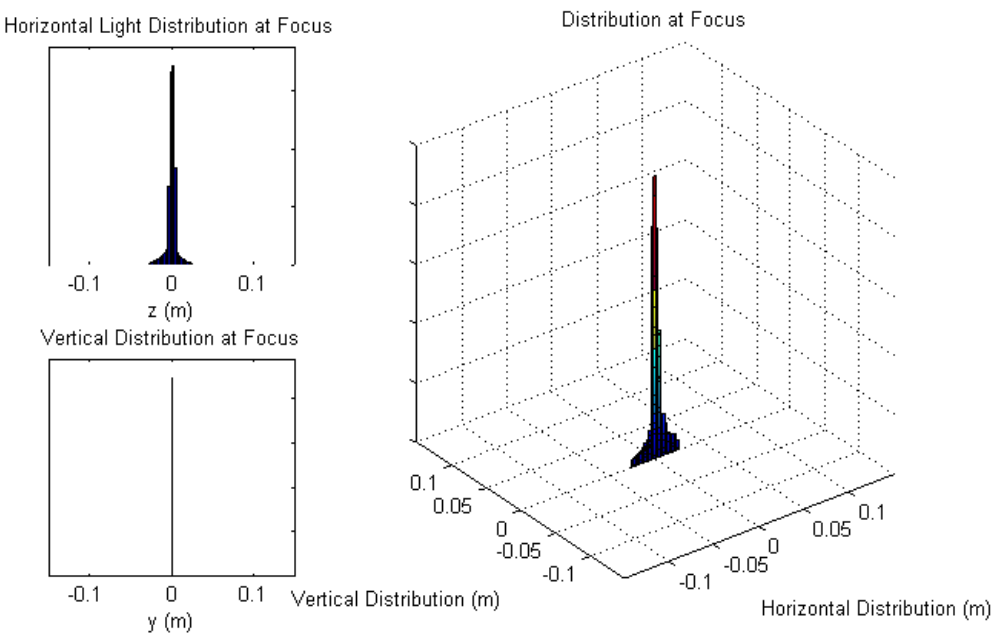

Figure 4.9: Light distribution at focus with a perfect reflector with circular crossbar profiles

UNIFORM PERCENT ANGLE DEVIATION

The first cases analyzed were those of a uniform percentage deviation in the angle. The center point of the reflector, at point C, is considered to be at 0° angle being the bottom of the reflector and light reflects by 90° onto the focus. A uniform angle percentage error on each axis makes it so that the parts of the reflector farther from the center point have a higher absolute deviation. This type of error represents an overall manufacturing error.

Table 4.1: Uniform 5% angle deformation

Focuse Area	**5x5 cm**	**10x10 cm**	**15x15 cm**	**20x20 cm**
% of light collected	0.5272	0.9632	1.0000	1.0000
Power concentrated (W)	688	1,257	1,305	1,305
Average Solar Concentration (Suns)	275	126	58	33

Table 4.2: Uniform 10% angle deformation

Focuse Area	**5x5 cm**	**10x10 cm**	**15x15 cm**	**20x20 cm**
% of light collected	0.1659	0.5274	0.8370	0.9693
Power concentrated (W)	216	688	1,092	1,265
Average Solar Concentration (Suns)	87	69	49	32

Table 4.3: Uniform 15% angle deformation

Focuse Area	**5x5 cm**	**10x10 cm**	**15x15 cm**	**20x20 cm**
% of light collected	0.0771	0.2774	0.5276	0.7555
Power concentrated (W)	101	362	688	986
Average Solar Concentration (Suns)	40	36	31	25

Table 4.4: Uniform 20% angle deformation

Focuse Area	**5x5 cm**	**10x10 cm**	**15x15 cm**	**20x20 cm**
% of light collected	0.0440	0.1659	0.3383	0.5276
Power concentrated (W)	57	217	441	688
Average Solar Concentration (Suns)	23	22	20	17

The four tables above show a varying percentage deformation in the manufacturing of positive 5%, 10%, 15%, 20%, which opens up the reflector. With a small deformation of 5% the focus is extremely acurate.

shows that over 95% of the light is focused within a 10x10 cm focus. This configuration achieves several hundred suns of concentratrion, which might even turn out to be excessive for cooking applications. The 10% angle deformation, in Table 4.2, seems to be the most aceptable condition of the four. While only about 50% is focused in a 10x10 cm focus it still concentrates over 1 kW of power within the 15x15 cm focus which makes it ideal for cooking. It concentrates almost 100 suns at the center of the focus allowing for high temperature and intense heats without proving excessive. Going up in percentage quickly drops the quality of the concentration. The 15% deviation is still able to focus close to 1 kW within at 20x20 focus, which will allow for less effective cooking because the heat will be distributed on a wider focus area. This condition is still acceptable for cooking applications in developing nations. Finally, the 20% angle defomation case does not prove to be a usefull design. Inverting the deformation so the reflector is being closed rather than opened has very little effect on the focus, the numbers are no more than one percent different from those shown in the resepctive tables above.

Considering the above simulations, a 10% uniform angle deformation is a good target for manufacturing acuracy. But it is important to consider that there will be many more types of

deformations on the surface, which will add up to make a less acurate reflector. This metric cannot be used as an absolute but it is very important to understand the effect of the manufactured shape on the focus of light.

Figure 4.10 shows a visual representation of the light concentration at the focus for the uniform 10% angle deformation. The larger graph on the right shows the distribution of light at the focus, the taller and redder the graphs the more light hitting that particulat point. Most of the light is focused at the center, and trails off outside the 20x20 focus area. The two smaller plots show the horizontal and vertical distribution independantly. The horizontal plot is very summetrical like the shape of the reflector on that axis, having elliptical profiles. The vertical distribution, instead, has a non uniform distribution about the focus because of the parapolic profile of the reflector in that direction. It has a higher curvature below the focus than above so a percent angle change has a larger effect on the more curved portions of the reflector. Overall, Figure 4.10 shows that with a 10% angle deformation the focus is still well concentrated in an area small enough to cook. It also seems that further lower order deviations can still be added to the reflector while still maintianing a good enough focus.

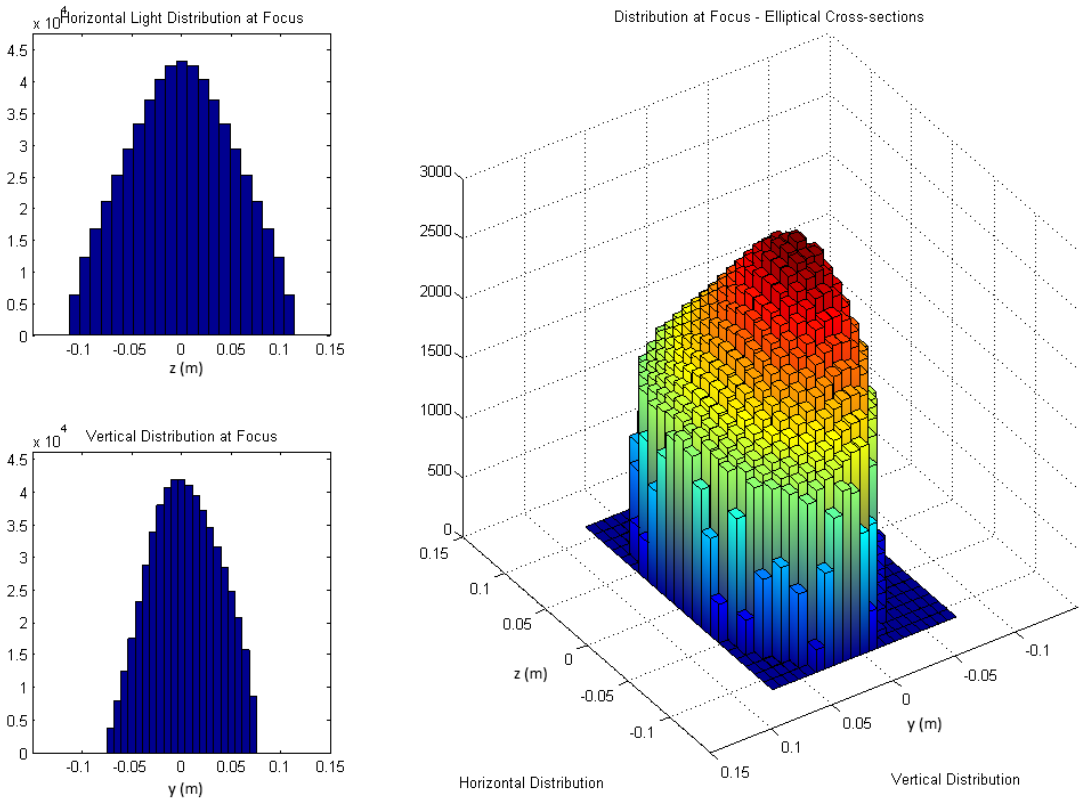

Figure 4.10: Uniform 10% angle deformation visualization of the focus. Horizontal and Vertical distributions on the left and a 3 dimensional color view on the right.

Tracing each light ray reflected from the Scheffler surface allows us to visualize light converging to the focus (Figure 4.11). The four subplots represent the four levels of deformation from 5% to 20%.

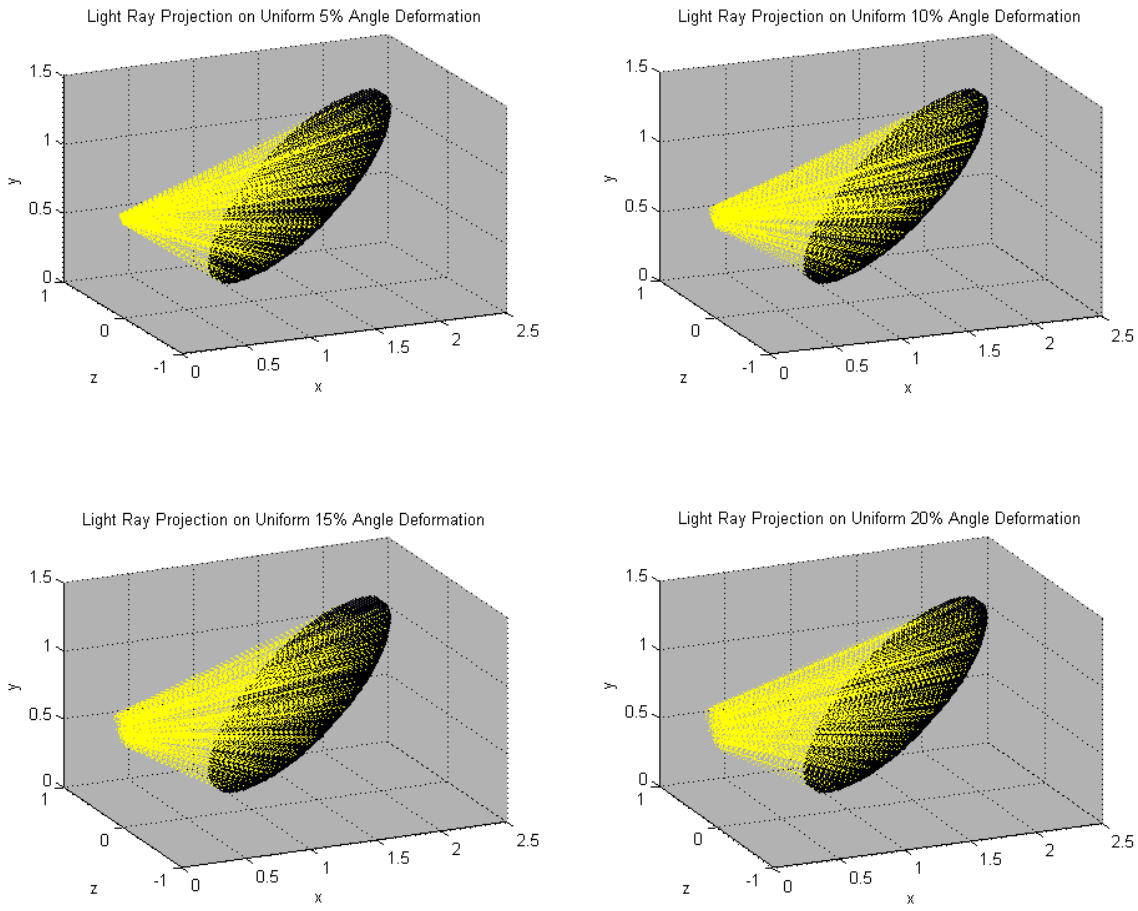

Figure 4.11: Ray tracing from the uniform angle deformed reflector surfaces to focus. Sun rays are incoming parallel to y-axis from above.

Figure 4.11 does lead to a very interesting realization - though the light rays are very sparse at the theoretical focus, they do seem to still be converging at a farther point. This is reasonable because the simulation opened up the reflector by a uniform percentage amount, decreasing the curvature or increasing the focal length. To see where and how the light rays would converge we could either extend the ray or we could invert the deformation so it is closing the reflector. Figure 4.12 shows the ray traces of the light converging before the focus, because the reflector is being deformed in the opposite direction as before. The first row of subplots shows the -10% angle deformation condition, which gave acceptable results at the focus as discussed earlier, now we see a very accurate convergence of the light rays about 20 cm from the theoretical focus. This new

convergence is extremely focused and would only require a small adjustment in the position of the cooking surface to correct. Similarly, the second row of subplots of the -20% angle deformation condition shows a considerably focused convergence about 30 cm from the theoretical focus. Though not as focused as the -10% condition, even with -20% deformation considerable light concentration can be achieved at the new focus. Increasing the deformation further leads a new focus even further from the original and considerably worse concentration.

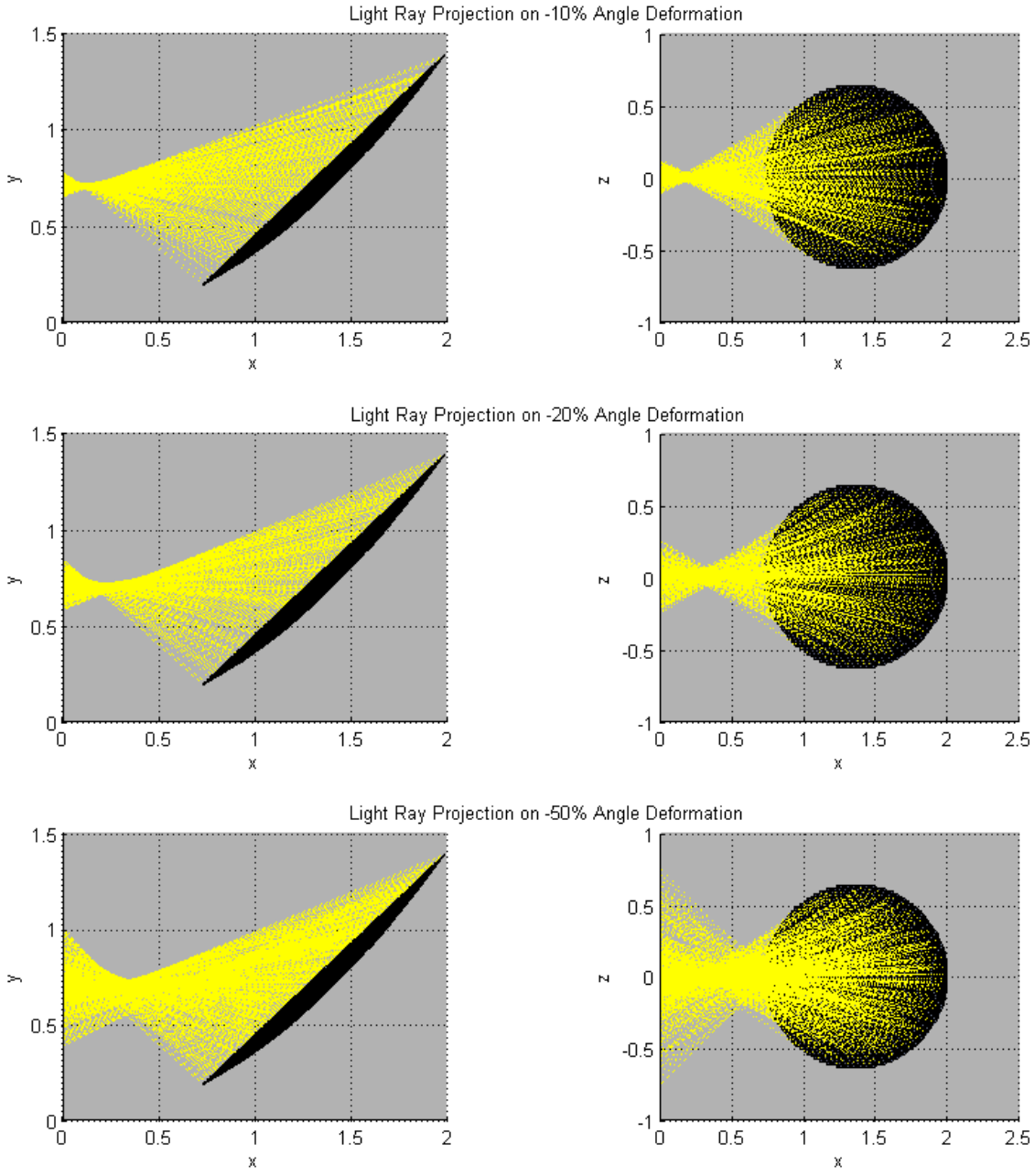

Figure 4.12: Convergence of light rays not at focus due to uniform angle deformation

The important conclusion of the uniform angle deformation caused by a manufacturing error is that as long as the deformation is uniform and small, less than 25%, the light rays will converge to a new focus slightly offset from the original with still a considerable solar concentration. The shape of the deformed reflector is not consistent with the Scheffler parabolic

geometry and so the hourly and seasonal adjustments will not be the same as with the Scheffler concentrator.

GAUSSIAN DEFORMATION

A deformation representative of small imperfections and wrinkles on the surface can be simulated with a Gaussian distribution of random angle deviations. For example, Figure 4.13 shows a sample Gaussian distribution from one of the runs. The average is always set to 0°, while the standard deviation is changed to widen the range and severity of the deformations. For this case the standard deviation (σ) is 1° and 95% of the points have an angle between ±2°.

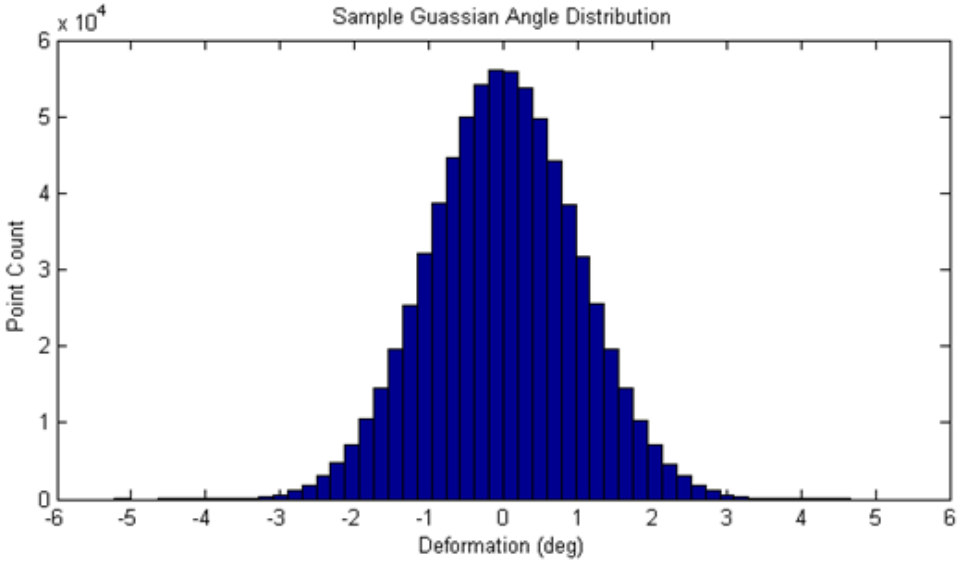

Figure 4.13: Sample Gaussian angle distribution with average of 0° and standard deviation of 1°

We ran simulations for Gaussian error distributions with 2σ between 1° and 3°. The tables below show the performance metrics for three conditions, the top being the least deformed. With 95% of the deviation being within ±1°, the first condition is very accurate with almost all of the light focusing in the 10x10 cm focus and achieving an impressive ~230 suns in a 5x5 cm focus. Increasing the random deformation decreases the concentration abilities of the reflector and at

2σ=2° the concentration is below 1kW in the 15x15 cm focus. This is still enough to cook well and quite acceptable, but it can quickly deteriorate the focus if it is superimposed with a uniform manufacturing deformation such as that described in the previous section. This is still a good target to consider when manufacturing the reflector. Increasing the deviation by one more degree drastically reduces the concentration to less than 50% in the 15x15 cm focus.

Table 4.5: Random Gaussian deformation, 2σ=1°

Focuse Area	**5x5 cm**	**10x10 cm**	**15x15 cm**	**20x20 cm**
% of light collected	43.92	86.68	98.00	99.79
Power concentrated (W)	573	1,131	1,279	1,302
Solar Concentration (Suns)	229	113	57	33

Table 4.6: Random Gaussian deformation, 2σ=2°

Focuse Area	**5x5 cm**	**10x10 cm**	**15x15 cm**	**20x20 cm**
% of light collected	13.98	43.86	70.49	86.64
Power concentrated (W)	182	572	920	1,131
Solar Concentration (Suns)	73	57	41	29

Table 4.7: Random Gaussian deformation, 2σ=3°

Focuse Area	**5x5 cm**	**10x10 cm**	**15x15 cm**	**20x20 cm**
% of light collected	6.49	23.22	43.77	62.58
Power concentrated (W)	85	303	571	817
Solar Concentration (Suns)	34	30	25	20

Unlike the uniform angle distribution, this random Gaussian deformation spans both positive and negative angles. This means that the light does not converge to a different focus because rays converge equally on both sides of the theoretical focus. Below are the graphical distributions of intensity on the focal plane (Figure 4.14). The plots recall the Gaussian distribution curve in both horizontal and vertical directions.

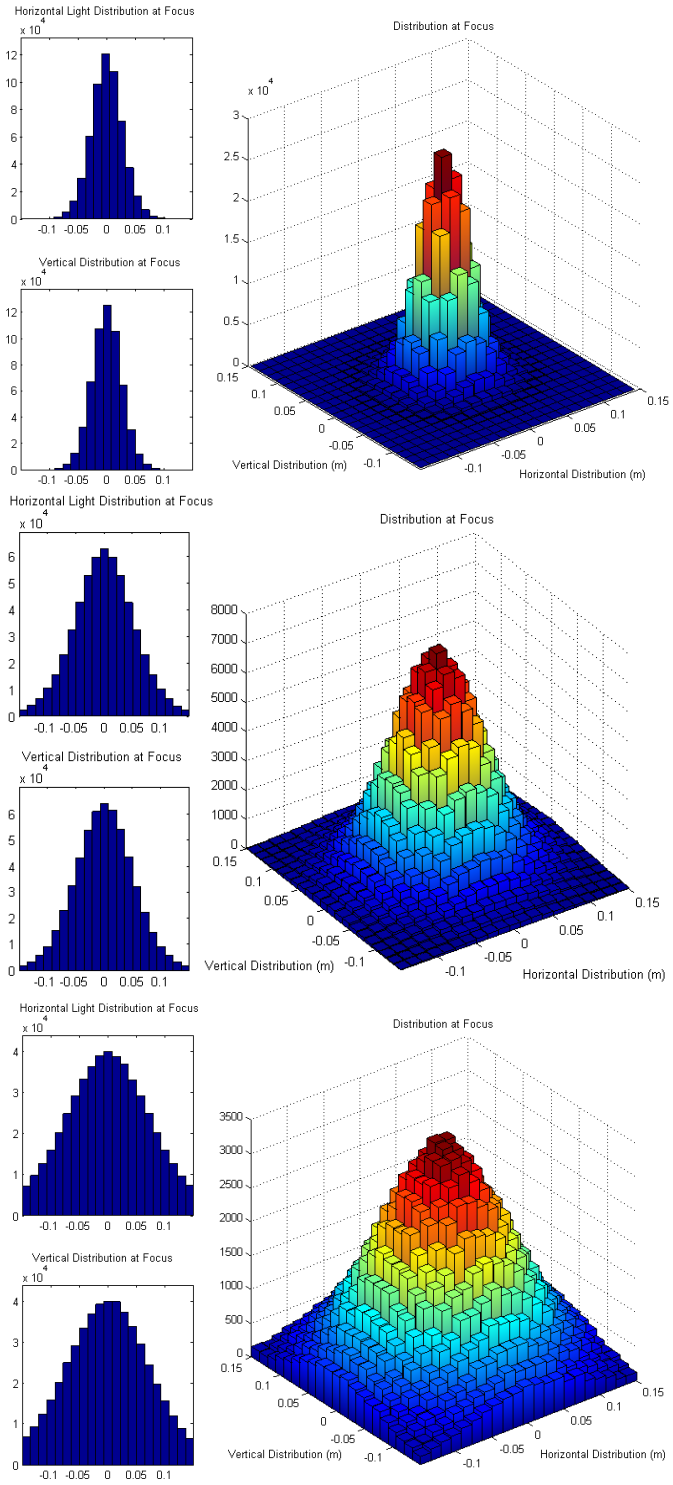

Figure 4.14: Gaussian distribution deformation visualization of the focus. From top left 2σ= 1°, 2°, and 3°. Horizontal and Vertical distributions on the left and a 3 dimensional color view on the right.

4.3 Global Ray Tracing from Any Surface

This second code is a full featured ray trace simulation which calculates reflected rays from any surface in space given an incoming light ray direction. A few features are then added to tailor the code to our application with the Scheffler reflector.

The code is vector based, taking the incoming light vector, calculating the normal vector of each point on the surface and finding the reflected light vectors. The unit normal vector is found by calculating the gradient of the surface, $\nabla = \left[\frac{dy}{dx}, \frac{dy}{dz}\right]$, since the vertical axis in the parabola coordinate system is y. The one major requirement is that all the points on the surface lie on a square grid on the x-z plane, so that the derivative in the x or z direction can be calculated from the two adjacent points in the respective directions. This can be easily obtained by using the meshgrid() function in Matlab or by using the reflector meshed surface outlined in Section 3.6 while still lying flat on the x-z plane. It is important to note that calculating the surface normal is done in the parabola coordinate system with the reflector dish laying on the x-z plane centered about the origin (similar to how it was positioned in the ellipse coordinate system, see Figure 3.6 and Figure 3.13), so that the mesh is aligned with the coordinate system. The surface and normal are then rotated to the appropriate position in the parabola coordinate system, as in Figure 3.14.

The gradient is found using the second order central difference method, which is a combination of the two first order backwards and forward difference methods, Equation 4.4 and Equation 4.5 respectively. The function being evaluated is the position of the surface in the y direction with x and z being independent variables. In the equation below we show the gradient in the x direction, which can be easily generalized to the z direction.

$$f(x_0 + \Delta x, z_0) = f(x_0, z_0) + \left.\frac{df}{dx}\right|_0 \Delta x + \mathcal{O}(\Delta x)$$

$$\left.\frac{df}{dx}\right|_0 = \frac{f(x_0 + \Delta x, z_0) - f(x_0, z_0)}{\Delta x} + \mathcal{O}(\Delta x)$$

4.4

$$f(x_0 - \Delta x, z_0) = f(x_0, z_0) - \left.\frac{df}{dx}\right|_0 \Delta x + \mathcal{O}(\Delta x)$$

$$\left.\frac{df}{dx}\right|_0 = \frac{f(x_0, z_0) - f(x_0 - \Delta x, z_0)}{\Delta x} + \mathcal{O}(1\Delta x)$$

4.5

Finding the difference between the two,

$$\left.\frac{df}{dx}\right|_0 = \frac{f(x_0 + \Delta x, z_0) - f(x_0 - \Delta x, z_0)}{2\Delta x} + \mathcal{O}(\Delta x^2)$$

4.6

Because the spacing between the points is not sufficiently small and the points are empirical we do not need to worry about rounding and truncation errors that arise in calculating the derivative. To make Equation 4.6 work in a computer code, the two adjacent points must be equally spaced by Δx and be aligned so there is no change in the z direction, and vice versa when calculating the derivative in the z direction.

The surface normal vector is then,

$$N_p = \begin{bmatrix} -\dfrac{dy}{dx} \\ 1 \\ \dfrac{dy}{dz} \end{bmatrix}$$

4.7

The sun vector is defined for equinox noon in the reflector's coordinate system (where the x-axis is parallel to the Earth's axis of rotation and the y-axis points toward the sun at equinox noon)

$$V_{sun} = \begin{bmatrix} 0 \\ -1 \\ 0 \end{bmatrix}$$

Once defined for equinox, the vector can be rotated about the z-axis by the solar declination for a particular day of the year. Now that the sun is angled about the axis of rotation of the Earth, we can rotate the sun vector about the x-axis by the hour of the day. All this is done with a 2D and a 3D rotation matrix, respectively.

Using vectors representing the incoming light and the surface normal, it is possible to calculate the outgoing light ray. If we break down the incoming vector in components parallel and perpendicular to the surface normal vector, we realize that the outgoing vector must have the identical perpendicular component and a negative parallel component as the incoming vector, see Figure 4.15.

$$V_i = u_{\parallel} + u_{\perp}$$

4.8

$$V_o = -u_{\parallel} + u_{\perp}$$

4.9

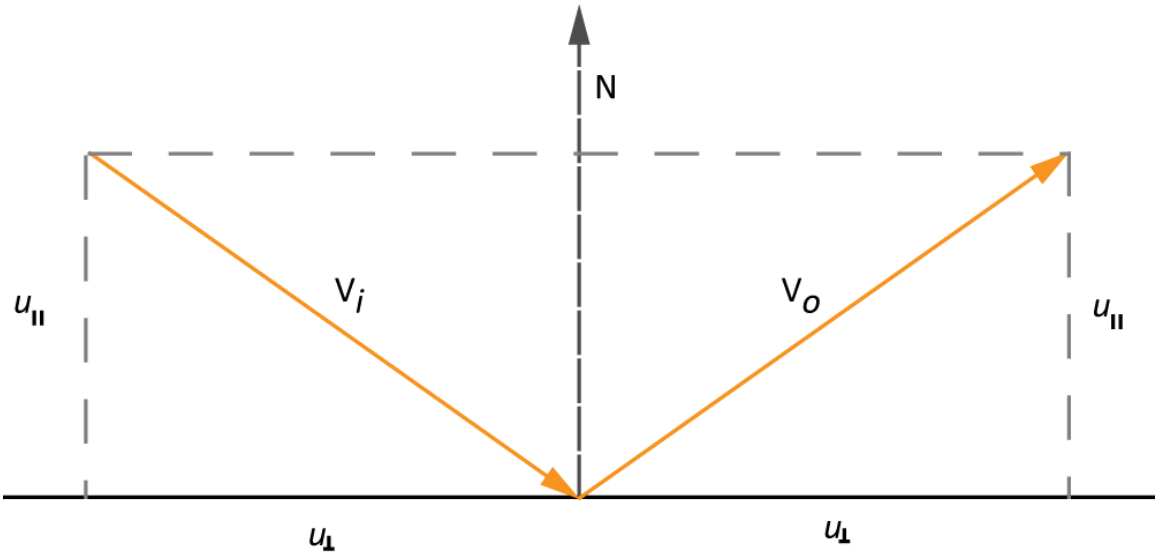

Figure 4.15: Ray reflection off of flat surface with normal vector N, absolute value of ray components parallel and normal to the surface remain unchanged after reflection.

We can also see that the parallel component is equal to the projection of the incoming vector onto the surface normal, more precisely the dot product times the unit vector of the normal.

$$u_{\parallel} = (V_i \cdot \hat{N})\hat{N}$$

4.10

Now solving for the outgoing vector,

$$u_{\perp} = V_i - u_{\parallel}$$

$$V_o = -u_{\parallel} + V_i - u_{\parallel} = V_i - 2u_{\parallel}$$

$$V_o = V_i - 2(V_i \cdot \hat{N})\hat{N}$$

4.11

Equation 4.11 can be applied to every point on the reflector with a known surface normal. The outgoing vectors can then be visualized by positioning them on the surface and extending them

as necessary, all accomplished with the Matlab 3D plot function. The ray trace code outputs the start and end points of every reflected vector as well as its corresponding surface normal in the form of a 3 dimensional matrix.

TEST CASE: PARABOLIC REFLECTOR

The test case run to demonstrate the accuracy of the ray tracing code was a classic parabolic reflector. A paraboloid of revolution was formed and the focus marked by a red dot. Incoming light rays were set to be parallel to the axis of symmetry of the parabola so that all the reflected rays would converge on the focus of the parabola.

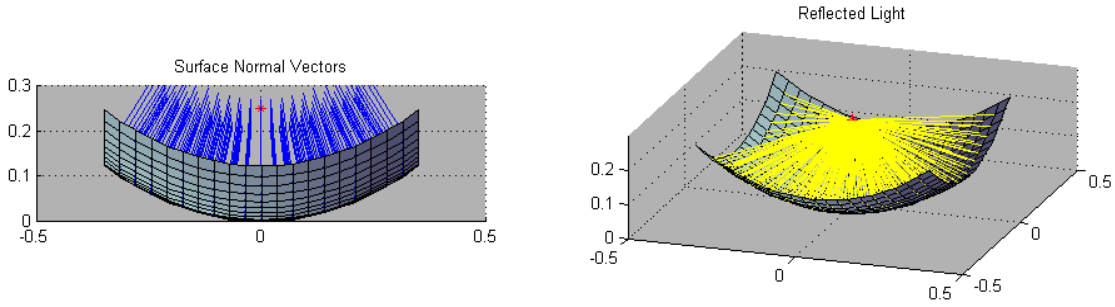

Figure 4.16: Ray trace analysis on parabolic dish with vertical incoming light rays. Graph on the left show the surface normal vectors in blue, graph on the right show light rays converge to the focus (red dot)

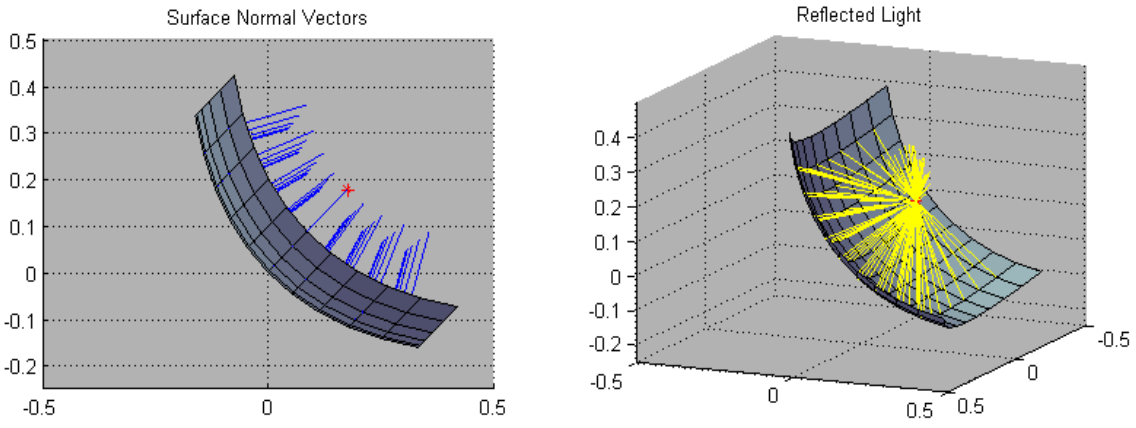

Figure 4.17: Ray trace analysis on parabolic dish with angled axis of symmetry and incoming light, all light rays converge to focus.

Figure 4.16 and Figure 4.17 show two conditions of the classic parabolic reflector. The first with a vertical axis of symmetry shows the simplest conditions and the light correctly converging to the focus. The second shows the case of a paraboloid with a tilted axis of symmetry, with the incoming light rays still parallel to the axis. The light still converges to the focus of the paraboloid. The ray tracing code is very effective with any surface with any incoming ray direction.

4.4 Theoretical Global Ray Tracing Analysis

This second code allows for very realistic simulations in which both the reflector and sun conditions can be set to any day of the year and hour of the day. It allows us to understand the effects the flexing the reflector has on the focus as the sun declination changes, how often it should be adjusted and the effects on daily tracking.

Perfect Reflector

First I shall simulate a perfect reflector at equinox at noon, when all conditions are prefect and light is shining down vertically from above. The reflected light rays converge perfectly at the focus since the conditions are those on which we built the reflector from, no sources of deviation is present. The two figures below show the results from this calculation from two different views. It is possible to see the direction of the incoming light onto the middle of the reflector and the resultant reflected rays converging at the focus perfectly. This reflector has no imperfections and it is perfectly adjusted to equinox conditions, so the focus is a point with no diffusion.

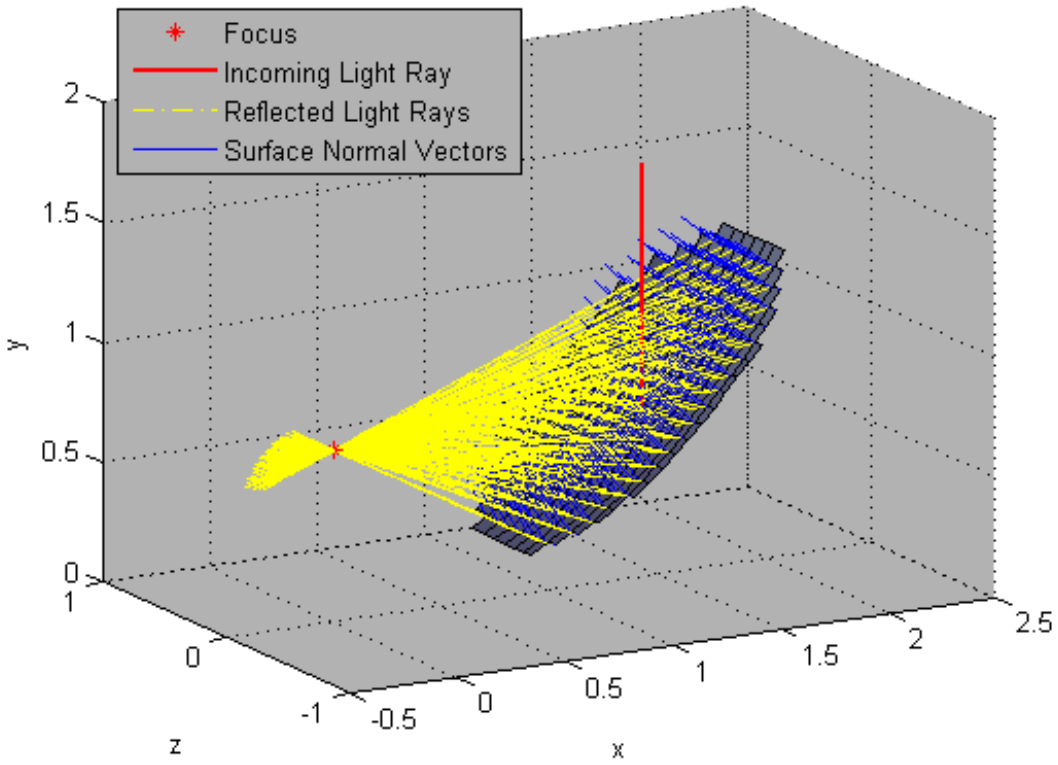

Figure 4.18: Ray tracing results for reflector at equinox noon is perfect configuration, isometric view

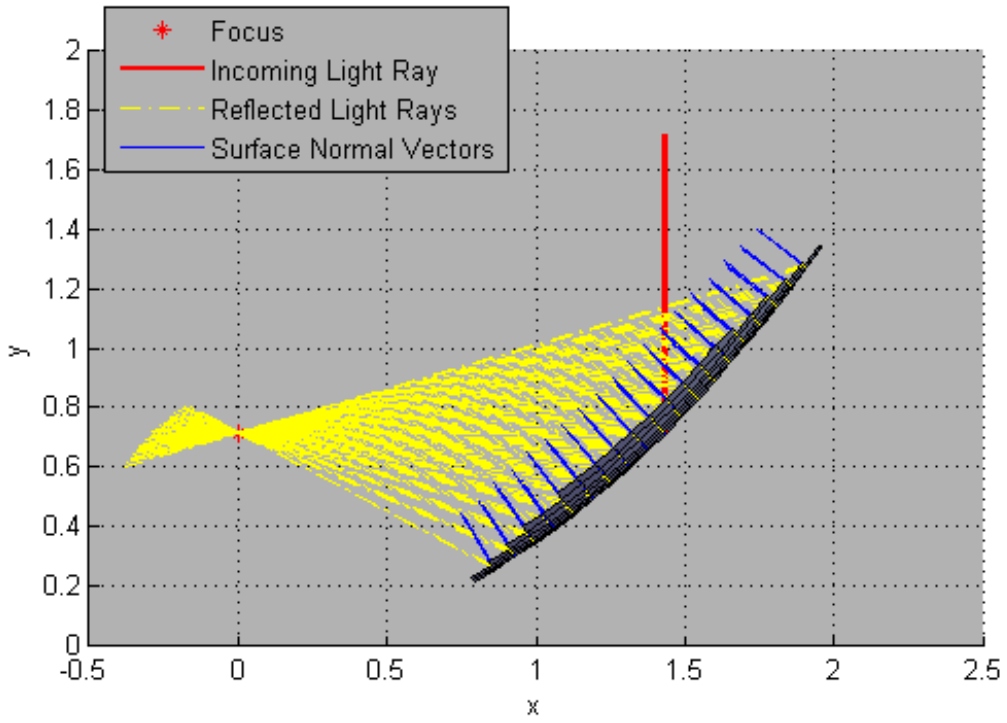

Figure 4.19: Ray tracing results for reflector at equinox noon in perfect configuration, side view

SEASONAL ADJUSTMENTS

The ability to simply adjust the shape of the reflector to compensate for the change of the seasons while keeping a fixed focus is one of the greatest strengths of the Scheffler design. As explained in Chapter 3: , the vertical profile must be closed or open throughout the year in order to track the sun as its declination changes. One important question that arises is, how often should the reflector be adjusted to maintain acceptable performance? There is not one answer because the declination of the sun changes at different rates throughout the year. Figure 4.20 shows how the change in declination closely resembles a sine curve, the greatest gradient occurs at the spring

and fall equinoxes (green and yellow, respectively) and zero gradient at the summer and winter solstices (red and blue, respectively).

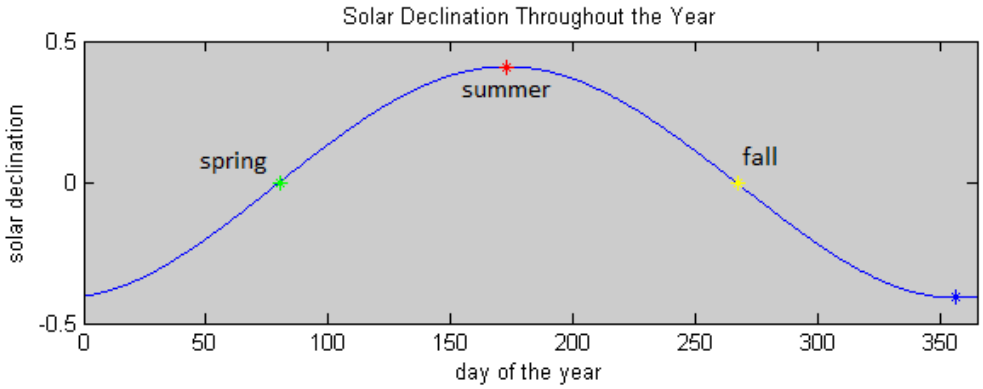

Figure 4.20: Solar declination throughout the year, colored points represents equinoxes and solstices

The changing gradient of the solar declination means that the reflector must be adjusted more frequently when closer to the equinoxes. Figure 4.21 shows the effect of keeping the reflector fixed at equinox configuration in the month following the spring equinox. It is possible to see that after one week the light still converges to a small area about 10 cm from the focus, but after two weeks the light hardly converges and misses the focus by a considerable amount. Finally, after a month the light is diffuse and far from the focus. It is reasonable to conclude that the reflector should be adjusted about every week when close to the equinox.

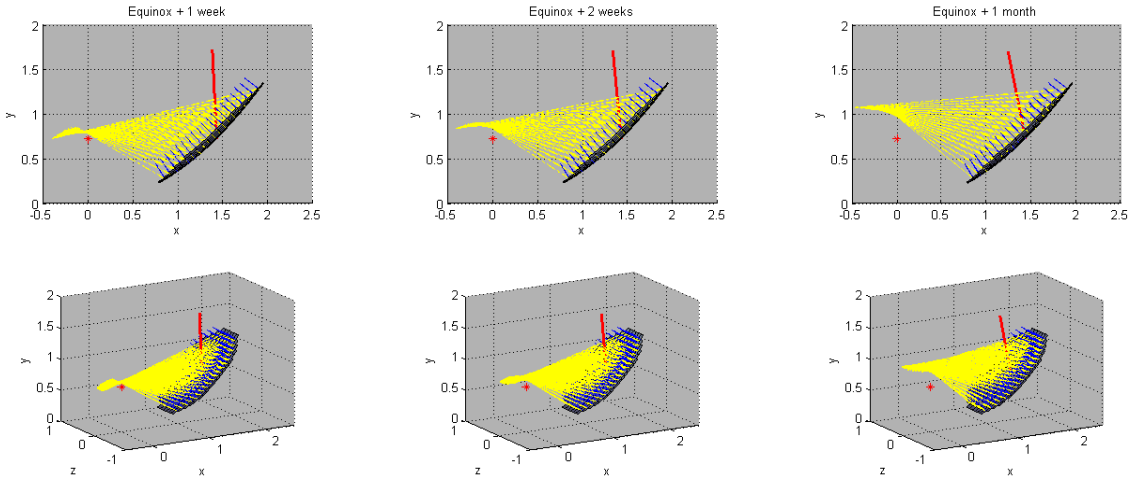

Figure 4.21: Loss of focus at equinox if reflector is not adjusted.

Conversely, the reflector needs to be adjusted much less frequently when close to the solstices. Figure 4.22 shows the change in the focus at the summer and winter solstices as the declination changes and the reflector is not adjusted. It can be seen that there is almost no movement in the focus after two whole weeks. Even after one month the focus is still close, slightly farther off target than after only one week during equinox. Approaching the solstices the reflector only needs to be adjusted every two or three weeks to maintain a good focus. Furthermore, the sun declination before and after the solstice is equal, so if the reflector is adjusted three weeks before the solstice, it will only move slightly off target in the following three weeks then start going back into focus until it is perfectly focused again after six weeks and not needing adjustment for at least another two weeks after that. During the bridge over the solstices the reflector can keep focus without being adjusted for over one and a half months.

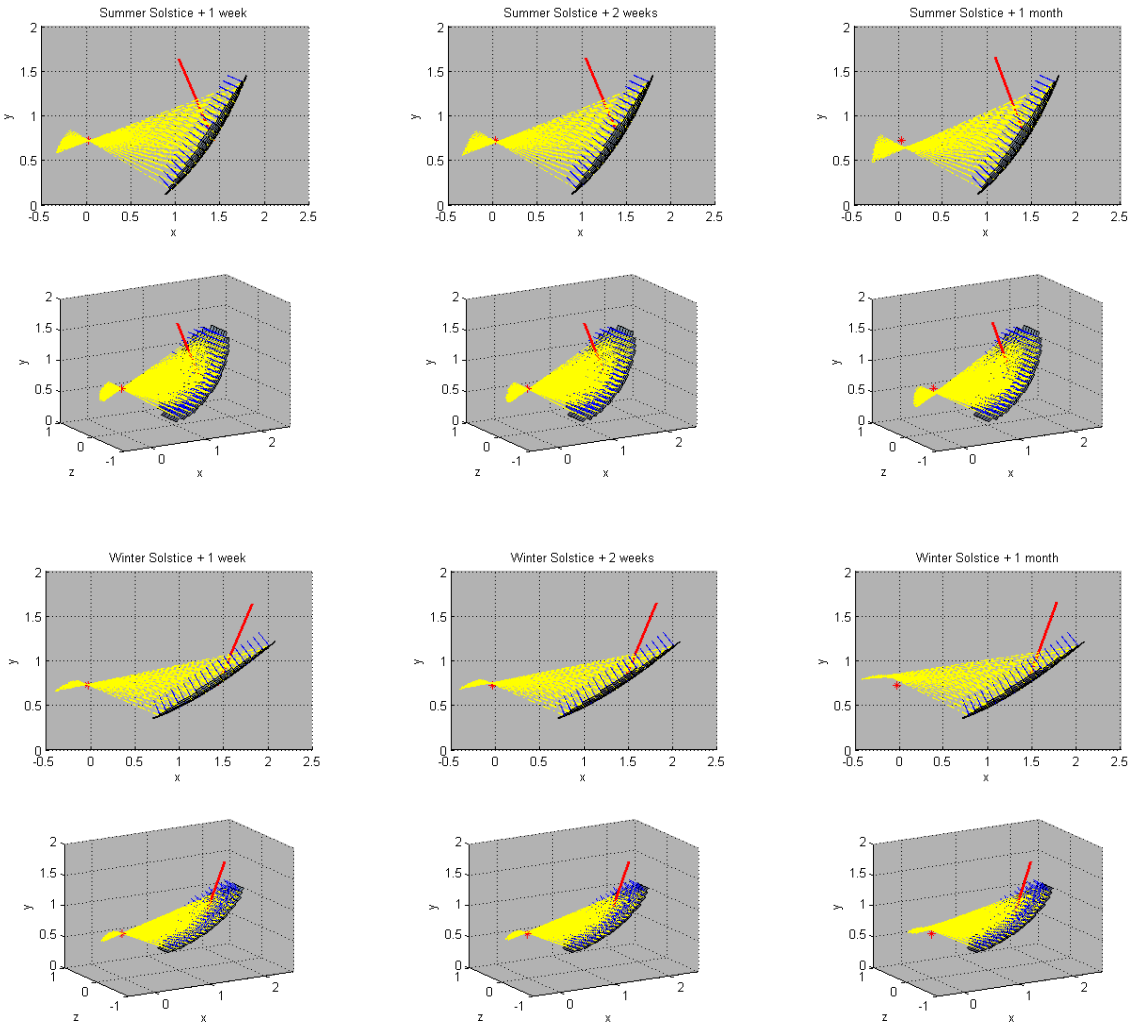

Figure 4.22: Change in focus at summer and winter solstices if reflector is not adjusted.

It is important to take into consideration that these analysis are performed on a perfect reflector. A real reflector might have some inherent diffusion due to poor manufacturing or wear (as analyzed in Section 4.2) and will most definitely have distortion on the focus at solstices due to the warping of the reflector as it is flexed. It is therefore a safe assumption that adjustments should be made at least every week when close to the equinoxes and about every two weeks when close to the solstices.

DAILY ADJUSTMENTS

One of the biggest strengths of the Scheffler design is its single axis daily tracking mechanism. The axis of rotation is antiparallel to the Earth axis so that the reflector maintains the same orientation toward the sun. You can imagine as if the sun and reflector are fixed and the earth is rotating under the Scheffler. Because of this technique, the Scheffler concentrator only needs to track the sun about a single axis greatly simplifying the process. To the lowest approximation, the reflector can be rotated by hand or with a geared hand-wheel, but even an automatic circuit/motor system can be very simple.

While the adjustment is very simply to perform, it does need to be performed every few minutes. Ideally an automated single axis tracker can update the rotation multiple times a minute to always maintain a perfect focus, but that may not be possible with a manual tracking system. Figure 4.23 shows the result of simulations of passing time with a fixed reflector and its effect on the position and quality of the focus. After five minutes the focus has moved by about 2.5 centimeters with little degradation of the focal area. After 15 minutes it will have moved the focus to 10 centimeters from its intended position, putting most of the light outside the target area, while after 30 minutes the quality of the focus is very low and displaced by about 15 to 25 centimeters. It is thus recommended to adjust the daily tracking every 5 minutes to maintain a high quality focus, and at least every 10 minutes to have a working concentrator.

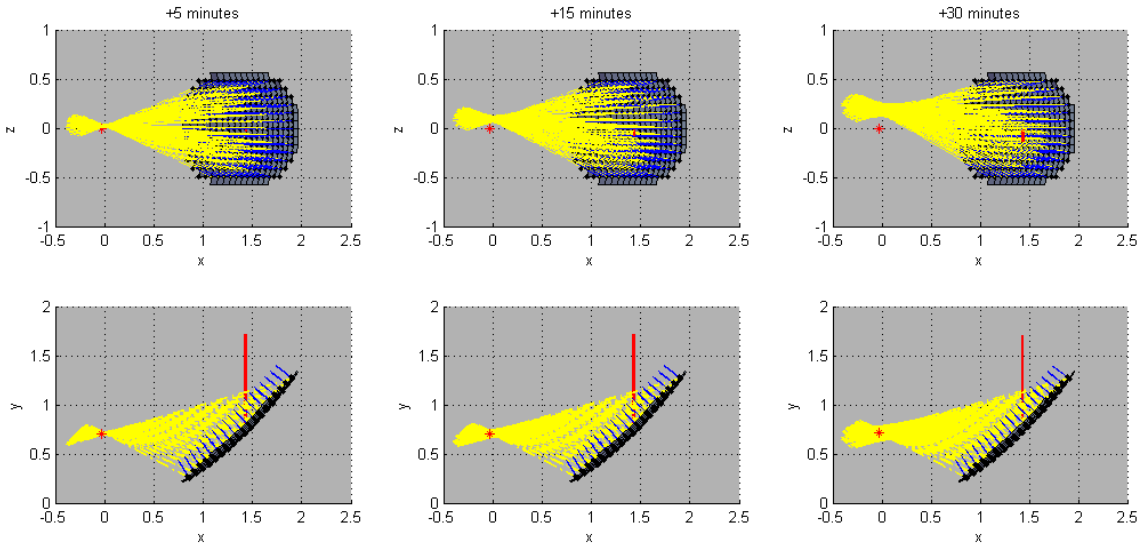

Figure 4.23: Effect of time change on a non-tracking reflector for 5, 15 and 30 minutes

4.5 A Rigid Reflector

After understanding how a Scheffler Reflector tracks the sun throughout the seasons and the hours of the day, it is very interesting to consider the condition where the reflector is rigid. The flexibility of the Scheffler Reflector is key to its ability to maintain a fixed focus with only one tracking axis.

Considering the condition of solar noon (at the equator for simplicity), as the year moves from an equinox to a solstice the incoming sun rays will become inclined at an angle $\delta_{\odot}$. To maintain a focus, the parabolic reflector would need to be rotated by an equal angle, $\delta_{\odot}$, so that its axis of symmetry remains parallel to the incoming light rays. Doing this would maintain a perfect focus but would cause the focus to move. If this rotation was performed about the center of gravity of the reflector, like the Scheffler design allows, the focus would inevitably move proportionally to the rotation as shown in Figure 4.24, where it has shifted downward by over 0.5 m. A different

kind of concentrator frame could be built to allow the reflector to rotate about the focus maintaining a fixed focus, but would be extremely complex.

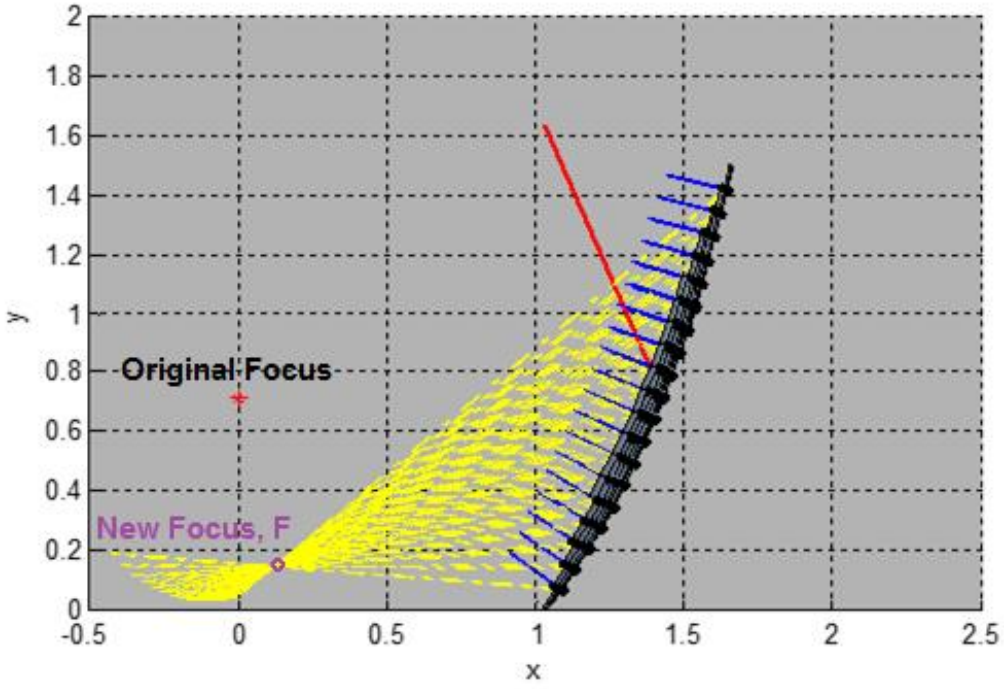

Figure 4.24: A ridged reflector tilted to match the solar declination at solstice at solar noon. The reflector still focuses light bu not at the original intended focus, red dot, moving over 0.5 m downwards..

Unfortunately, after this rotation, the daily tracking axis that goes from the midpoint of the reflector, C, and the focus, F, is no longer parallel to the axis of rotation of the Earth. Therefore, this configuration will not be able to track the sun while rotating about the C-F axis as the Scheffler reflector does. The focus will be worse farther away from solar noon since the axis of symmetry of the parabola will be rotating about a different axis than the incoming light rays from the sun.

An alternative option is for the reflector to still rotate about the polar axis of the Earth which does not pass through both C and F. In this scenario, the focus will be maintained but it will move proportionally to daily tracking rotation, negating the advantages of a single axis tracking reflector. Figure 4.25 shows that at solstice the focus will move sideways by an additional 0.5 m by

4 pm. It is thus possible to maintain focus with a ridged reflector, but it will be a moving focus dual-axis concentrator instead of a Scheffler Reflector.

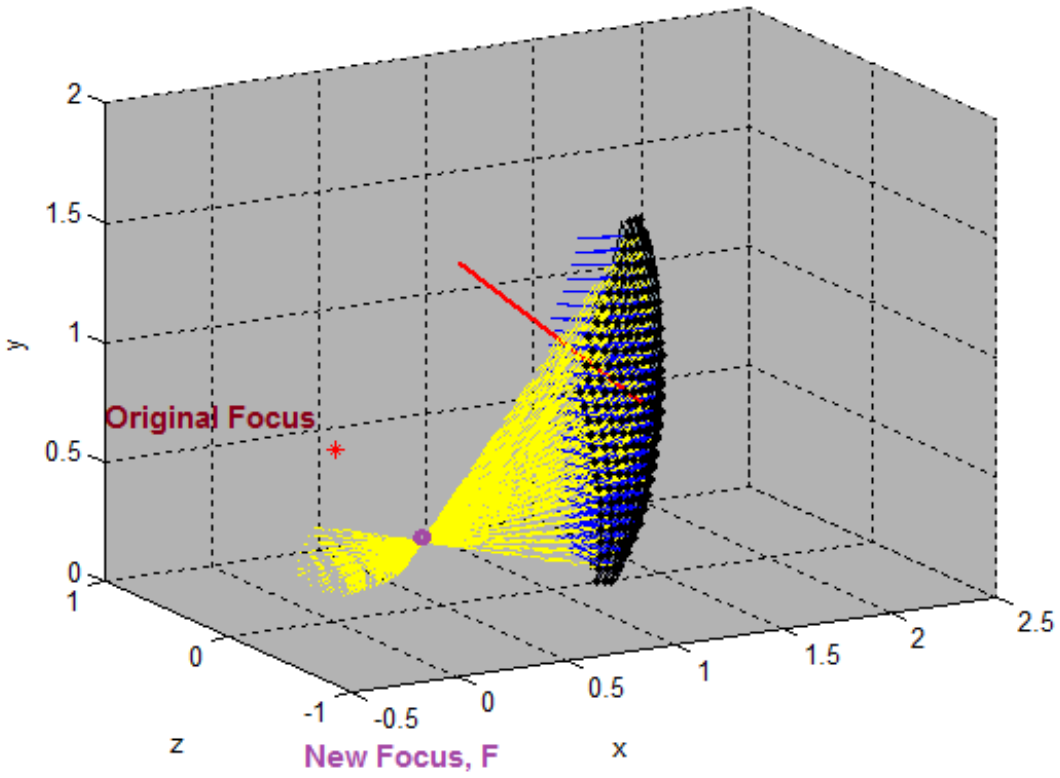

Figure 4.25: A rigid reflector tilted to match the solar declination at solstice and rotated about the polar axis for 4 pm condition. The reflector still focuses but the focus moves considerably as it tracks the sun hourly, by about 0.5 m sideways at 4 pm.

Another possible approach to focusing a ridged reflector is to simply adjust it to an angle such that the ray from the center of the reflector, point C, aims directly for the focus. With this configuration, all the rays will be directed in the general direction of the focus but will not converge to a point. Figure 4.26 shows this approach for a ridged perfect reflector optimized for equinox during summer solstice at noon. It can be seen on the left that the rays converge past the focus on the vertical plane and before the focus on the horizontal plane. This creates a rather poor focus even with a perfectly shaped reflector. The daily tracking will keep the center ray still aligned with the focus will maintain its poor quality, see Figure 4.27.

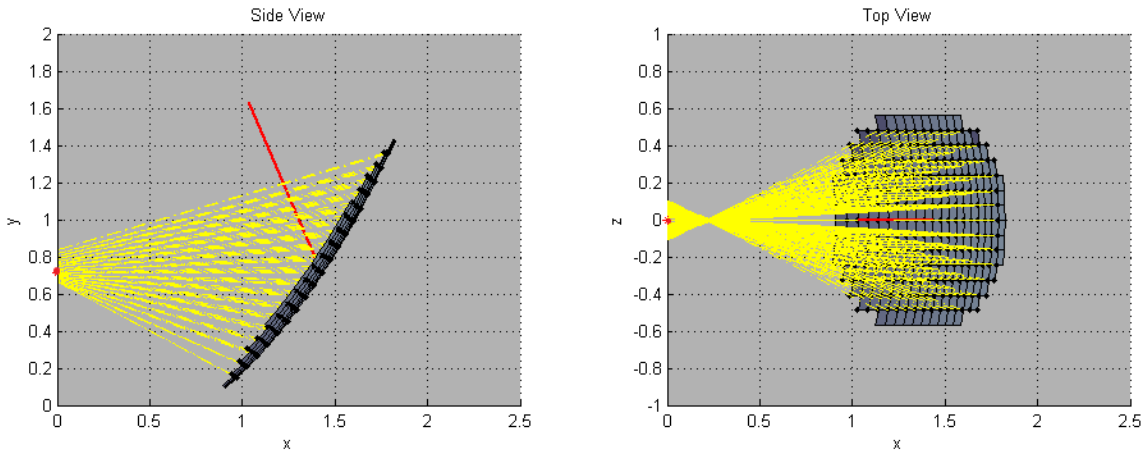

Figure 4.26: Ridged reflector at summer solstice at noon tilted so that the center ray passes through the focus, red dot.

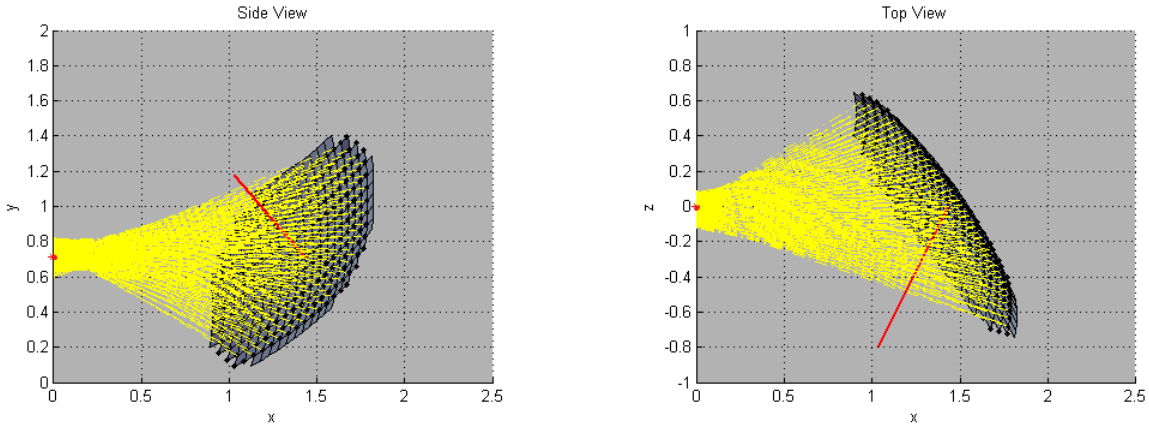

Figure 4.27: Ridged reflector at summer solstice at 4 pm tilted so that the center ray passes through the focus, red dot.

CHAPTER 5: DISH PROTOTYPES

Alongside the computational analysis of the Scheffler reflector, its dynamics and allowable tolerances, various prototyping techniques were investigated to create an inexpensive reflector. The prototyping was done in collaboration with undergraduate physics students and as a mechanical engineering senior project which I acted as an advisor for.

5.1 Foam Mold and Fiberglass Prototype

The first step to creating a repeatable manufacturing method to create a high quality reflector is to create a mold. Though a mold is an expensive piece of equipment, it gives the research team the opportunity to explore a myriad of construction materials and methods, as well as the possibility to construct high quality reflectors that can be used.

The male mold for a 1.8 square meter reflector that can theoretically concentrate 1.2 kW of solar power was constructed from high density urethane board measuring approximately 2 by 1.2 meters. The convex shape of the paraboloid was machined using a large CNC machine from the Matlab generated solid model of the desired reflector. After sanding and fixing the machined surface, the mold was coated with Duratech primer and high gloss coating and smoothed to 2000 grit resulting in a very nice finish. We were able to construct this one time mold because the polyurethane board was donated, otherwise the cost would be very high and not feasible for developing nations. Disregarding the initial cost, the mold allows for the prototyping of very inexpensive reflectors for about $30.

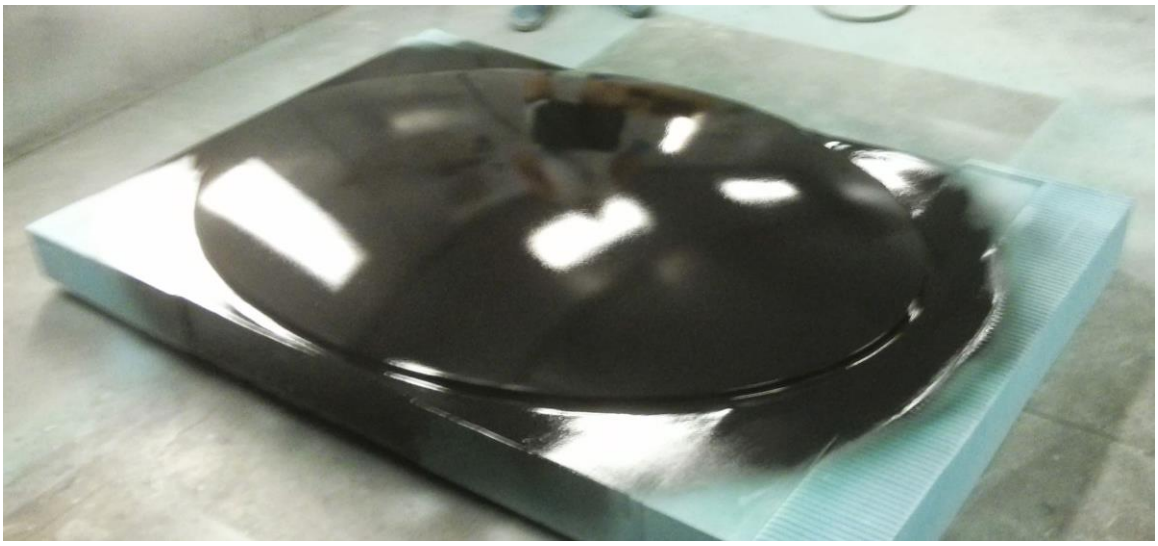

Figure 5.1: High density urethane mold with high gloss top coat

The first prototype produced with the mold was a two ply fiberglass dish. To minimize the cost of the fiberglass, we used two layers of 24 ounce per square foot 0/90 fiberglass cloth instead of doing several layers of the conventional 6 once per square foot cloth. This choice of very thick fiberglass cloth helped simplify and speed up the layup process but required more resin and a lot of time to soak the thick cloth thoroughly. Ultraviolet setting resin was used to allow plenty of time to perform each layup inside a paint booth.

The two ply fiberglass reflector cost us about $30 in materials and a couple of hours to complete the layup. The results were impressive, the elliptical structure was strong but also very flexible. It can yield elastically past buckling without fracturing which is highly desirable since the Scheffler reflector requires the surface to deflect throughout the year. It also has an extremely accurate shape, thanks to the foam mold we constructed, creating a very small focus during the preliminary tests. Adhesive aluminum coated Mylar was used to make the front surface reflective. The texture of the heavy weight fiberglass cloth shows through the front surface of the reflector

to a very small degree, but tests show that this effect is smaller than the effect of the subtending angle of the sun.

Figure 5.2: First fiberglass prototype before application of reflective Mylar coating

Moving forward, physics undergraduate students are exploring applications of the fiberglass reflector and a wide array of reflective materials that can be used as an alternate to the aluminum coated Mylar. A first complete prototype was tested with good results, Figure 5.3, the focus was approximately 15 by 15 centimeters without a properly focused shape and various reflective surface coatings. A finished prototype, with a uniform reflective surface and accurately focused, could achieve much higher concentrations.

Figure 5.3: Fiberglass reflector prototype with various reflective surface materials

5.2 Latex Cement and Burlap Prototype

The last prototype made on the mold, that I supervised, was a burlap fiber with a latex cement matrix composite. The materials were chosen to improve accessibility over fiberglass and ultraviolet setting resin in developing nations. This type of composite is used in a few applications, including roofing, in developing nations. The latex cement is supposed to be less brittle than concrete and allow the composite to not crack while flexing during drying.

The reflector was made with two plies of burlap infiltrated with latex cement, costing us about $15 but which would be considerably less expensive in developing nations. The reflector resulted in a surprisingly thin and light structure that was not as rigid as desired. It would need structural reinforcements to maintain a perfect shape under its own weight, but was flexible

enough to withstand the necessary deformation. While it was concluded that this composite is not appropriate to be used for the Scheffler reflector due to its low strength, it fits the requirements for a dual mirror polar tracking reflector, a derivative of the Scheffler reflector that the team ideated here at Cal Poly which does not require a flexible parabolic mirror, see Appendix A:.

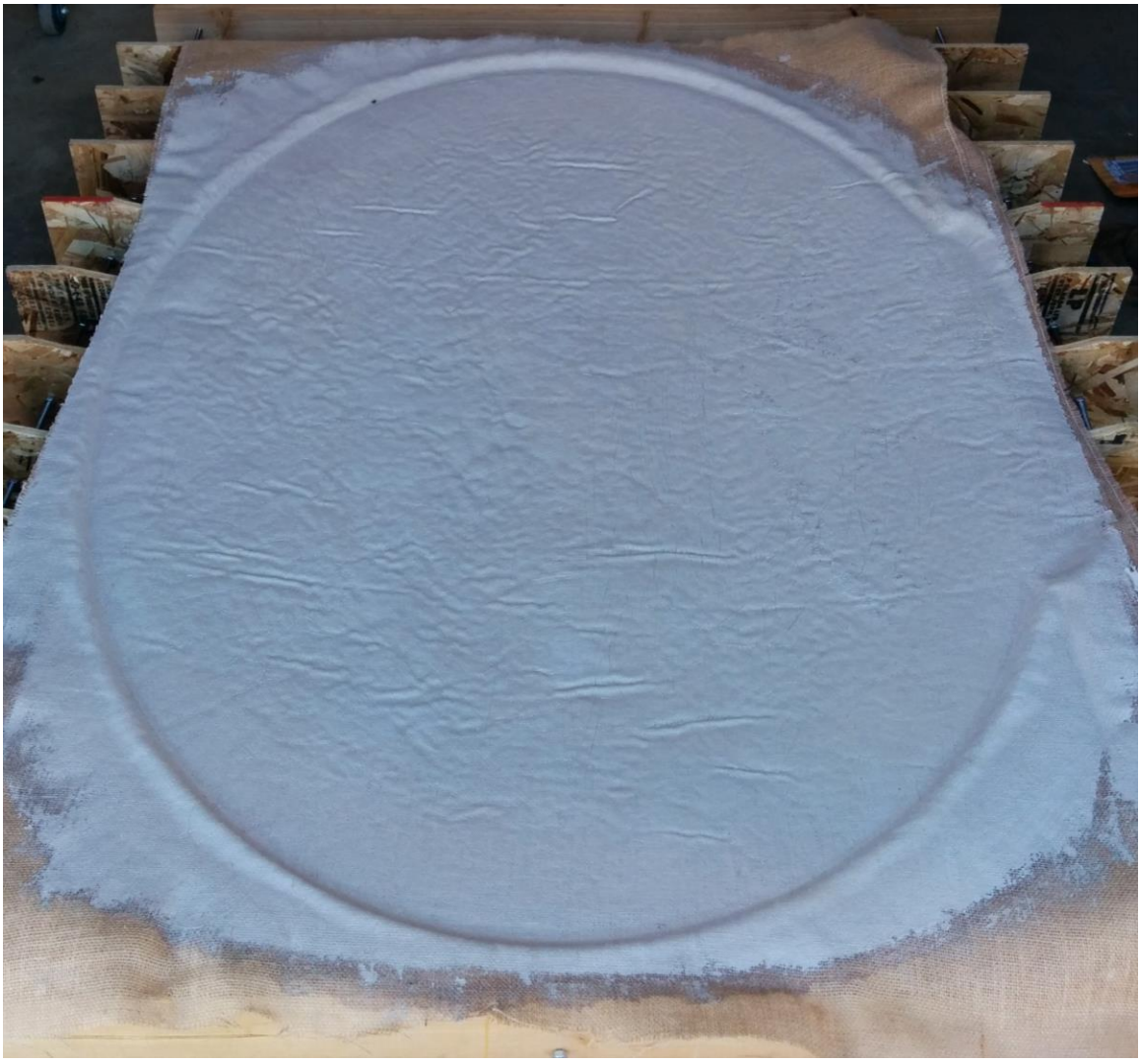

Figure 5.4: Reflector prototype made with latex cement and burlap composite

5.3 The Senior Project Team Design and Prototype

The task of exploring new construction techniques and ideating a non-conventional Scheffler reflector was contracted out as a senior project for a group of mechanical engineering students. The senior project team was formed by three students who chose the project out of spread of industry sponsored projects. The ME senior project is a 3 quarter course of design-build-test structure with various milestones set by the senior project advisor professor and by the project sponsor, me. The three students were: Nicholas Fuller, Jason Morgan, and Darren Sholes. (Sholes, Morgan and Fuller)

Their goal in the project was to find a way to construct a reflective parabolic Scheffler dish with materials that are readily available in developing nations with no need of advance manufacturing techniques and minimizing cost, while I provided them high level analysis. Their first step was to brainstorm a large number of concept ideas, many unconventional and farfetched. All the concept ideas from the initial brainstorm are showing in Figure 5.5 with some being redlined on a go/no-go basis.

Ideation/Brainstorming

System Concepts:

- ~~Basket Weave out of local plants~~
- ~~Use the rib cage and hide of deceased local animals~~
- Make different approximations of Scheffler for different seasons (that do not flex) out of:
  - Cob, Adobe, or Mud Brick
  - Cardboard
  - Inflatable
- Use similar design to current Scheffler but use _____ for the ribs:
  - "natural" composites
  - Wood
  - PVC Pipe
  - Bamboo
  - Kenaf
  - Fiberglass coated cardboard composite
  - Aluminum Poles
  - Bone/Ribs
- ~~Weave old bike tubes around ribs to form dish.~~
- Segmented "puzzle" concept
  - Attached or hinged pieces create a polygonal approximation of elliptical Scheffler shape.
- Tent Design
  - Stretch canvas around outer rim and use hooks and string at different lengths and locations to approximate scheffler shape
  - Use poles as "ribs" and run them through slots in canvas or tent-like material to approximate the shape of the dish.
- ~~Umbrella Design~~
  - Similar to tent but source off taut surface is central
  - Dish folds together for easy storage
- Sheet Metal
  - Bend/Hammer one large piece of sheet metal into the shape of the Scheffler and check against mold.
  - Bend smaller pieces of sheet metal and attach them to form the shape of the dish.
- Cardboard/Paper Folding
  - Similar to "fancy" paper airplane kits. In the immortal words of Jason Morgan: "Cut, Fold, Duct Tape. Scheffler."
- ~~Pin Impression Board~~
- Pipe (Heliostat Array)

Structural Materials:

- Cob, adobe, mud brick
- ~~Brick~~
- Cardboard
- Concrete
- Aluminum
- "Natural" Composites
- Bamboo
- Sheet Metal
- Conduit
- PVC/ABS
- Wood
- Chicken Wire
- Steel Tubing
- Canvas
- Kenaf
- Fiberglass-Coated Cardboard Composite
- Aluminum Poles
- ~~Bike Tubes~~
- ~~Cow Ribs~~
- ~~Bone~~
- ~~Sand~~

Reflective Material:

- Highly-Polished Aluminum Strips
- Sheet Metal
- Aluminum –Coated Mylar
- Space Blankets
- Aluminum Foil
- Mirror
- Mirror Pieces
- Glass
- Broken Glass
- Aluminum Cans
- Potato Chip Bags
- ~~White Paper~~
- White Paint
- Corrugated Steel

Figure 5.5: List of all possible construction methods or ideas for the Scheffler reflector by the senior project team

The initial concept ideas contained several very interesting and feasible possibilities that hadn't been thought of before. The three main concepts that were explored were sheet metal forming, stretch fabric, and cob concrete.

The sheet metal dish would allow for a cheap, widely available construction material with great strength and workability. The metal would be formed with an English Wheel or alternately with an anvil and hammer. The team found that metal sheet forming had a steep learning curve but that a skilled worker could make very accurate surfaces, especially if given a template or

method to check the shape. Additionally, the dish could be polished after shaping to create a reflective surface without the need of a reflective coating. Their preliminary prototypes were able to achieve a focus of about 10 by 10 centimeters, with a reduced size reflector.

A stretched fabric dish would be formed in a similar way to how a tent and umbrella hold their shape, using sail making methods to achieve an accurate shape. They explored the possibility of using natural fibers as the cloth and bamboo as a frame. This method of construction could be feasible with the help of experienced sail makers to perfect the shape making process.

One of the most attractive methods in terms of accessibility in developing nations was using cob/concrete. The ancient composite material is very easily found and many people have experience with it. The biggest challenge in using this material would be making it flexible yet strong enough to maintain its shape. The latex cement and burlap reflector discussed in Section 5.2 was a derivative of this idea attempting add some flexibility to the structure.

Finally, the construction method that was prototyped and tested was a derivation of the stretched fabric idea. They constructed a reflector from thin wooden strips and glue, borrowing the construction method of wooden boats. A template mold was created from plywood sections to define the radii of the lateral ribs, as shown in Figure 5.6. The ribs for the dish would be made from laminated, curved wooden section. Thin strips of wood, such as balsa, would be laid over the ribs in the opposite orientation. The curvature would be obtained by bending two slats glued over each other along the length, when the glue dried, the curve would be maintained.

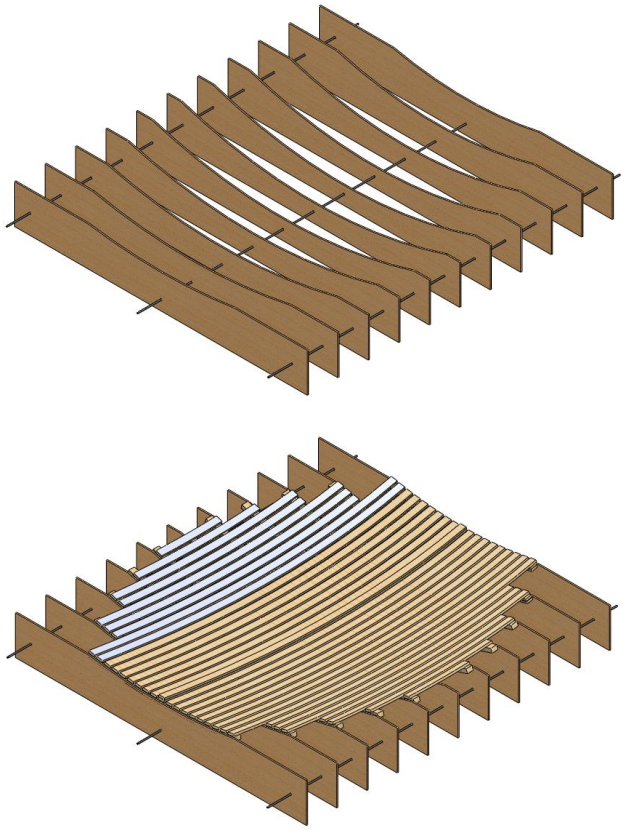

Figure 5.6: Plywood female mold of the reflector (left), wooden reflector finished still in the mold (right)

Results were impressive, the wooden reflector was structurally sound yet flexible. The manufacturing technique was rather simple and inexpensive, Figure 5.7. All the light was concentrated in a 20 by 20 centimeter focus with their first prototype. The major source of imperfections were due to the low experience with woodworking and more refined reflectors could be manufactured with some practice. The dish was created with just over $100 of material, but the cost could be greatly reduced by producing multiple reflectors from one mold. It is also important to consider that these materials are considerably less expensive in developing nations, compared to California. For the full report, which includes detailed construction technique and results, see Appendix B:.

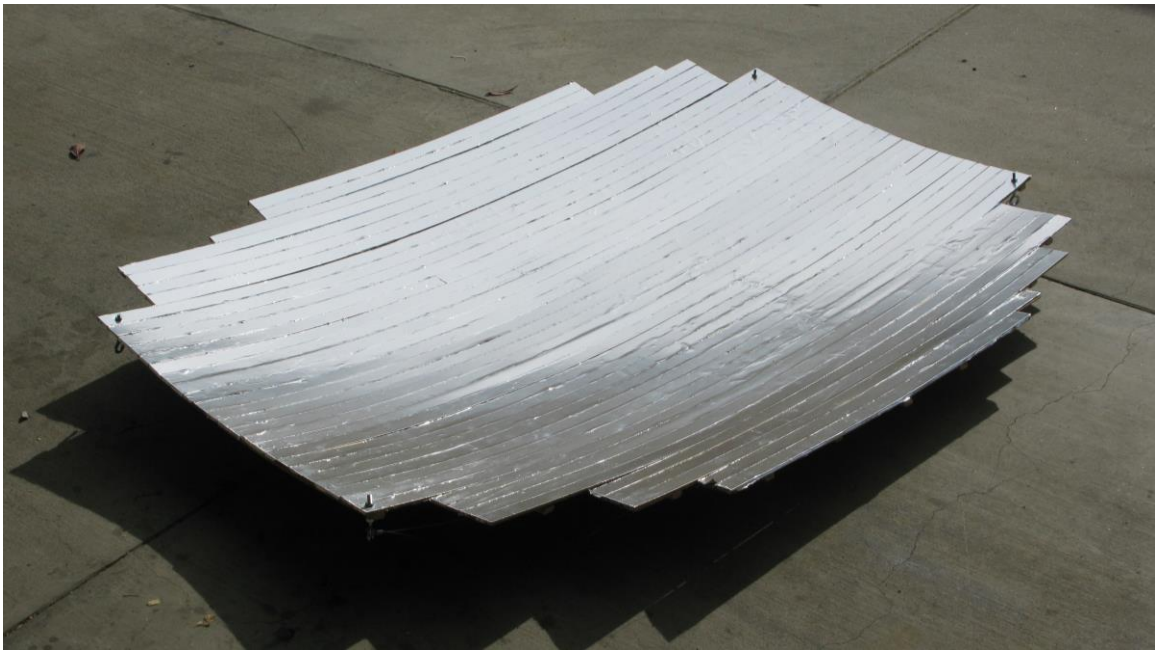

Figure 5.7: The finished wooden reflector prototype with reflective aluminum coated Mylar

CHAPTER 6: CONCLUSION

The intent for this project was a combination of research, analysis, design, and project management. The four goals of developing in-depth understanding of the Scheffler reflector dynamics, analyze the sensitivity of the focus to deformations and deviations, to design a reflector constructed from accessible materials, and to drive the raw material and manufacturing down were all successfully advanced. Much more work is left to be done before the Cal Poly Scheffler Reflector group can deploy their design in developing nations, but new students are already building upon the advancements we accomplished in 2012-2014.

A strong analysis tool was able to improve on our understanding of the dynamics of our solar concentrator. The sensitivity analysis brought a quantitative level of understanding of the manufacturing tolerances and quality required to produce a high quality concentrator. We were also able to explore various permutations of the design. Most importantly, this analysis and the foam mold allowed for the creation of various new prototypes and laid the foundation for new manufacturing methods of the parabolic dish.

A total of three different reflector prototypes were created from very different materials and techniques. The wooden reflector proved that with good design and manufacturing technique, a reflector can be made with very simple materials and without high tech machining hardware. The fiberglass prototype was especially significant because it confirmed that creating a sub $50 parabolic reflector for the Scheffler concentrator is possible. In combination with the design efforts from other members of the group on other components of the reflector, we are now confident that a sub $100 Scheffler reflector is a reality that Cal Poly can achieve in the near future.

BIBLIOGRAPHY

Alberti, Simone, Tyler Murphy and Pete Schwartz. *Redirecting Sunlight with Polar Tracking in Developing Countries... and Elsewhere*. Research Paper. San Luis Obispo: California Polytechnic State University, 2013.

Duffie, John A and William A Beckman. *Solar Engineering of Thermal Processes, fourth ed*. Hoboken: John Wiley & Sons, Inc, 2013.

Ezzati, MAjid and Dainel Kammen. "The health impacts of exposure to indoor air pollution from solid fuels in developing countries: knowledge, gaps, and data needs." *Environ Health Perspectives* (2002): 1057-1068.

Groulx, Dominic and Benjamin Sponagle. "Ray-Tracing Analysis of a Two-Stage Solar Concentrator." *Transactions of the Canadian Society for Mechanical Engineering* 34.2 (2010): 263-275.

Munir, A., O. Hensel and W. Scheffler. "Design principle and calculations of a Scheffler fixed focus concentrator for medium temperature applications." *Solar Energy* 84 (2010): 1490-1502.

Rapp, Jason. *Construction and Improvement of a Scheffler Reflector and Thermal Storage Device*. Senior Project. San Luis Obispo: California Polytechnic State University, 2010.

Rogers, Steven, et al. "Concentrating Sunlight with an Immobile Primary Mirror and Immoble Receiver: Ray-Tracing Results." *Solar Energy* (2011): 132-138.

Scheffler, Wolfgang, O Hensel and A Munir. "Design principle and calculations of a Scheffler fixed focus concentrator for medium temperature applications." *Solar Energy* (2010): 1490-1502.

Sholes, Darren, Jason Morgan and Nicholas Fuller. *Low-Cost Scheffler Solar Concentrator for the Developing World*. Senior Project. San Luis Obispo: California Polytechnic State University, 2013.

Sproul, Alistair B. "Derivation of the solar geometric relationships using vector analysis." *Renewablew Energy* (2007): 1187-1205. Document.

Szokolay, Steven. "Solar Geometry." *Plea Notes* 1 (1996).

Wolfgang, Scheffler. "Introduction to the Revolutionary Design of the Scheffler Reflectors." n.d. *Solare Bruecke.* September 2012.

APPENDIX A: DUAL MIRROR SOLAR CONCENTRATOR

Redirecting Sunlight with Polar Tracking in Developing Countries… and Elsewhere

Simo Alberti*, Tyler Murphy, Pete Schwartz
Cal Poly Physics Department
**Cal Poly Mechanical Engineering Department*
pschwart@calpoly.edu

Abstract

A correctly oriented mirror rotating anti-parallel with the earth's rotation will reflect incident sunlight parallel to the rotation axis in either direction onto a stationary target. The mirror's orientation on the rotation axis (declination) must be adjusted for the seasonal variation in the sun's altitude but throughout the day the mirror tracks on a single axis. While this system may not improve tracking for industrial solar electricity production, it could be a game-changer in developing countries where concentrator construction and seasonal declination adjustment could be done by hand. The easily constructed, functionally single axis polar tracking may greatly increase accessibility to effective solar cooking and other small-scale industries requiring intense heat; assisting developing economies in leap-frogging the increasingly unavailable or undesirable carbon-intensive step that industrial societies took.

Introduction

Harnessing solar energy would be much easier if the sun didn't move. For low-precision concentration, the complexity of construction could be reduced by an order of magnitude if sunlight came from a fixed direction. However, in order to achieve sustained solar concentrations greater than 2 "suns" throughout the day, the reflector surface must track the sun's apparent motion. Complexity increases not only because of the tracking mechanism itself, but also due to the structural rigidity, lightness, and precision necessary for a structure to track on two axis. We present a single-axis, polar-tracking, flat mirror heliostat that simply and inexpensively redirects sunlight to a stationary location where it can be subsequently concentrated, redirected, or otherwise utilized. Daily tracking can be done by a simple comparator circuit, a clockwork mechanism, or by hand. The trade-offs of having only one tracking axis are that the mirror's declination must be adjusted weekly (or daily near equinox when the sun's altitude changes at the greatest rate), and that the orientation of the stationary target and the mirror must be along the earth's rotation axis.

Our innovation fits between conventional tracking heliostats and the Scheffler Concentrators. A flat mirror on a dual axis tracker can redirect sunlight to a stationary concentrator, such as the high-flux solar furnaces[1] at the National Renewable Energy Laboratory and the Institute of Solar Research in Cologne, Figure 1a. The dual-axis tracking requires sophisticated computer controlled

[1] High Flux Solar Furnace at National Renewable Energy Laboratory (NREL) in Golden Colorado, DLR Institute for Solar Research in Cologne, Germany

coordination, which is not a drawback for this already expensive and precise system. However, dual axis tracking would greatly increase the cost of a low precision, hand-made solar concentrator. Polar or planetary mount tracking is common in astronomy, where counter rotating a telescope parallel to the earth's rotation allows the telescope to remain fixed on the same celestial direction. Polar tracking for solar energy has so far been used only in Scheffler Concentrators,[2] where a parabolic mirror rotates on a polar axis, concentrating sunlight to between 50 and 500 suns onto a stationary target, Figure 1b. There are about 10,000 such devices in use, mostly for cooking in Asia and Africa. Seasonal adjustment of the polar tracking Scheffler Concentrator requires that the flexible parabolic mirror change in both declination and curvature. The construction of a movable, deformable mirror requires moderate training, time and resources.

The Scheffler reflector *concentrates and directs* sunlight with one curved reflector while in our design a polar tracker *directs* the sunlight with a flat mirror to a stationary location for subsequent *concentration* or redirection by a secondary device, Figure 1c. Doing so decouples tracking from concentration, making possible a wide variety of stationary concentrating geometries, some of which may be less complicated or more appropriate for a given project than other solar concentration or redirection techniques. The advantage of our polar tracking dual mirror concentrator (1c) is a potential decrease in cost because both single axis tracking of a flat mirror, and stationary concentration technologies are inexpensive. The comparative advantage of the Scheffler design (1b) is that they either have no secondary mirror, reducing reflective losses, or have a smaller secondary that is easier to accommodate geometrically. The comparative advantage of the dual axis high flux solar furnace (1a) is freedom to place the two mirrors not on the earth's rotational axis. Thus, our polar tracking dual mirror solar concentrator geometry (1c) is unique with its own advantages and disadvantages, and could be particularly compelling where cost is very important and a person could conveniently do seasonal declination adjustments.

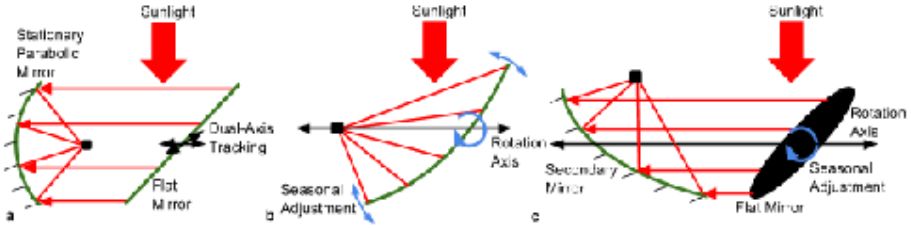

Figure 1 Illustration of three solar concentrators and tracking methods: **a)** NREL high flux solar furnace with 2-axis flat heliostat and stationary parabolic concentrator, **b)** Scheffler solar concentrator with single axis deformable parabolic mirror (tracking seasonally by rotating declination and flexing, blue arrows) **c)** polar axis dual mirror concentrator with a single axis flat primary mirror and a parabolic secondary mirror (tracking seasonally by rotating declination of primary mirror, blue arrow)

The Polar Tracking Redirects Sunlight to Stationary Target

Figure 2 illustrates the apparent path of the sun for equinox, and winter and summer solstice. In order to properly track the sun, a heliostat must rotate daily to compensate for the apparent daily

[2] a) Scheffler, W., 2006. Introduction to the revolutionary design of Scheffler. In: SCIs International Solar Cooker Conference, Granada, Spain, 2006. b) A. Munir, O. Hensel, W. Scheffler, Solar Energy 84 (2010) 1490–1502

path of the sun about the earth, and must also traverse north and south annually to account for the apparent change in altitude of the sun's daily path.

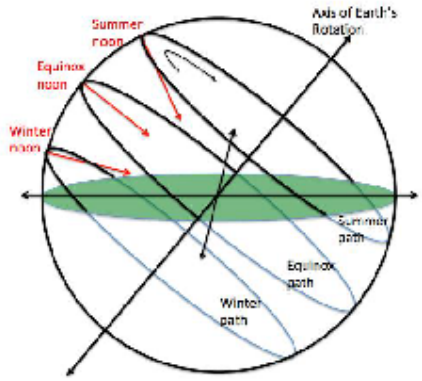

Figure 2 The sun's apparent path for a place at about 50° North Latitude. Red rays indicate direction of sunlight at noon at the season indicated.

A flat mirror rotating counter parallel to the earth's rotation will maintain the same orientation with respect to the sun and is said to be "polar tracking".[3] If the mirror is mounted such that it reflects sunlight parallel to this rotation axis (see Figure 3a), the reflected light will remain in the same place throughout the day. The mirror could reflect the sunlight upwards (Figure 3a), or downwards (Figure 3b) along the rotation axis.

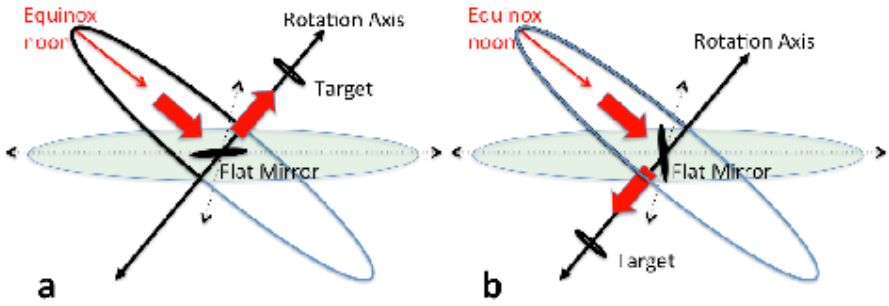

Figure 3 Mirror in the northern hemisphere at the latitude of Fig. 1 reflects sunlight along the earth's rotation axis **a)** upward to a target located to the north, and **b)** downward to a target located to the south.

[3] Because the earth also orbits the sun once per year, the sun's apparent orbit is about 0.3% slower than the earth's rotation.

During Equinox, the direction of incident sunlight is perpendicular to the rotation axis as in Figure 3, and so the mirror's perpendicular would be oriented at a 45° with respect to both the rotation axis and the direction of incident sunlight. Because the direction of incoming sunlight changes by about 23.5° northward June 21 and southward in December 21, the mirror's perpendicular must be rotated by about 12° northward in June (Figure 4a), and southward in December (Figure 4b).

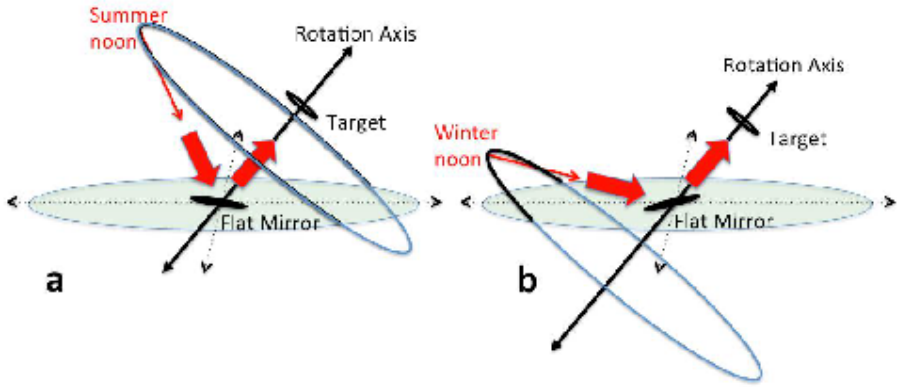

Figure 4 The upward-facing mirror in the northern hemisphere at **a)** summer solstice, and **b)** winter solstice. Note the slight change in angle of the black circular mirror between these two figures and Figure 3a), which corresponds to equinox.

While the angle between the mirror and rotation axis (declination) must be changed throughout the year to account for the seasons, the mirror still rotates daily about the same axis, simplifying daily tracking to that of a single axis.

Solar Concentration Application

A possible solar concentration application at the equator at equinox is shown in Figure 5, whereby the reflected rays from a polar tracking, flat mirror are incident upon a stationary, parabolic mirror with a central axis that is parallel to the mirror's rotation axis. Figure 6 depicts an indoor cooking facility in the tropics at equinox, where the sun is near straight overhead and the polar axis is near horizontal. An *upward* facing mirror in temperate latitudes may be more appropriate for concentrating with a Fresnel lens as in Figure 7 because rays should focus upward for cooking.

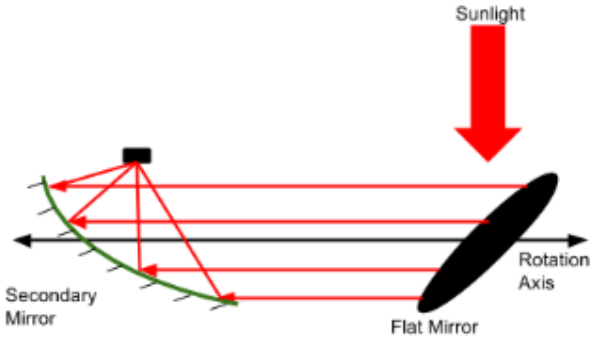

Figure 5 Parabolic mirror concentrator. The light reflected to the left from the rotating flat mirror is incident upon a stationary parabolic mirror (green) with a central axis that is parallel to, but displaced upwards from the rotation axis of the flat mirror in order to place the focus away from the rotation axis. This concentrator is configured for noon during equinox at the equator.

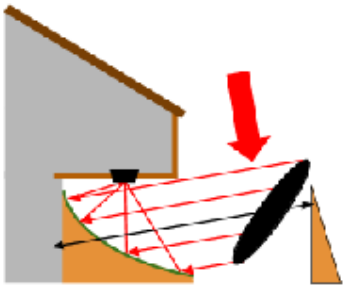

Figure 6 Tropical indoor solar concentrated cookstove at about 10° Latitude. This geometry allows the focused light to be upward and the cooking facility to be indoors and sheltered.

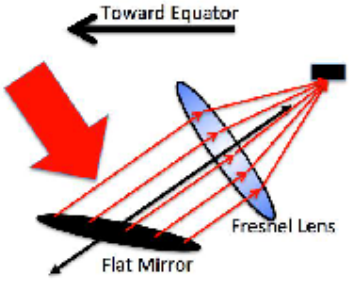

Figure 7 Fresnel lens concentrator. The light reflected upward from the rotating flat mirror is incident upon a stationary Fresnel lens (blue) oriented perpendicular to and centered on the rotation axis. The axis is tilted at 35° (Cal Poly's Latitude) with respect to the horizon, and the black arrow indicates the direction of the equator.

Another application for redirecting sunlight for buildings could have the target itself be a flat mirror that simply reflects the sunlight to the desired location, such as in a north-facing window as shown in Figure 8. Similarly, if the pot in Figure 6 were removed, the focused light would enter the living space and defocus, providing heat and light to the room.

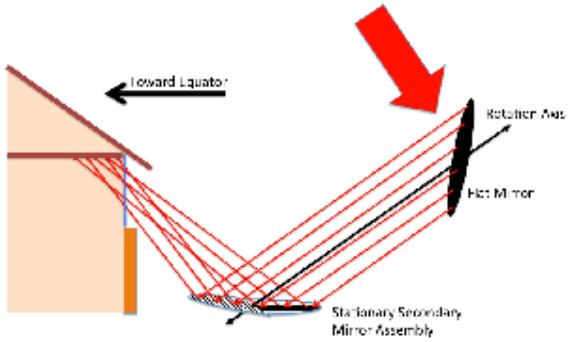

Figure 8 An inexpensive heliostat. The redirected sunlight is incident on flat mirrors, reflecting heat and light through a window that would otherwise not receive sunlight.

Ray-Tracing Results

In order to establish the necessary tolerances for a concentrator such as in Figure 6, a Matlab-based ray-tracing program simulates sunlight for time of day and time of year as well as for various types of imperfections. The results help define the tolerances on the surface of the secondary reflector and the alignment of the two reflectors necessary for adequate performance.

The primary reflector was assumed to not have significant deformation since it is a flat surface, which leaves the secondary mirror surface and alignment as the only source of imperfections. Because the flat primary mirror is inexpensive, we make the primary mirror big enough for the secondary mirror to always be fully illuminated. The code simulates a circular sun of uniform intensity subtending an angle of 0.533°.

For the purpose of the simulation, the secondary mirror accepts light of a circular cross section of 1 meter radius, giving the reflector an effective area of 3.14 m^2 and a power of 3.14 kW assuming solar flux of 1 kW/m^2. We neglect reflective losses although they may be significant. The two mirrors are placed approximately two meters apart and a target area (cooking surface) is a 10 cm radius circle. With a perfectly shaped reflector the sun subtending angle results in a 2 cm diameter focus corresponding to a concentration greater than 5,000 suns. Figure 9 shows a visual representation of the tray tracing of this reflector with an imperfect surface during midday of equinox at the equator.

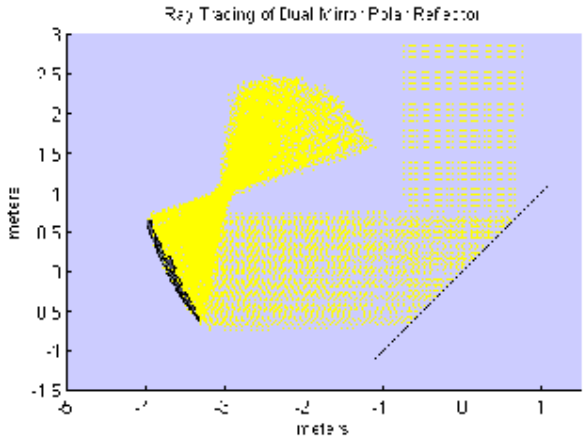

Figure 9 Visual representation of an imperfectly manufactured polar tracking dual axis reflector focusing light from a real sun. The secondary mirror is configured with the highest tolerances (poorest quality) that allow for an efficiency, ignoring reflective losses, above 90% of ±2° and ±4 cm surface roughness.

We introduce three types of imperfections into the system and evaluate the quality of the focus based on the percentage of light that hits a 10 cm radius target (efficiency) and the average sunlight intensity in a 1 cm radius target inside of the 10 cm target.

The first imperfection is a misalignment between the axis of the secondary mirror and the axis of the light reflected off the primary mirror. This imperfection is important because it can represent both an error in assembling the reflector or the error that arises in improperly adjusting the primary reflector seasonally. The blue data set in Figure 10 shows the degradation of the focus as the axes become misaligned by up to 5 degrees. The percentage of light focused degrades very quickly after 2° because the focal point moves outside the target area. By noticing that the light is pointed outside of the target area the misalignment can be diagnosed and corrected by bending the rotation axis slightly, so this imperfection is not a major area of concern.

We also simulated surface roughness with localized angular and displacement deformations on the secondary reflector surface. For example, an outward bump in the reflective surface of the dish has a displacement from the surface and parts which are at angles different than the ideal dish surface. Computationally this was simulated by adding a random, uniformly distributed angle between ±x degrees and/or displacements between ±x centimeters to the perfect shape of the secondary reflector for each ray upon reflection. This represents inaccuracies on the surface due to shaping the of the secondary reflector. Deformation in angles have a significant impact on the focus, though the reflector will still focus about 80% of the light with concentrations of over 1000 suns with angular deformations between ±3°. Conversely, deformation in surface displacement has negligible effect on the focus even at ±5 cm.

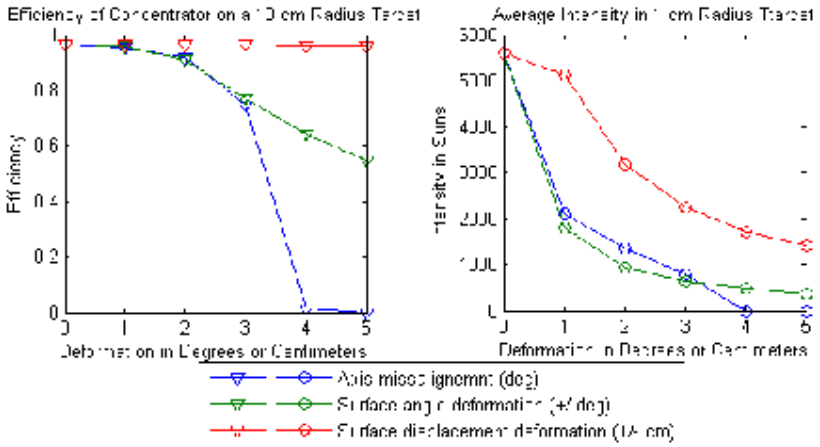

Figure 10 Degradation of focus for given manufacturing tolerances in percent of light falling on a 10 cm radius target (left) and average intensity of radiation on a 1 cm radius target (right).

It may be instrumental to observe the effect of the superposition of the imperfections. The blue data in Figure 11 show a reflector with both angle and displacement deformations, as would be expected from a hand shaped secondary reflector, with perfectly aligned axes. We see that 90% of the light is focused with tolerances of ±2° and ±2 cm, while over 75% is focused with tolerances of ±3° *and* ±3 cm, both with solar intensities of over 500 suns. The green data in Figure 11 show a combination of all types of imperfection showing a quick degradation in the focus mostly due to the axis misalignment. The axis misalignment must have a tolerance of ±1° to focus more than 90% of the light.

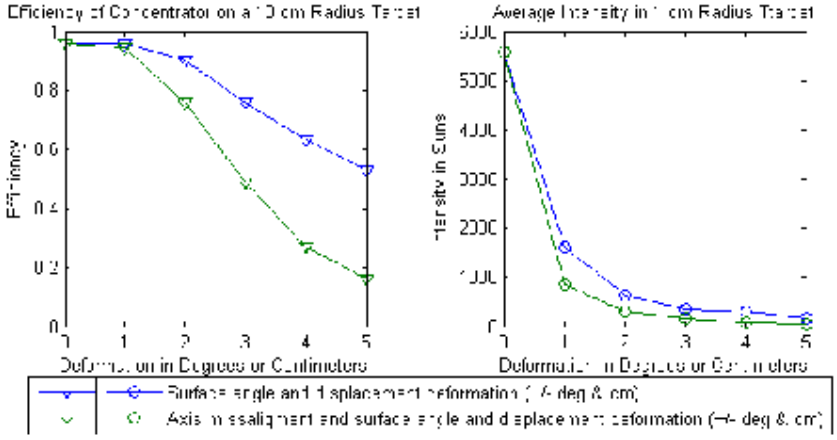

Figure 11 Degradation of focus for given a combination of manufacturing tolerances in percent of light focused

Ray-tracing results for the proposed 3.14 kW solar cooking facility identify tolerances for a design where 90% of the incident sunlight reaches a 10 cm radius circle, corresponding to a concentration of about 1000 suns. Inclusion of 90% reflectivity coefficient for both reflectors reduces the power concentrated to 2.3 kW. To achieve this level of concentration the misalignment between the axes must be no more than 2° regardless of other imperfections. Additionally the manufacturing tolerances of the secondary mirror must be less than what is shown in Figure 9: ±2° and ±4 cm.

Accessibility to Concentrated Solar in Developing Countries

Like Scheffler, our goal is not to minimize the cost of a technology for sale, but to bring to people the means of technology production itself. Thus, barriers to acquire a technology should be thought of in terms of complexity, or level of expertise needed to construct and maintain a technology, as well as cost and availability of materials. Driving down costs through optimized, centralized production does not bring the same value to developing countries as it does to industrialized nations. Human labor is readily available in developing areas, so saving time with economies of scale is not as important.[4] Additionally, producing something by hand employs and empowers locals to be self-sufficient. However, it requires that they be appropriately prepared for the task's level of complexity.

Cooking for the poor in developing countries is usually done by burning wood or some other biomass inside often poorly ventilated kitchens. The resulting indoor air pollution claims more children's lives than malaria.[5] Where fuel is scarce, families struggle to obtain fuel with results that may include deforestation, long difficult trips, and exposure to violence. Solar cooking provides an inexpensive, safe alternative that is free of emissions and other environmental degradation, but solar cooking technologies are often not adopted because they are not convenient or powerful enough. Our new design offers convenience and effectiveness similar to natural gas or electricity.

This new design doesn't rely on scarce or expensive materials, and can be adapted to most sunny environments. Only the tracking automation requires machinery, which could be as simple as a clock or a closed-loop circuit comparing signals from (for instance) two photodiodes and small electric motor. The secondary mirror can be shaped in the earth or formed out of any readily available material that can hold its shape, some possible examples are show in Figure 12. Reflectivity can be provided by aluminized mylar (ubiquitously available from discarded snack bags), aluminum foil, or by tiled broken mirror pieces.

[4] E. F. Schumacher, Small Is Beautiful: A Study of Economics As If People Mattered, Blond and Briggs, 1973

[5] Ezzati M, Kammen DM (November 2002). "The health impacts of exposure to indoor air pollution from solid fuels in developing countries: knowledge, gaps, and data needs". *Environ Health Perspect.* **110** (11): 1057–68

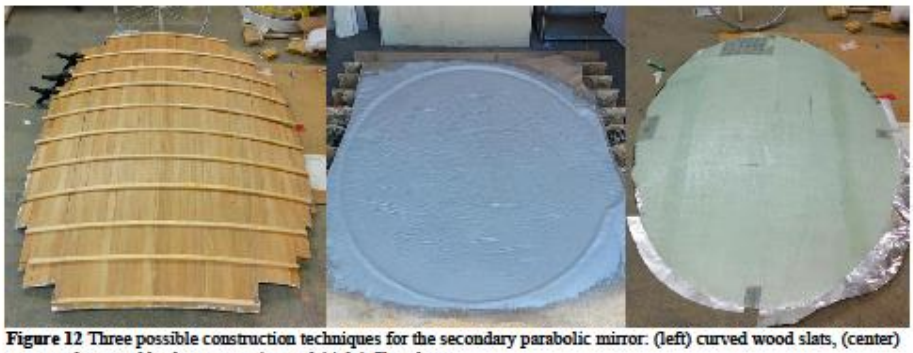

Figure 12 Three possible construction techniques for the secondary parabolic mirror: (left) curved wood slats, (center) concrete latex and burlap composite, and (right) fiberglass.

Conclusion

Sunlight can be reflected to a stationary point during the day with a heliostat rotating on a single axis, polar mount. The reflected light can then be concentrated or otherwise processed at a stationary position, reducing complexity. In developing countries and for residential uses everywhere, seasonal declination needs only to be adjusted occasionally by hand. The ease of construction and maintenance may allow communities everywhere to construct their own solar concentration facilities.

Acknowledgements

We acknowledge independent solar consultant, Steve Horne, for valuable guidance in the production of this paper.

APPENDIX B: MECHANICAL ENGINEERING SENIOR PROJECT THESIS COVER PAGE

Low-Cost Scheffler Solar Concentrator for the Developing World

A Senior Project

presented to

the Faculty of the Mechanical Engineering Department

California Polytechnic State University, San Luis Obispo

In Partial Fulfillment

of the Requirements for the Degree

Bachelor of Science, Mechanical Engineering

by

Darren Sholes, Jason Morgan, Nicholas Fuller

December, 2013

APPENDIX C: MATLAB CODE HEADDER


```
% Simo Alberti
% MSME Thesis
% 10/12 (Mo/Yr Start)

% Scheffler Design Master Code

close all
clear
clear classes
clc

diary('last.txt')
syms x xl yl

%% Run Configuration

% Deformation Type ========================================================
DefType = 10;
errTheta = .00001;   % degrees or percent based on Rnd selection

    % 0 - % - All error equal to errTheta
    % 1 - % - Uniform random distribution between +/- errTheta
    % 2 - deg - Gaussian distribution with mean=0 and stdev=errTheta
    % 10/12 - Circular profile ribs, same as above - NEEDS GLOBAL!!!!

if DefType == 2 || 12
    errTheta = deg2rad(errTheta);
end

% Display Flags ===========================================================
T_flag = 0;     % Text?
F_flag = [9];   % Figures?
    % 1 - Parabola and dish plots                   - n = 11
    % 2 - Seasonal changes of parabolic profile     - n = 11
    % 3 - Crossbars, 2D and 3D                      - n = 11
    % 4 - Flat 3D model                             - n = 101

    % 5 - Global 3D model                           - n = 101

    % 6 - Deformation Ray Tracing                   - n = 101
    % 7 - Deformation Focus Distribution            - n = 1001

    % 8 - Reflection Focus Distribution (???)       - n = 1001
    % 9 - Reflection Ray Tracing                    - n = 21

    % 11 - Power plot                               - n = 101
    % 12 - Resolution Convergence to 1001           - n = 101
    % 13 - 3D model with parabolic lines            - n = 101

    % 21 - Write DXF solid model                    - n = 101

Rayext = 1.2;

if max(F_flag == 1) || max(F_flag == 2) || max(F_flag == 3)
    n = 11;
elseif max(F_flag == 4) || max(F_flag == 5) || max(F_flag == 6)
    n = 101
elseif max(F_flag == 7)  || max(F_flag == 8)
    n = 1001
elseif max(F_flag == 9)
    n = 21
else
    n = 101
end

% Conditions ==============================================================

today = floor(date2doy(now));

Time = TimeYear;
TimeEquinox = TimeYear;

% Hour of the day wrt noon
Time.Hour_Sun = 12 + 0/60;              % Hour of the Day
Time.DotY_Sun = 173;          % Day = for Equinox - Spring = 80 and Fall = 267
                                %       for Solstice - Summer = 173 and Winter = 356
```